



Magnetolectric effect: principles and applications in biology and medicine—a review



S. Kopyl^{a,**}, R. Surmenev^{b,c,***}, M. Surmeneva^{b,c}, Y. Fetisov^d, A. Kholkin^{a,c,e,*}

^a Department of Physics & CICECO - Aveiro Institute of Materials, University of Aveiro, Aveiro, Portugal

^b Physical Materials Science and Composite Materials Centre, Research School of Chemistry & Applied Biomedical Sciences, National Research Tomsk Polytechnic University, Tomsk, Russia

^c Piezo- and Magnetolectric Materials Research & Development Centre, Research School of Chemistry & Applied Biomedical Sciences, National Research Tomsk Polytechnic University, Tomsk, Russia

^d Research & Education Centre 'Magnetolectric Materials and Devices', MIREA – Russian Technological University, Moscow, Russia

^e School of Natural Sciences and Mathematics, Ural Federal University, Ekaterinburg, Russia

ARTICLE INFO

Keywords:

Magnetolectric effect
Multiferroics
Piezoelectricity
Brain stimulation
Tissue engineering
Drug delivery
Wireless power transfer

ABSTRACT

Magnetolectric (ME) effect experimentally discovered about 60 years ago remains one of the promising research fields with the main applications in microelectronics and sensors. However, its applications to biology and medicine are still in their infancy. For the diagnosis and treatment of diseases at the intracellular level, it is necessary to develop a maximally non-invasive way of local stimulation of individual neurons, navigation, and distribution of biomolecules in damaged cells with relatively high efficiency and adequate spatial and temporal resolution. Recently developed ME materials (composites), which combine elastically coupled piezoelectric (PE) and magnetostrictive (MS) phases, have been shown to yield very strong ME effects even at room temperature. This makes them a promising toolbox for solving many problems of modern medicine. The main ME materials, processing technologies, as well as most prospective biomedical applications will be overviewed, and modern trends in using ME materials for future therapies, wireless power transfer, and optogenetics will be considered.

1. Introduction

A class of multiferroic structures exhibiting magnetolectric (ME) effect, which is a linear coupling between the applied magnetic field and generated electric voltage, has been attracted more and more research attention over the last years [1–5]. The coupling between electric and magnetic properties in ME materials provides exceptional opportunities to develop electric charges without any wire connections, which allows less-invasive integration into devices. Recent reviews [6–10] show progress in the fundamental understanding, development, and characterization of novel ME materials, as well as that these materials and structures are promising in microelectronics and related engineering applications, for instance, as high-speed memories, compact ME antennas [11,12], magnetolectric sensors [13,14], etc.

Despite the fact that the ME effect was known for many decades, scientists have only recently learned how to synthesize materials with

strong ME effects at room temperature [15,16], which is of particular importance for biomedical applications of ME materials.

As is well known [17], the human body is an extremely complex engineering system of trillions of interconnected cells that has been optimized over many years of evolution. Intrinsic electric fields at the subcellular level play an important (if not decisive!) role in these interactions, and this plethora of electrophysical effects determine fundamental physiological mechanisms [18,19]. ME materials may enable cells to react remotely at nano- and microscales, thus opening up unprecedented possibilities for biomedical applications. By controlling their own electric fields that underlie cell-to-cell and cell-to-cell interactions, ME materials are expected to play an important role in the development of imaging and treatment methods that allow eliminating collateral damage and significantly improve the effectiveness of modern treatments [20–22].

The use of ME materials in biology and medicine is still in its infancy, so there are a few publications and no reviews. The recent introductory

* Corresponding author.

** Corresponding author.

*** Corresponding author.

E-mail addresses: svitlanakopyl@ua.pt (S. Kopyl), rsurmenev@mail.ru (R. Surmenev), kholkin@ua.pt (A. Kholkin).

review [23] focuses only on the characterization of modern magnetic field sensors suitable for biomedical applications such as magneto-cardiography, magnetotomography, magnetomyography, magneto-neurography from a physical point of view and provides a brief overview of recent studies in this field. Another review [24] considers the problems associated with the development and application of a new type of 'smart' medical materials based on ME composites, mainly for bone tissue regeneration, capable of creating additional stimuli that affect the regeneration process.

In this work, we provide an extensive comprehensive overview of the principles of the ME effect, modern processing technologies, as well as current developments in their applications in biomedical research. We discuss a number of applications in tissue engineering, brain stimulation, cancer treatment, and drug delivery. Magnetolectric effect for wireless power transfer and optogenetics will be considered, as well as current trends and prospects in the use of ME materials for future treatment methods.

2. Principles of magnetolectric effect: from single-phase materials to composites

The magnetolectric (ME) effect is defined as a change in the electric polarization P of a substance under the influence of a magnetic field H (direct effect) or a change in the magnetization M of a substance under the action of electric field E (converse effect) (see Fig. 1) [25]. ME effects are observed in multiferroic solids that simultaneously possess both the ferromagnetic and ferroelectric ordering, as well as in other materials that acquire electric polarization under the action of a magnetic field.

Generally, in multiferroic crystals, the polarization P and magnetization M are related to the electric E and magnetic H fields by the following relations [26]:

$$P_i = P_i^S + \varepsilon_0 \varepsilon_{ij} E_j + \alpha_{ij} H_j + \frac{1}{2} \beta_{ijk} H_j H_k + \gamma_{ijk} H_j E_k \dots \quad (1a)$$

$$M_i = M_i^S + \mu_0 \mu_{ij} H_j + \alpha_{ji} E_j + \beta_{jik} E_j H_k + \frac{1}{2} \gamma'_{ijk} E_j E_k \dots \quad (1b)$$

where P_i^S and M_i^S are the spontaneous polarization and magnetization, respectively, ε_0 and μ_0 are the magnetic and electrical constants, ε_{ij} and μ_{ij} are the relative electrical permittivity and magnetic permeability of the substance. The tensor α_{ij} determines the magnitude of the linear ME effect in the material, and the tensors β_{ijk} and γ'_{ijk} determine the magnitude of the nonlinear ME effects.

In practice, in order to eliminate the influence of the electrical conductivity of materials, ME effects are investigated in a dynamic mode by applying an alternating magnetic or electric field to the samples. The magnitude of dynamic effects is characterized using ME coefficients:

$$\alpha_E = \frac{\delta E}{\delta H} = \frac{u}{b \delta H} \text{ in } V/(\text{Oe} \cdot \text{cm}) \text{ for the direct ME effect,} \quad (2a)$$

$$\alpha_B = \frac{\delta B}{\delta E} = \frac{\delta B}{u/b} \text{ in } \text{G} \cdot \text{cm}/V \text{ for the converse ME effect,} \quad (2b)$$

where δE and δB are the amplitudes of the ac electric field and magnetic induction in the substance, caused by a change in the magnetic δH and electric δE fields, respectively (parameters u and b are defined in Fig. 1).

The ME effect was first observed in 1960 in Cr_2O_3 single crystals [27, 28], where its magnitude at room temperature is $\alpha_E \approx 20 \text{ mV}/(\text{Oe} \cdot \text{cm})$. To date, ME effects have been found in dozens of different single-phase materials [29]. However, in ME crystals, the effects are small in magnitude $\alpha_E \sim 1\text{--}20 \text{ mV}/(\text{Oe} \cdot \text{cm})$ and are observed (with rare exceptions, for example, in Cr_2O_3 , BiFeO_3 , $\text{Y}_3\text{Fe}_5\text{O}_{12}$, $\text{SrCo}_2\text{Ti}_2\text{Fe}_8\text{O}_{19}$) at low temperatures $T \sim 4\text{--}20 \text{ K}$, or in high magnetic fields $H \sim 10\text{--}50 \text{ kOe}$, which complicates their practical use [30].

Much larger ME effects were found at room temperatures in artificially created composite materials containing ferromagnetic (FM) and piezoelectric (PE) phases. In such composites, ME effects arise as a result of a combination 'product-property' of the magnetostriction of the FM phase and piezoelectricity in the PE phase due to the mechanical coupling of the phases across the interfaces [31,32]. When the ME composite is placed in an external magnetic field H , the FM phase is deformed due to magnetostriction, this deformation is transferred to the PE phase, and the piezoelectric effect results in the generation of an electric field E (direct ME effect). While an electric field E is applied to the composite, the converse piezoelectric effect results in a deformation of the PE phase, this deformation is transferred to the FM phase, and due to the inverse magnetostriction (Villari effect), the magnetic field B is changed (converse ME effect).

Fig. 2a–c schematically depicts the main types of two-phase ME composites with connectivity types 0-0, 0-3, 1-3, and 2-2, respectively [33]. The numbers indicate the number of coordinates along which deformation is transmitted in each of the phases, with the first number referring to the FM phase and the second to the PE phase. Particulate composite (a) of 0-0 type is FM and PE particles embedded in a neutral matrix. Composite (b) with the connectivity of the 0-3 type contains FM particles located in a PE matrix. Composite (c) with the connectivity of 1-3 type is FM rods in a PE matrix. Particles and rods in 0-0, 0-3, and 1-3 composites can be distributed in the matrix both randomly or in a certain order. Composite (d) of 2-2 type is a planar heterostructure containing two or more alternating FM and PE layers. Additionally, it is worth highlighting the core-shell nanocomposites (e), consisting of nanoparticles, the core of each is made of FM material, and the shell is made of PE material [34,35]. The properties of ME composites can be engineered by selecting phase materials of the structure, phase volume ratio, and changing the particle and sample sizes.

According to the 'product-property' concept, the magnitude of the direct ME effect in the above-mentioned composites is qualitatively well described by the formula

$$\alpha_E = \frac{\delta E}{\delta H} \approx \frac{\delta E}{\delta S} \cdot \frac{\delta S}{\delta H} \approx A \cdot h \cdot q, \quad (3)$$

where A is the coefficient that depends only on the geometry of the composite, and the dielectric characteristics of its phases, $h(E)$ is the piezomodulus of the PE phase, $q(H) = \partial \lambda / \partial H|_H$ is the piezomagnetic modulus of the FM phase, $\lambda(H)$ is the dependence of the magnetostriction of the FM material on the magnetic field. It follows from (3) that the characteristics of ME effects in composites can also be controlled using external H and E fields. Of great interest for applications are 2-2 type layered structures containing alternating FM and PE layers, which are relatively easy to manufacture. In such composites, FM layers with high conductivity and PE layers with low conductivity are spatially separated and retain their physical properties, which makes it possible to effectively polarize the PE layers.

It is worth adding that the stress coupling mechanism leads to an increase of the ME effect in composites by a factor of $Q \sim 10^2\text{--}10^3$ due to a sharp increase in deformations when the frequencies of the fields coincide with the frequency of the acoustic resonance of the sample [36].

Recently, a variety of composite materials with high ME conversion efficiency have been created. Fig. 3 shows the values of the ME

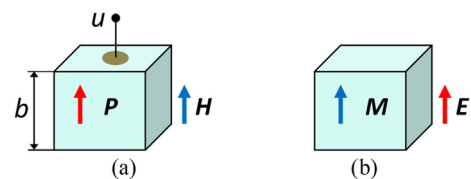


Fig. 1. Geometry of the direct (a) and converse (b) magnetolectric effects. U is the voltage appearing under the action of applied magnetic field H .

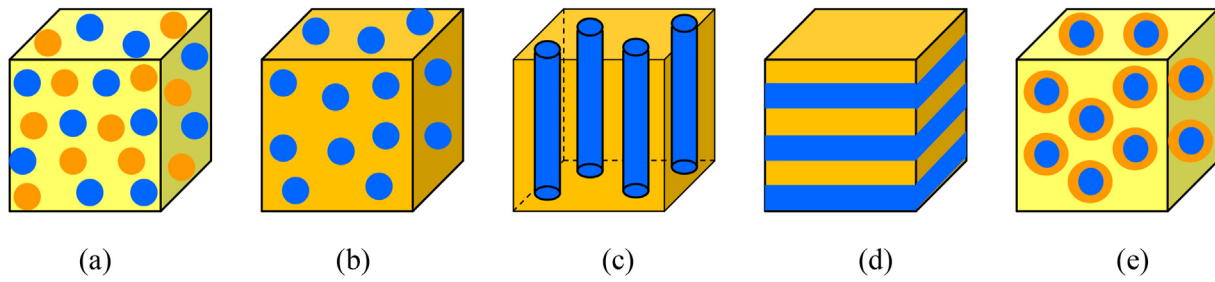


Fig. 2. Composite ME materials of various types of connectivity: (a) 0–0; (b) 0–3; (c) 1–3; (d) 2–2; (e) - core-shell nanocomposite. Highlighted in color: yellow - dielectric matrix; orange - piezoelectric; blue - ferromagnet.

coefficient for some particulate composites and heterostructures in the off-resonant and resonant excitation modes.

It follows from (2) and Fig. 3 that to increase the ME effect in composites, one should use ferromagnets with a high piezomagnetic coefficient q (metals - Ni, Co, alloys - FeCo, FeGa, Metglas, Terfenol-D, ferrites NFO, CFO) and piezoelectrics with a high piezoelectric modulus ratio to dielectric constant d/ϵ (ceramics of the PZT and PMN-PT types, LNO, BTO, AlN crystals). Flexible structures based on biocompatible polymeric piezoelectrics of the PVDF type are promising for applications, too [2]. It is seen from Fig. 3 that for particulate composites, the magnitude of the ME coefficient α_E is $\sim 1\text{--}100$ mV/(Oe cm) while for planar structures it is about $1\text{--}50$ V/(Oe cm) and increases to hundreds V/(Oe cm) at the frequencies of acoustic resonance.

The ability to mutually transform magnetic and electric fields makes it possible to use the ME effect in multiferroic materials in various fields

of science and technology. The direct ME effect forms a basis for sensors of permanent and low-frequency alternating magnetic fields with a sensitivity of up to $\sim 10^{-11}$ T, operating at room temperature [21], solid-state inductors and transformers tuned by an electric field [1,38], energy harvesters, converting alternating-current (AC) magnetic fields into direct-current (DC) voltage [39], etc. The converse ME effect is used in compact low-frequency antennas [1], electrically tunable resonators and microwave filters [40], data storage elements switched by an electric field [41]. One of the most promising directions is the use of biocompatible ME materials in medicine [24,42,43].

3. Magnetolectric composite materials

Magnetolectric (ME) composites allow either polarization in response to an applied magnetic field or induce magnetization caused by

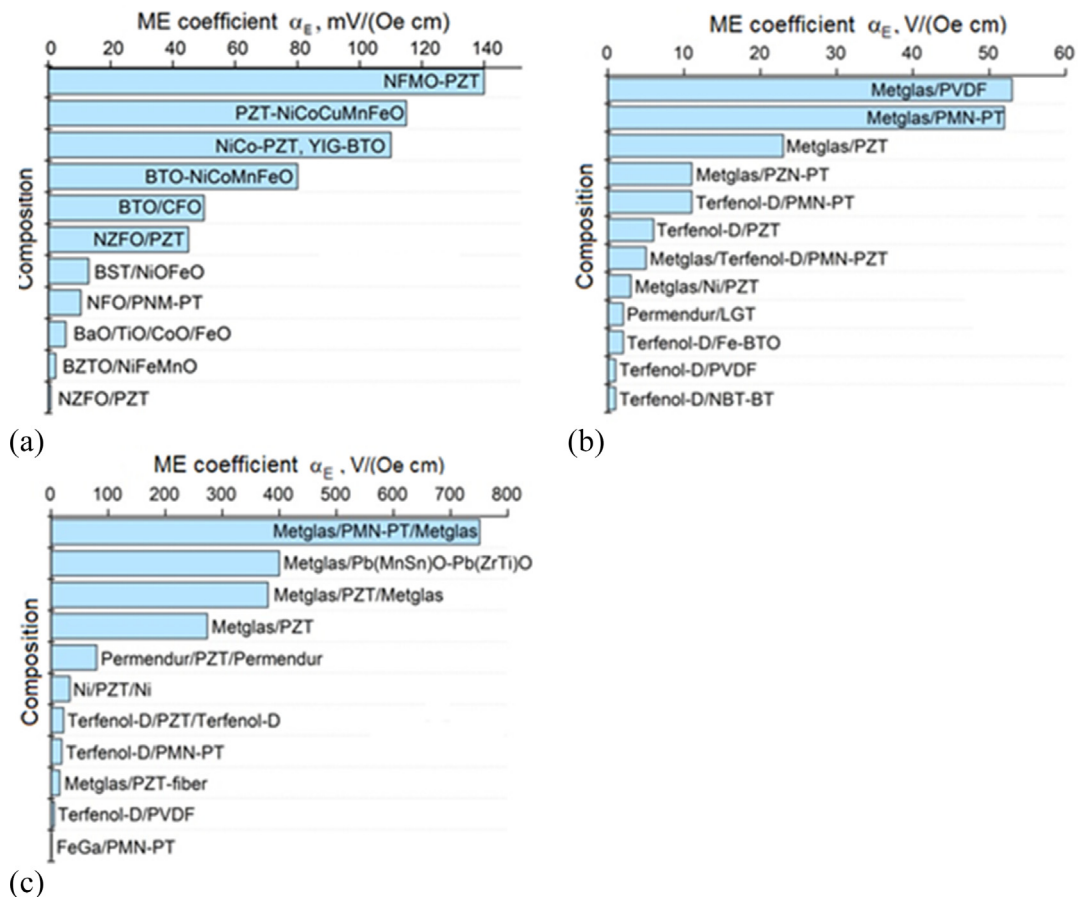


Fig. 3. Values of ME coefficients for: (a) particulate composites; (b) laminated heterostructures in off-resonance regime; (c) laminated heterostructures in resonance regime. Adapted from Ref. [37].

an externally applied electric field, allowing ME effect at room temperature [44], which is particularly important for biomedical applications of ME composites. Moreover, the coupling between electric and magnetic properties in ME composites provides exceptional opportunities to develop charges without any electrical connections, which allows less-invasive integration into sensors, energy harvesters, wearable and implantable electrodes, etc.

Extensive overviews of electroactive, in particular piezoelectric materials and composites, are reported elsewhere [45]. Electroactive electrospun nanofibers are well-reviewed for various biomedical applications such as cardiac or nerve tissue regeneration, wound healing, skeletal muscle and bone regeneration, a therapeutic platform for drug delivery, biosensing, etc. [46]. Magnetic actuation of the ME composites provides electrical and mechanical stimuli to the neighboring cells [47]. Also important is that the ME composites enable, under the exposure of the external magnetic field, the remote stimulation of a specific tissue, e.g. bone, nerve, etc [46,48].

Strain-induced ME effects have given rise to significant ME properties in the various composites (polymer-based or hydrogel-based) that combine the piezoelectric and magnetostrictive phases such as polyvinylidene fluoride (PVDF) and metglas or Terfenol-D, respectively. The developed composites allow the increase of ME coefficients in the materials of up to 370 V/(Oe cm) under an externally applied magnetic field at room temperature [49], which is close to that of human body temperature, thus making them prospective for a broad range of tissue engineering applications [44].

In general, the application of magnetic fields to stimulate cells and tissues is intensively studied in various tissue engineering applications [50–52]. As an example, magnetic poly(L-lactic acid) (PLLA) scaffolds obtained via a freeze-drying approach containing Fe-doped hydroxyapatite nanoparticles are also reported [50]. Silk fibroin magnetoactive nanocomposite films and membranes with cobalt ferrite (CoFe₂O₄) nanoparticles have also been developed for dynamic bone tissue engineering strategies [53]. The application of electrically responsive scaffolds can also be connected with nerve regeneration [54].

ME materials in the form of core-shell nanoparticles have gained particular interest for various drug delivery systems allowing control via external magnetic field over tissue regeneration processes, wireless powering of miniature implantable devices without any harmful damage of tissues, allowing to avoid repeated surgeries and thus infection apposition or even more complicated consequences [55,56], which are reviewed in detail in the following sections.

Various ME composites were also reported in the form of laminates, e.g. Terfenol-D/P(VDF-TrFE), Terfenol-D/PZT/PVDF, core-shell particles, etc [47,57]. Usually, the piezoelectric phase in the ME composite is a lead-containing ceramic such as PZT-5H [58]. A high generated output voltage and significant value of deliverable power (~0.6 mW) were achieved in the case of the composite Terfenol-D/Metglas/PZT-5H for wireless powering of an embedded device for biomedical applications [58]. Moreover, higher energy powers have been reported so far, e.g. power of ~10 mW is generated at an applied magnetic flux density of 318.9 μ T in case of a laminated composite of two Galfenol and one PZT layers [59]. Terfenol-D/P(VDF-TrFE) composites were found to provide both mechanical and electrical stimuli to MC3T3-E1 preosteoblast cells triggered by a remotely applied magnetic field. It was reported that the proliferation of cells is enhanced up to ~25% when they are cultured under mechanical (up to 110 ppm) and electrical stimulation (up to 0.115 mV). This demonstrated that ME cell stimulation via magnetic, mechanical, and electrical cues is a perspective approach for various tissue engineering applications [47].

Hydrogel-based ME microenvironments for tissue stimulation have been also reported [60]. Polymer-based ME materials demonstrated suitable bioactivity to provide magnetically and mechanically activated biophysical electrical stimuli capable of improving cellular processes [61]. PLLA microspheres and magnetic microsphere nanocomposites composed of PLLA and magnetostrictive CoFe₂O₄ nanoparticles

combined with a hydrogel matrix allowed mimicking the tissue's hydrated environment and simultaneously served as a support matrix [61]. Hybrid composites, which contain multiferroics, most frequently BiFeO₃, were reported for use in tissue engineering to significantly enhance cell viability and proliferation [62].

A study of hybrid ME films of P(VDF-TrFE)/CoFe₂O₄ revealed that both proliferation and differentiation of the C₂C₁₂ myoblast cells are enhanced via the application of mechanical and/or electrical stimulation with higher values of maturation index under mechano-electrical stimuli [51]. These composites allowed mechanical (13·10⁻³ μ m/mm²) and electrical stimulation of cells (16.15 μ V and 64 μ V), in case of magnetic and mechanical bioreactors, respectively.

A composite of P(VDF-TrFE)/CoFe₂O₄ has been reported as a new magnetic field responsive bioactive coating to enhance cellular osteogenic differentiation. This composite allowed the authors to understand the molecular mechanisms of osteogenic differentiation when magnetic responsive coating and static magnetic field are combined [64]. It was revealed that the most appropriate magnetic fields for cellular adhesion and proliferation are 2000 and 2600 Oe, respectively, which enable an attractive remote-control approach to develop and design a new type of magnetic field responsive biomaterials for bone tissue engineering.

The magnetic micro-environment achieved by the inclusion of 7.5 wt % Fe₃O₄ nanoparticles in the PLLA/PGA scaffold significantly promoted cell differentiation over time [52,65]. The enhancement effect is due to the fact that magnetic nanoparticles embedded in scaffolds facilitate cell adhesion via activation of various signaling pathways with the extending of culture time promoting cell differentiation [66]. More details on the results obtained on magnetic field simulation of magnetically responsive materials and subsequent effects are presented in the following sections.

As already mentioned, the current state-of-the-art magnetolectric composites contain high amounts of lead-based ferroelectrics, such as lead zirconate titanate (Pb [Zr_xTi_{1-x}]₂O₇, PZT) and lead magnesium niobate-lead titanate (Pb(Mg_{1/3}Nb_{2/3})O₃-PbTiO₃, PMN-PT), endowing them with excellent piezoelectric response [49]. However, over the last 15 years, a lot of studies have been done to decrease the amount of lead and other hazardous materials in commercial electronics and other products, primarily due to health and environmental concerns. This has motivated the search for lead-free materials with piezoelectric characteristics similar to those of PZT and PMN-PT [67]. Furthermore, the majority of ME transducers developed so far are laminates and composites with different designs, such as 0–3, 1–3, and 2–2 [68]. In the case of ME composites, Metglas® is mostly used as a magnetostrictive layer [63]. Generally, amorphous metallic glass (e.g., Metglas® 2605SC (Fe₈₁B_{13.5}Si_{3.5}C₂)) assumes the form of an amorphous ribbon [69], with no comparable alternatives having been reported thus far (Fig. 4). Metglas® comprises magnetic grains with shiftable domain boundaries under an applied AC magnetic field, enabling the material to change its overall shape. The resulting vibrations are transferred to the PZT, which develops a voltage in response to the induced strain [63]. Therefore, a thin-film laminate converts an externally applied low-frequency AC magnetic field into a voltage across the transducer via mechanical coupling between the magnetostrictive and piezoelectric phases.

Various ME composites have been developed, e.g., bilayer laminates [(Ba_{0.85}Ca_{0.15})(Zr_{0.1}Ti_{0.9})O₃ - CoFe₂O₄] (α_{ME} of ~615 mV/(Oe cm), trilayer laminates (α_{ME} ~ 803 mV/(Oe cm) [70], and [Ba(Zr_{0.2}Ti_{0.8})O₃-0.5(Ba_{0.7}Ca_{0.3})TiO₃]/CoFe₂O₄]/[Ba(Zr_{0.2}Ti_{0.8})O₃-0.5(Ba_{0.7}Ca_{0.3})TiO₃] (α_{ME} ~ 740 mV/(Oe cm) [71]. Alternatives to magnetostrictive Metglas-based materials with considerable ME properties have been reported [72,73]. However, their energy harvesting performance is limited, and can only be maximized under high-strength magnetic fields; thus, they cannot achieve sufficient power transfer under safety levels and novel magnetostrictive materials which can overcome this problem are highly demanded, which is one of the main objectives of the current research endeavors.

Recently, a novel magnetostrictive material, Fe_{100-x}Ga_x compound, was discovered [69]. This alloy is more suitable for ME transducers

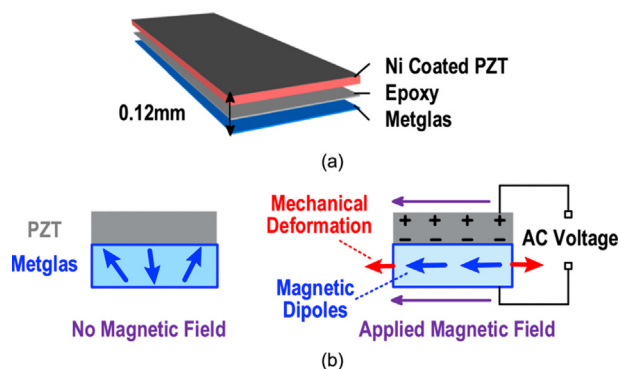


Fig. 4. State-of-the-art in the field: (a) laminate structure and (b) operating principles of the PZT/Metglas ME transducer. A piezoelectric layer (pink) (Ni-coated PZT) and a Metglas (magnetostrictive layer (blue)). © [2020] IEEE. Reprinted, with permission, from Ref. [63].

owing to its superior properties compared to the conventionally used Metglas® 2605SC, such as lower Young's modulus (65 against 160 GPa) and significantly higher magnetostriction constant (320 against ~30 ppm) [69]. Typically, Fe–Ga alloys are magnetically soft, mechanically robust, ductile with large [74] or giant [75] magnetostriction. In general, magnetostriction in the rare-earth-free Fe–Ga alloys increases with the increasing content of non-magnetic Ga, peaking in the metastable (A2+D0₃) two-phase region [76]. The dependence of the magnetostriction on the stoichiometry of Fe–Ga alloys has been extensively studied. In the case of Fe₈₃Ga₁₇, the λ_{100} magnetostriction coefficient can reach 0.02% [77]. In Fe₈₁Ga₁₉ alloys, an enhanced magnetostriction coefficient of $\lambda_{100} = 0.039\%$ was measured [78]. Magnetostriction values of ~140–150 ppm were observed in a ~5 μm long section of a 150 nm diameter Fe–Ga/Cu nanowire, which was the same as that found on the macroscale [79]. However, to date, little is known about the strain distribution and magnetostriction both at the nanoscale/microscale due to the experimental challenges faced during characterization [80]. For example, as the size of Fe–Ga alloys decreases to the nanoscale, shape anisotropy significantly hinders the actuation and sensing of the samples [79]. Thus, to engineer magnetostrictive devices with high sensitivity and reliability, it is vital to understand the fundamental interactions between the lattice strain, dimensionality, and magnetic moment under the influence of an external magnetic field. The materials with higher magnetostriction can be potentially suitable candidates for the higher energy-scavenging performance of ME composites.

4. Biomedical application of magnetoelectric materials

4.1. Piezoelectric materials in tissue engineering

The term biopiezoelectricity is used to describe piezoelectricity found in biological systems. In addition, some of the hard tissues such as dentin, bone, cementum, etc., and some soft tissues such as hair, tendon, muscle, cartilage, pineal gland, ligament, etc. reveal intrinsic piezoelectric effect in the human body [81,82]. The piezoelectricity of bone was discovered for the first time by Fukada and Jasuda [83], which at a later stage was connected with the piezoelectric nature of collagen [84]. The piezoelectricity mainly originates from the liquid-crystalline or nanocrystalline structure of complex extracellular matrix (ECM) components such as keratin, elastin, glycosaminoglycans, collagen, and hydroxyapatite. It is known that there are circulating microcurrents in the human body, which determine the mechanisms of tissues regeneration and metabolic processes. In Fig. 5, the most important tissues in the human body are listed, where electrical activity is observed.

Electric fields are pervasive in many biological processes. For example, in neuronal wound healing, neuronal cells experience a constant electric field of up to 140 mV/mm [48,85]. Thus, the inclusion of

electroactive materials in neuronal wound healing environments can be used to guide axons to grow along specific paths [86]. Other types of tissues are also dependent on electric stimuli to help them to grow, reconstruct, and regenerate. While the inclusion of electroactive materials can be used to guide osteoregeneration, neuronal differentiation, and proliferation, there are many challenges associated with designing materials that can apply electric fields in a minimally and/or noninvasive manner.

Biochemical stimulation is the most frequently used strategy for cell regeneration, while application of physical stimuli, including magnetic, mechanical, or electrical fields, is a promising yet scarcely investigated alternative approach up to now [87]. In addition, the fabrication of materials with a potential control of their behavior *in vitro* and *in vivo* via either externally applied magnetic field or intrinsic properties such as piezoelectric or electroactive is in high demand [88].

It has been reported that the bone should be exposed to mechanical strain between 100 and 2000 microstrain with ~ strain 100 repetitions a day to achieve a balance in bone remodeling and healing [89]. By being exposed to such mechanical stress, bone generates the charge density of $\sim 7 \times 10^{-11} \mu\text{C}/\text{cm}^2$ (at 1 N/m² of stress), resulting in a balance between bone resorption and a new bone formation [43,90]. During wound healing, similar behavior of electrical signals was reported [91]. It has also been demonstrated that endogenous electrical fields affect both cell migration and wound healing. However, electrical stimuli influencing the natural tissue healing process may not exist at the defect site, i.e. at bone replacement and bone fracture. Therefore, the use of *ex-situ* electrical stimuli can potentially replace natural endogenous electrical stimuli and thus restore/accelerate tissue healing [43]. *Ex-situ* electrical, ultrasonic, and electromagnetic stimulation enables acceleration of bone repair/healing. In particular, electrical stimulation is revealed to enhance bone healing through the changes in cell adhesion, alignment, proliferation, and migration to the defect site [43,92,93]. At a later stage, electrically active smart biomaterials have served the purpose of generating electrical stimulation *in situ* [43,94]. Different approaches have been used to alter cell behavior to accelerate bone healing via the design of the polarized surfaces for bone replacements [43,95].

Different ferroelectric and piezoelectric materials were used in tissue engineering applications such as polymers PLLA, PVDF, PVDF-TrFE, poly-3-hydroxybutyrate-co-3-hydroxyvalerate (PHBV), poly-3-hydroxybutyrate (PHB), ceramics (BaTiO₃, BN, ZnO, BiFeO₃, and hydroxyapatite) and composites thereof [45,48,96]. Several of them produce piezoelectric output in the range, which is very close to that of the endogenous potentials (0.15–1.2 V) naturally existing at the healing site of a wound. Piezoelectric nanocomposites combine relatively high piezoelectric charge coefficients of a piezoceramic and flexibility of a piezoelectric polymer matrix, thereby allowing regeneration of bone, cartilage, and other tissues [45]. However, the effect of piezocharge and/or piezoelectric potential on the regeneration process has not been studied in sufficient detail so far [45].

PVDF and also its copolymers (e.g. P(VDF-TrFE), polyvinylidene fluoride hexafluoropropylene, etc.) are the piezoelectric non-biodegradable polymers most frequently used for tissue engineering applications due to intrinsic piezoelectricity [97]. In further, most of the studies describing cell response under dynamic stimulation used namely PVDF (also its copolymers) as a support for cell proliferation and differentiation.

Electrospinning is typically used to prepare various types of nanofibrous composite scaffolds, e.g. PVDF/Fe₃O₄ [44] or PVDF with hybrid nanofillers of graphene oxide/CoFe₂O₄ [98] and others [48,88].

Utilizing the piezoelectric effect requires applied alternating mechanical stimuli, which may have several of their own challenges. For example, when ultrasound exposure is used as a stimulus, ultrasound waves may be attenuated by the body tissues [99]. This means that ultrasound stimulation is limited in its efficiency to stimulate regions deep inside the body. Therefore, there is still a challenge to develop electroactive materials that enable delivering electric fields to more remote

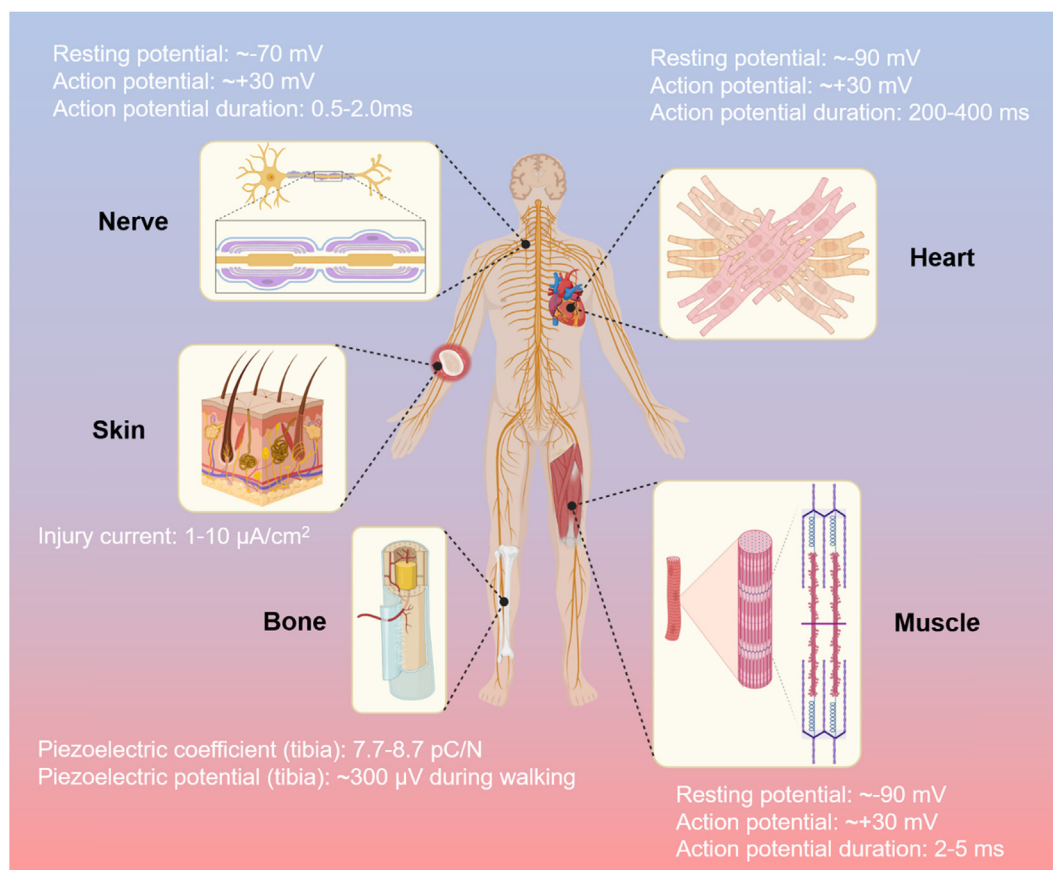


Fig. 5. Electrical activity in the human body. Adapted from Ref. [46] with permission from Elsevier. © 2021 Elsevier Ltd.

regions in the body. A short summary of the cellular responses to these composite materials is given in Fig. 6.

Piezoelectric BFO^+ films with a thickness of about 10–20 nm were obtained on the surface of SrTiO_3 implants (Fig. 6a). The results of PFM revealed that the films generated a constant, built-in electropositive field of 75 mV, which enables a strong interaction with the electronegative bone potential (from -87 to -52 mV). As a result of such stimulation, both bone healing and osseointegration of the coated implants in rat femoral defects were achieved (Fig. 6b). Possible mechanisms were proposed that is BFO^+ nanofilms promoted the adsorption of fibronectin (isoelectric point 4.8–6.4) and also upregulated the expression of cadherin 16 (*Cdh 16*) (mediating intercellular adhesion), *Cd44*, *Vcl*, *Itgb3*, and *Actb* (mediating crosstalk between cells) and osteogenic genes (*Spp1*, *Bmp2*, and *Wnt5a*) via activation of the PI3K-AKT signaling pathway (*Src*, *Akt1*, and *Pten* genes are responsible for bone formation, osteogenesis, and remodeling). As a result of this stimulation, cortical-like bone deposition was triggered, accompanied by the osseointegration of the coated implants. The alternative mechanism responsible for the obtained results can be the polarization of the piezoelectric materials due to body movements, which stimulated the adsorption of bioactive proteins followed by apatite deposition from the ions of Ca^{2+} and PO_4^{3-} [45].

Exposure to physiological loads or mechanical vibrations/deformations at an implantation site results in the generation of electrical signals on the surface of piezoelectric material, which occur similarly to collagen fibrils in cartilage and bone matrix by the formation of the negative charges via dipole reorientation. The formed electrical signal (Fig. 6c) subsequently triggers intricate cell signaling pathways, for example, by the opening of voltage-gated Ca^{2+} channels in cell membranes, which increases intracellular Ca^{2+} contents followed by activation of the calmodulin/calcineurin pathway following dephosphorylation of nuclear factor of activated cells (NF-AT),

translocation of dephosphorylated NF-AT into the cell nucleus and cooperative binding with other transcription factors. The described process regulates gene expression of specific signal proteins (bone morphogenic proteins, growth factors (TGF- β)), which are important for bone and cartilage formation [45].

The piezoelectric response of PVDF can be significantly increased via a poling process [103]. This is a process that utilizes a high external electrical field and allows aligning the molecular chains of the polymer to increase polarization proportional to the concentration of electroactive β -phase and/or γ -phase. As an example, poling procedure is described in Ref. 89. In addition, a poling approach may also affect cellular response. The negatively poled β -PVDF samples with $d_{33} \sim -32 \text{ pC}/\text{N}$ reveal a more pronounced ability to stimulate protein adsorption and osteogenic differentiation (ALP activity) of hASCs compared with either unpoled samples or positively poled ones under dynamic conditions (frequency 1 Hz, maximum amplitude 1 mm) (Fig. 6d) [101]. In comparison with PVDF, P(VDF-TrFE) reveals a higher piezocharge coefficient, which can be further increased by annealing at 135°C due to the increased amount of electroactive β -phase. As a result, under dynamic compression (frequency 1 Hz, deformation 10%), surface piezoelectric potential in the case of the annealed samples is significantly increased as compared to as-spun P(VDF-TrFE) samples without annealing. The scaffolds revealed streaming potentials of $61.1 \pm 1.5 \mu\text{V}$ and $25.2 \pm 2.5 \mu\text{V}$, respectively. An increased piezoelectric response of the P(VDF-TrFE) samples after annealing promoted osteogenic activity as compared to as-spun ones. In addition, the former samples expressed more pronounced levels of both osteogenic markers (osteocalcin, ALP, mineralization and upregulated osteogenic related genes (Runx2 and ALP (early markers), OCN and OPN (late/mature bone markers), but downregulated collagen I (Col I) (immature fibrocartilage marker) at day 28. On the contrary, as-spun samples revealed

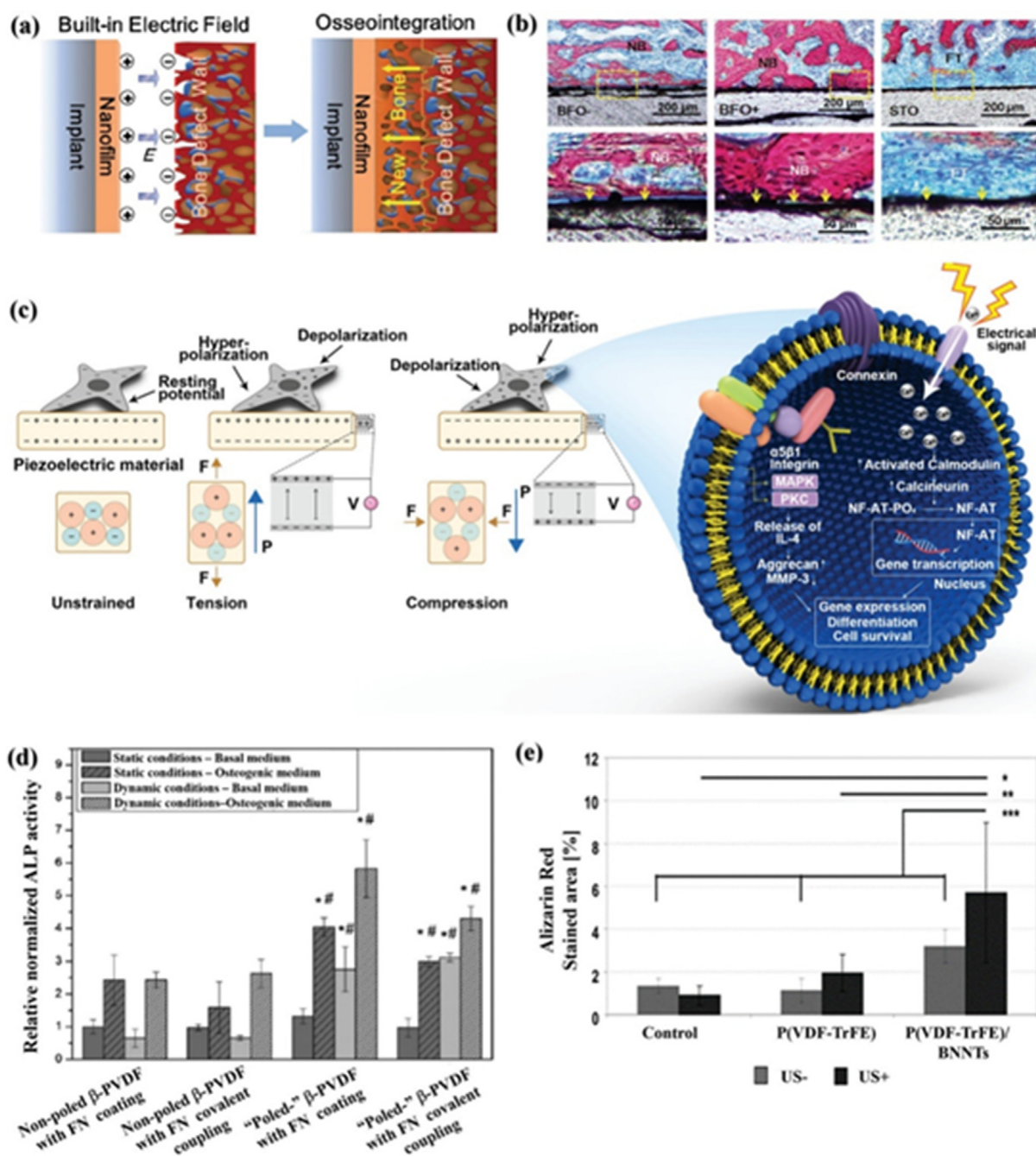


Fig. 6. The impact of a piezoelectric material or a thin film on cell behavior *in vitro*. (a) A schematic representation of fast osseointegration between electronegative bone and electropositive implant; (b) Histological results revealing enhanced osseointegration with BFO⁺ (BiFeO₃ films with downward polarization and positive potential) coated SrTiO₃ implants in comparison with uncoated or BFO⁻ (BiFeO₃ films with upward-oriented polarization and negative potential) coated SrTiO₃ implants (arrows in yellow: bone-material interfaces, NB: nascent bone, FT: fibrous tissue); (c) Schematic view of electric charge generation induced by mechanical strain on piezoelectric material surface triggering the signaling pathways of the cells; (d) Alkaline phosphatase (ALP) activity at 15 day of static and dynamic culture of human adipose stem cells (hASCs) on different PVDF films using either regular or osteogenic medium ($*p \leq 0.005$); (e) The effect of ultrasound stimulation of SaOS-2 cells seeded on P(VDF-TrFE) and hybrid P(VDF-TrFE)/BNNT films using a medium for differentiation (bright-field microscopy after staining with alizarin red) [45]. The images in Ref. [45] were adapted from as follows: (a,b) with the permission from Ref. [100] Wiley-VCH © 2017 WILEY-VCH Verlag GmbH & Co. KGaA, Weinheim; (d) with the permission from Ref. [101] © 2014 Wiley Periodicals, Inc.; (e) with the permission from Ref. [102].

chondrogenic activity compared to annealed P(VDF-TrFE) ones. The as-electrospun materials stimulated the synthesis of GAGs, collagen types II/I ratio, and upregulated expression of chondrogenic genes, e.g. chondroadherin (late/mature hyaline cartilage marker), Sox9 (early chondrogenic transcription factor), collagen II and IX (late/mature hyaline cartilage and hypertrophic chondrocytes marker), downregulated expression of aggrecan (early hyaline cartilage marker) and Col I (increased for the other). In addition, collagen II or IX expression

increased until day 14, and thereafter the expression decreased. At the same time, dynamic compression in the case of non-piezoelectric control has not revealed any significant response of the cells [104]. It was also reported that ultrasound stimulation of cast-annealed P(VDF-TrFE)/BN nanotube nanocomposite films, revealing 80% higher d_{31} piezocharge coefficient, stimulated differentiation of SaOS-2 osteoblast-like cell as compared to the plain P(VDF-TrFE) films, developed surface potential in the range of 20–60 mV (Fig. 6e) [105].

4.2. Magnetoactive and magnetoelectric materials for tissue engineering

It is well established that stimulation via magnetic field enables activation of numerous sensitive receptors on the cell surface and also related signaling pathways to promote cell activity [106,107]. In addition, the magnetic field that acts on the bone defect in a specifically tailored manner can enhance cell activity and thus increase the bone healing rate. Besides, magnetic field stimulation can promote integration between scaffolds and host bone, increasing both Ca and newly formed bone contents. Numerous sensitive receptors on the cell surface can also be activated, thereby enhancing cell activity and promoting new bone formation and fracture repair [52,108,109].

The magnetoactive 3D porous scaffolds for the effective proliferation of osteoblasts in a biomimetic microenvironment were reported [87]. The scaffolds are obtained through the development of nanocomposites comprised of a piezoelectric polymer PVDF and magnetostrictive CoFe_2O_4 nanoparticles, using a solvent casting method guided by overlapping the structures of a nylon template with three different fiber diameter sizes (60, 80, and 120 μm), and thus, varied porosity. The magnetoactive composites possess a structure, which is very similar to that of trabecular bone with pore size in the range from 5 to 20 μm owing to the inherent process of crystallization of PVDF with the nanoparticles interconnected with larger pores, formed after removing the nylon templates [87]. A physically active microenvironment was prepared through the bone-mimicking structure of the scaffolds combined with the physical stimuli provided by a magnetic custom-made bioreactor on a magneto-responsive scaffold. In this study, a novel bioreactor based on magnetic stimulation has been developed, allowing for advanced tissue engineering strategies [110]. It can act as a valuable tool for mimicking *in vitro* the human stimulations provided by the electrically active tissues that are present in the body. The magnetic stimuli application (23 mT at a frequency of 0.3 Hz) to cells seeded on the ME leads to an increase in the cell viability of almost 30% with respect to the cell culture under static conditions, which could mimic what occurs in the human body and for the application in immobilized patients [110]. It could also be important for growing well-formed cellular tissues *in vitro* more effectively and rapidly, which could be further implanted in the human body without the material. In the case that magnetoactive materials are implanted in the human body, it may provide a suitable platform to evaluate the remote stimulation and thus for the effective growth and cell differentiation in immobilized patients.

A novel approach for tissue engineering applications has been achieved with ME composite biomaterials. As an example, ME Terfenol-D/PVDF-TrFe composites promoted $\sim 25\%$ of MC3T3-E1 preosteoblast cells proliferation when cultured under mechanical and electrical stimulation remotely controlled via varying magnetic fields [111]. The surface charge also stimulated enhanced cell proliferation for muscle regeneration [112]. However, the studies with piezoelectric biomaterials reporting the effect of dynamic conditions have been scarcely performed [97].

3D ME inverse opal scaffolds allowing the generation of localized electric fields under external magnetic field exposure are presented in Fig. 7 [113]. The scaffolds are composed of biodegradable piezoelectric PLLA and hybrid ME nanoparticles ($\text{CoFe}_2\text{O}_4/\text{BiFeO}_3$) and are designed to mimic porosity and piezoelectric properties of the native microenvironment of cancellous bone. The protocol to prepare ME inverse opal scaffolds is presented in Fig. 7a, which includes fabrication and assembly of monodispersed gelatin microspheres into a hexagonally close-packed (*hcp*) lattice followed by thermal annealing to introduce necking between adjacent gelatin spheres. After that, a solution with the scaffolding material composed of hybrid ME $\text{CoFe}_2\text{O}_4/\text{BiFeO}_3$ core-shell nanoparticles dispersed in a PLLA solution is infiltrated into the voids of the gelatin lattice in vacuum conditions (Fig. 7a(i)). In the end, the obtained gelatin lattice is etched selectively by immersing the samples at 60 °C in deionized water, which resulted in the fabrication of a ME scaffold with an ordered porous network (Fig. 7a(ii)). The prepared gelatin

microspheres revealed a uniform diameter of $\sim 440 \mu\text{m}$. Fig. 7b presents an image of the ordered *hcp* gelatin microspheres. A magnified image shows that the gelatin lattice is composed of well-connected microspheres with uniform void spaces. The fabricated ME inverse opal scaffolds obtained after removal of gelatin spheres with various magnifications are shown in Fig. 7c. It is clearly seen that the ME scaffolds possess a uniform, well-ordered structure. Fig. 7d reveals a cross-sectional view of the scaffold with a well-defined, long-range ordered interconnecting porous network with a uniform size. The fabricated cobalt ferrite nanoparticles are cuboidal in shape with an average size of $\sim 12 \text{ nm}$. The core-shell cobalt ferrite@bismuth ferrite nanoparticles demonstrate an average size of 20 nm (Fig. 7e). The energy-dispersive X-ray mappings presented in Fig. 7f show a uniform shell composed of iron, bismuth, and oxygen around the core of cobalt ferrite. The EDX mappings of a typical ME scaffold are shown in Fig. 7g and reveal that the ME nanoparticles are uniformly distributed in the volume of the scaffold. MicroCT analysis of the cobalt ferrite@bismuth ferrite/PLLA scaffolds revealed an overall porosity of $\sim 86\%$. In its turn, a cross-sectional MicroCT image of the same scaffold is shown in Fig. 7h and also reveals a porous and well-ordered structure of the scaffold.

The magnetic field (13 mT at the frequency of 1.1 kHz) resulted in electric stimulation of human-derived MG63 osteoblast cell proliferation, which is a model for primary osteoblast cells, was studied on 3D scaffolds and 2D membranes. As a result, a 134% increase in cell proliferation was obtained for stimulated 3D scaffolds compared with non-stimulated ones. An increase of 43% of stimulated 2D membranes was obtained compared with non-stimulated ones, which signifies the importance of 3D scaffolds to provide a suitable microenvironment to host the cells [113].

It was reported that cancellous bone is piezoelectric and reveals a 3D interconnected porous structure, which is crucial to maintain its biological functions. Magneto-electrically induced proliferation of MG63 cells cultured under the influence of alternating current (AC) magnetic fields was studied (Fig. 8a). Fig. 8b clearly shows a pronounced increase in cell proliferation seeded on ME scaffolds under exposure to a magnetic field in comparison with the untreated scaffolds. The cell viability of the 3D ME scaffolds exposed to a magnetic field increased by 134% ($p < 0.001$), in comparison to the samples without treatment. This result confirms the significant impact of ME effect-induced cell proliferation on 3D porous scaffolds. Fig. 8c presents an SEM cross-section image of a 3D ME scaffold seeded with cells after exposure to a magnetic field. The top and the bottom of the scaffold, marked as red squares in this SEM image, are shown as magnified SEM images (Fig. 8d and e). On the top surface of the ME scaffold, the presence of many well-adherent cells interacting and growing on the walls of the scaffold is observed (Fig. 8d). The presence of many cells that successfully migrated within the scaffold is revealed on SEM images obtained from the bottom region of the scaffold. It can also be observed that the cells are well adherent and interacting with the curved walls of the scaffold. The results obtained were further confirmed by confocal laser scanning microscopy (CLSM) of the 3D ME scaffold (Fig. 8f and g) [113].

Usually, the important stage prior to cell adhesion on the surface is protein adsorption [114]. Thus, the success of any cellular tests *in vitro* should take into account surface-protein interactions. Proteins expression of integrin $\alpha 5\beta 1$ -mediated FAK/ERK signaling pathway was studied to understand the molecular mechanisms responsible for osteogenic differentiation on poled $\text{CoFe}_2\text{O}_4/\text{P}(\text{VDF-TrFE})$ nanocomposite films under the dynamic regulation of magnetic field [115]. The expression level of proteins, including $\alpha 5$, $\beta 1$, *p*-FAK, and *p*-ERK is significantly upregulated on 2600/2600/0 at 4 days, compared with the 2000/2000/0 and 2600/2600/0 (Fig. 9A-F), which is attributed to a transformation from a low-affinity binding state of $\alpha 5\beta 1$ -FN to a high-affinity binding state of $\alpha 5\beta 1$ -FN strengthen integrin-mediated FAK/ERK signaling pathway, when the temporal dynamic regulation of magnetic field was performed on poled nanocomposite film. A mechanism of recognition and strengthening process between integrin FN and $\alpha 5\beta 1$ is designed to enhance osteogenic differentiation of cells based on integrin-mediated

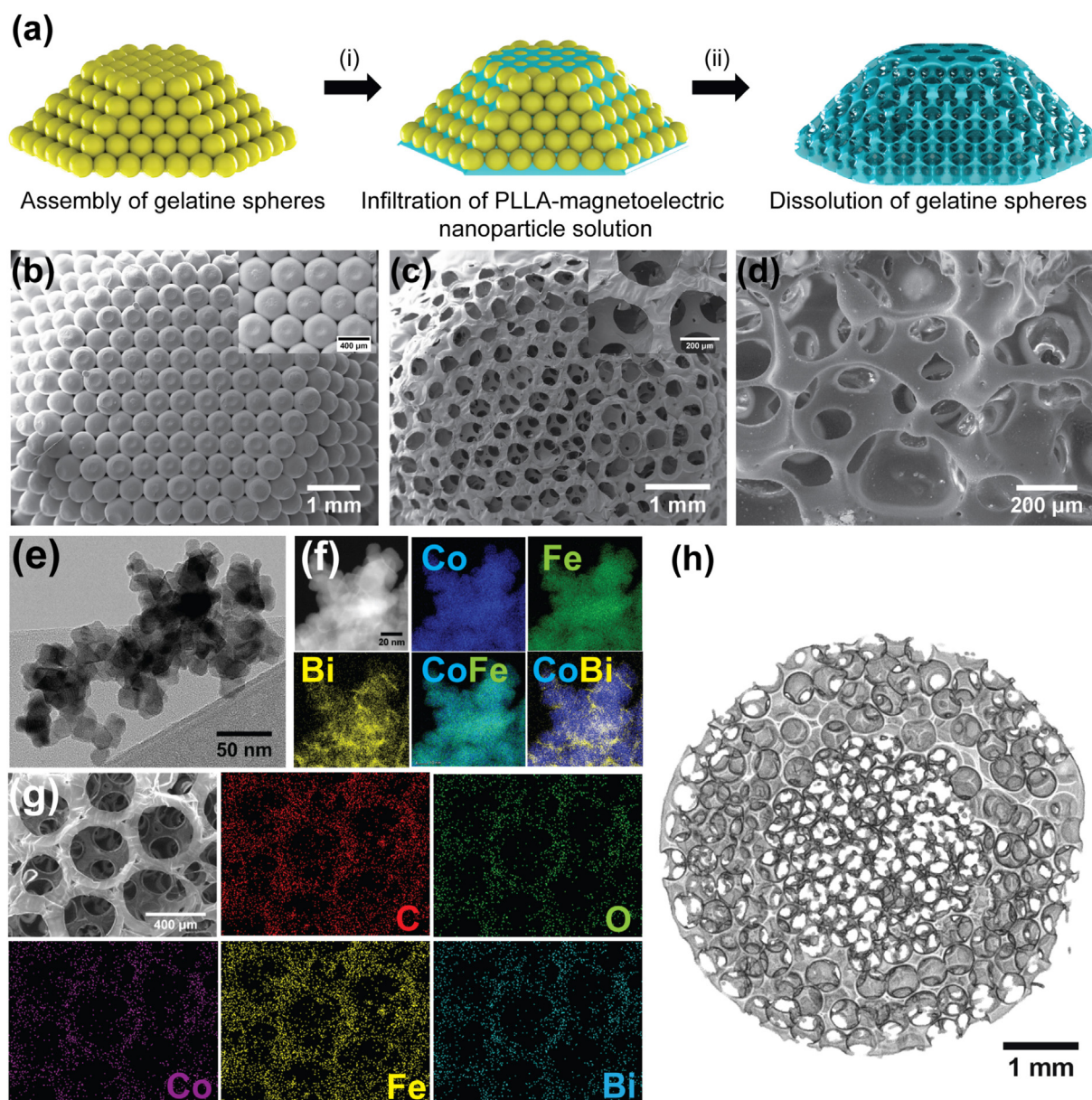


Fig. 7. The fabrication scheme of ME inverse opal scaffolds and the results of ME nanoparticles and scaffolds properties. (a) Fabrication steps scheme dealing with the assembly of the spheres of gelatin followed by (i) their infiltration with the solution of PLLA and ME nanoparticles and (ii) gelatin spheres removal to prepare 3D porous ME scaffolds. SEM images of the assembled gelatin template (b) (a magnified image is shown as an inset). (c) SEM image of the top-view of a 3D ME scaffold (a uniform porous structure is revealed in the inset). (d) SEM image of a ME scaffold cross-sectional view. (e) TEM image revealing many overlapped cobalt ferrite@bismuth ferrite nanoparticles. (f) high-angle annular dark-field detector (HAADF) scanning-transmission electron microscope (STEM) image of the overlapped cobalt ferrite@bismuth ferrite nanoparticles and corresponding EDX maps for Fe, Co, and Bi, with the superimposed images of the hybrid core-shell cobalt ferrite@bismuth ferrite nanoparticles. (g) SEM image of the ME scaffold and the corresponding EDX maps obtained for Co, C, Fe, O, and Bi revealing a uniform distribution of ME nanoparticles within the scaffold. (h) Cross-sectional reconstructed 3D micro-CT image of a scaffold with a porosity of 86% Reprinted with permission from Ref. [113] © 2019 Elsevier Ltd.

FAK/ERK signaling pathway (Fig. 9G).

Materials with a proper microenvironment providing mechanical and electrical cues to cells have been created mimicking the morphology and physical environment of bone since it reveals piezoelectric nature and allows generating electrical cues with mechanical stimulation, e.g., walking [88]. The ME composite materials can generate mechanical and electrical cues indirectly upon the external magnetic field proving the concept of remote stimulation of the immobilized patients [87]. For that purpose, bioinspired magnetoactive 3D scaffolds for bone engineering have been reported (Fig. 10).

The obtained scaffolds are based on piezoelectric PVDF and magnetostrictive CoFe_2O_4 nanoparticles. The improved proliferation of

preosteoblasts by means of the application of magnetic stimuli is revealed [66], which is attributed to both local magnetomechanical and ME response of the scaffolds induced subsequent cellular mechano- and electro-transduction processes via the change of the magnetic field (Table 1) [87].

Electrospun hybrids of PVDF/ CoFe_2O_4 /GO scaffolds were seeded with mesenchymal stem cells and then exposed for up to 21 days (8 h per day) to extremely low-frequency electromagnetic fields (1 mT, 50 Hz) produced by the home-made magnetic generator, which was placed inside the CO_2 incubator [98]. The differentiation value increased with the employment of bioreactor and was also reinforced after neural differentiation media treatment. Thus, fabrication of ME scaffolds for neural

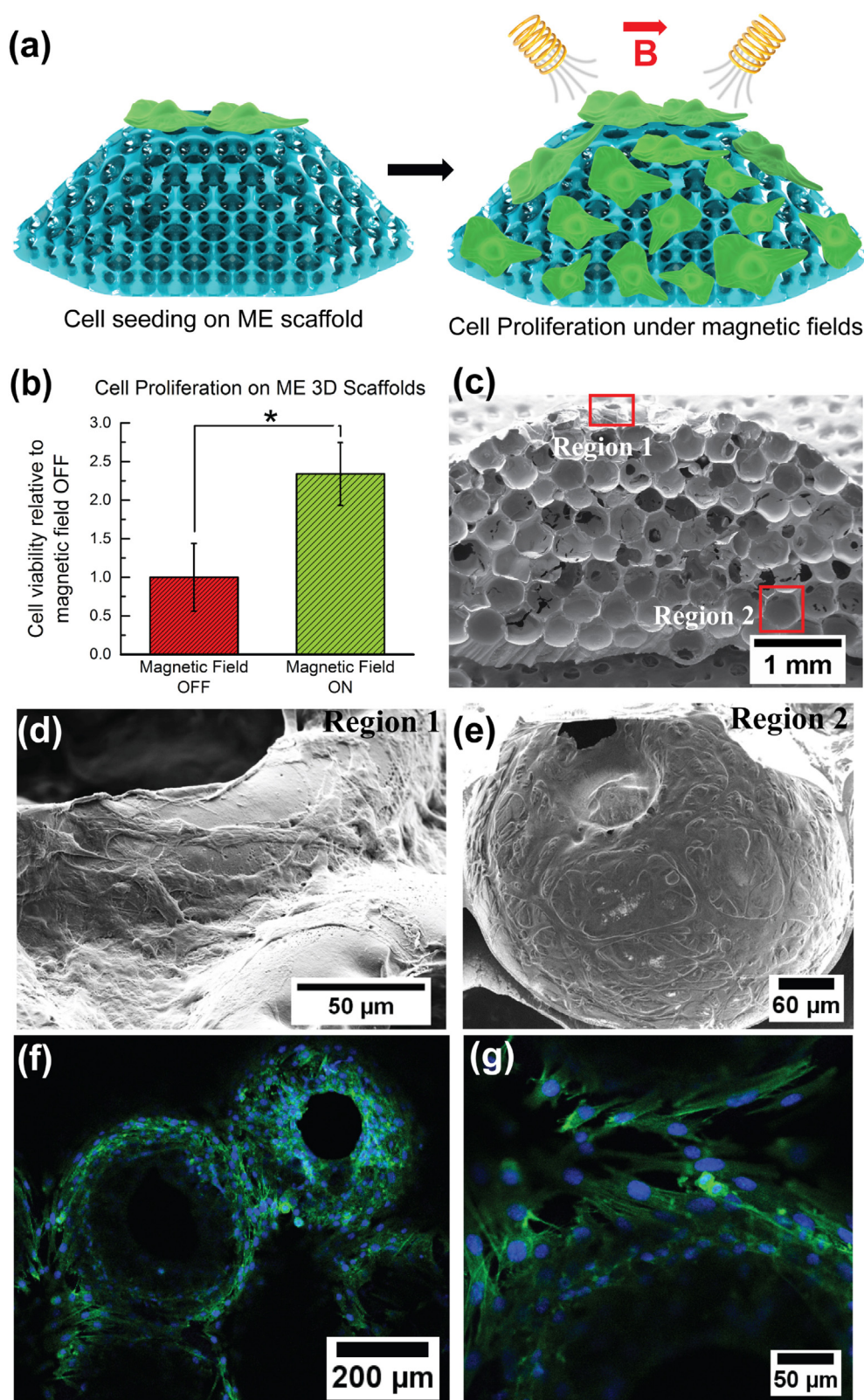


Fig. 8. Effect of magnetic stimulation of 3D ME scaffolds seeded with cells. (a) A scheme revealing the ME effect induced enhanced cell proliferation on the prepared 3D scaffolds exposed to AC magnetic field. (b) A comparison of cell viability assay of cell proliferation on ME 3D scaffolds without and with magnetic field stimulation (* $p < 0.001$). (c) SEM image revealing the 3D ME scaffold cross-section seeded with cells and subjected to a magnetic field. A magnified image of the (d) region 1 reveals the SEM image at the top of the scaffold, where many interacting/attached cells are seen. (e) An SEM image for region 2, where there are many cells growing on the inside wall of the scaffold, is seen. (f and g) CLSM images of the 3D ME scaffolds with MG63 cells after magnetic field exposure. Phalloidin-stained f -actin in green and Hoechst-stained nuclei in blue reveal a uniformly grown layer of adherent MG63 cells along the curved walls of the scaffold [113]. Reprinted with permission from Ref. [113] © 2019 Elsevier Ltd.

cell differentiation with no need for chemical differentiation media was achieved. However, it should also be noted that no ME coupling was discussed in detail in the study; thus, the physical mechanisms of the observed phenomena are not clear.

ME coupling was also revealed at the nanoscale in the case of electrospun nanofibrous PVDF/Fe₃O₄ (10 wt% of PVDF) scaffolds when an

individual nanofiber was studied [49]. It means that even magnetically active materials with Fe-containing compounds studied mostly at the moment reveal the ME effect observed at the magnetic field up to 2000 Oe, which has not been given sufficient details so far. Thus, more research should be done to derive the effect of magnetic field-induced polarization due to magnetostriction of the magnetic phase. The

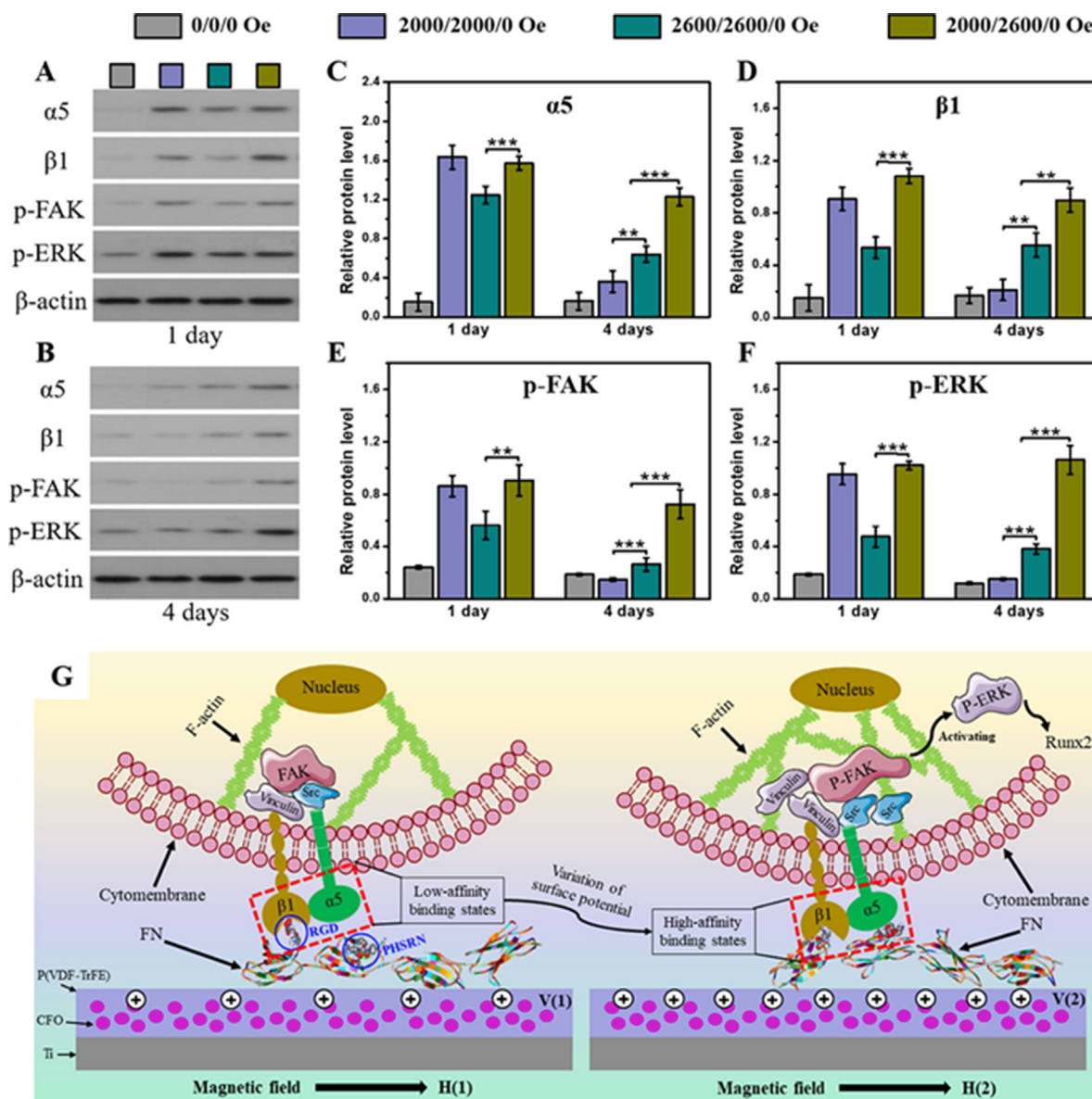


Fig. 9. Proteins expression of integrin-mediated FAK/ERK signaling pathway on the surface of 10% poled cobalt ferrite/P(VDF-TrFE) nanocomposite film. (A–F) The relative expression levels of α5, β1, p-FAK, and p-ERK on the film with temporal dynamic regulation of magnetic field normalized to β-actin. (G) Schematic diagram of cellular osteogenic differentiation on magnetically responsive cobalt ferrite/P(VDF-TrFE) nanocomposite film with temporal dynamic regulation of the magnetic field. Reprinted with permission from Ref. [115]. Copyright © 2018, American Chemical Society.

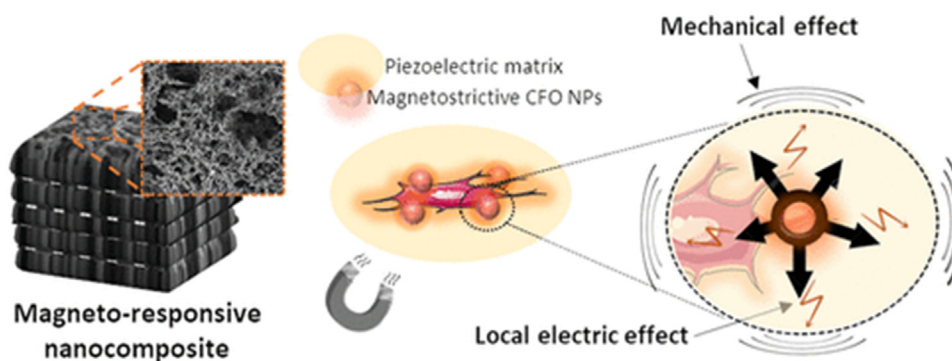


Fig. 10. A scheme of a magneto-responsive nanocomposite and its effect on a cell under an external magnetic field exposure. Reprinted with permission from Ref. [87]. Copyright © 2019, American Chemical Society.

Table 1

A summary of piezoelectric, magnetoactive, and ME composites and their potential for bone engineering. Redesigned based on the results reported elsewhere [43]. BT – barium titanate (BaTiO₃), PU – polyurethane, BM-MSCs – bone marrow mesenchymal stem cells.

Structure	Composite	Results	Magnetic field	ME coupling,	Reference
Piezoelectric					
Porous	HA/BT	Biocompatible, cell viability enhanced on HA composites with up to 70% BT	–	–	[116]
	BT/akermanite nano-bioceramic	No cytotoxic effect	–	–	[117]
	Lithium Sodium Potassium Niobate	Improved attachment and proliferation of osteoblasts	–	–	[118]
Fibre	PVDF	Excellent osteoblast cell spreading	–	–	[119]
	BT/PLLA	Randomly oriented fibrous composite encouraged BM-MSCs spreading/differentiation	–	–	[120]
	ZnO/PU	Promote <i>in vitro</i> fibroblasts cell adhesion, proliferation, differentiation	–	–	[121]
Membrane	BT/P(VDF-TrFE)	Promote fast bone regeneration both <i>in vitro</i> and <i>in vivo</i>	–	–	[122]
		Both enhanced <i>in vitro</i> osteoinductivity and <i>in vivo</i> bone regeneration, used as osteoinductive barrier membrane	–	–	[123]
3D printed	BT	Scaffold for bone tissue engineering	–	–	[124]
		Enhance <i>in vitro</i> osteogenic differentiation	–	–	[125]
Magnetoactive					
3D printed (selective laser sintering)	PLLA/polyglycolic acid (PLLA/PGA) doped with Fe ₃ O ₄ 20 nm in size	Stimulated cell adhesion and viability, and enhanced proliferation rate and ALP activity	Permanent 0.35 T	–	[52]
		Significantly induced substantial blood vessel tissue, fibrous tissue, and new bone tissue formation at 2 months postimplantation in a rabbit bone defect <i>in vivo</i>			
Composite	Bioactive glass incorporated with BiFeO ₃ (2–15 wt%)	Enhance up to three times mouse preosteoblast MC3T3 cells viability/proliferation exposed for 30 min/day	200 or 350 mT	–	[62]
Magnetoelectric					
Hydrogel-based scaffold	CoFe ₂ O ₄ /Methacrylated Gellan Gum (GGMA)/PVDF	Provide cell viability superior to 80% <i>in vitro</i>	220 mT	$\Delta d_{33} \approx 6$ pC/N	[60]
Film	CoFe ₂ O ₄ /PVDF	Mechanical (0.013 $\mu\text{m mm}^{-2}$) and electrical (16.15 μV and 64 μV , magnetic and mechanical bioreactor, respectively) stimulation of C2C12 myoblast cells	± 220 mT	–	[51]
Composite	Terfenol-D/P(VDF-TrFE)	Enhanced MC3T3-E1 preosteoblast cell proliferation up to $\approx 25\%$ while being cultured under mechanical (up to 110 ppm) and electrical stimulation	230 Oe (frequency 0.3 Hz)	0.115 mV	[47,97,111]
Scaffolds	PVDF/CoFe ₂ O ₄	Local magnetomechanical and ME response induced subsequent cellular mechano- and electro-transduction processes	230-0 Oe	0.115 mV	[87]
Composite membrane	CoFe ₂ O ₄ /P(VDF-TrFE) (10 wt%)	Enhanced BM-MSCs osteogenic differentiation, and also regulated the osteoimmunomodulatory environment to improve bone regeneration	2300 Oe (DC)	54 mV	[126]
Film	CoFe ₂ O ₄ /P(VDF-TrFE) (10 wt%)	Synthetically programming the preferred magnetic field of cell adhesion and proliferation periods during cell growth significantly enhanced cellular osteogenic differentiation	0–3000 Oe	$\Delta V \approx 93$ mV	[115]

nanoscale ME effect is still to be demonstrated in the macroscale form of electrospun nanofibrous samples, which typically have a porous, randomly oriented nanofibrous structure.

There are also a few results on ME composites, which composition deviates from traditional ME structures containing both magnetostrictive and piezoelectric phases. As an example, in the study [127], the authors

use the term ME effect in the case of a high-frequency magnetic field generating an electric current by charging conductors. Thus, a digital light processing (DLP) 3D printing method was used to prepare a biocompatible and stretchable nanocookie conduit (NC@conduit, NC@C) integrating features of mesoporous carbon sheets and protein permeable elastomers for the purpose to regenerate a peripheral nerve

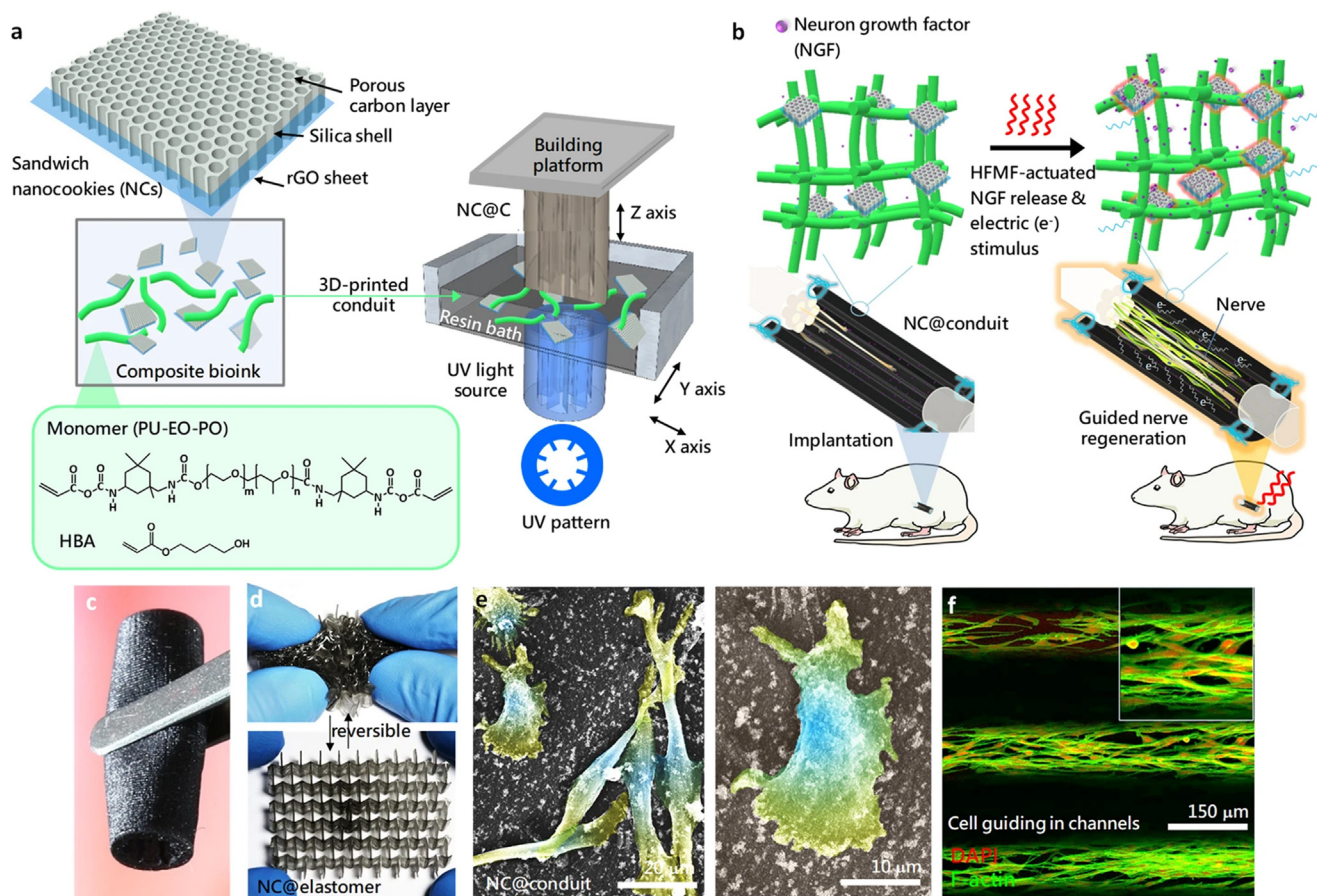


Fig. 11. 4D Printing of stretchable NC@C with ME conversion capability for growth factors release and simulation of cells for neurite sprouting. (a) Composite bioink consisting of 4-hydroxybutyl acrylate, urethanepolyethylene glycol-polypropylene glycol monomer, initiator, and NCs made through 3D printing for NC@C fabrication. (b) NC@C under the treatment of a high-frequency magnetic field facilitated ME conversion for growth factor release and cell stimulation to induce neuron cell differentiation. (c) Image of a 3D printed NC@C revealing elastic properties of the composite. (d) The stretchable properties of NC@C revealed. (e) SEM image of cells adhered to the surface of NC@C. The surface roughness of the NCs improved cell attachment. (f) CLSM images of cells proliferating on NC@C with microchannels. DAPI-stained nuclei (red) and phalloidin-stained F-actin (green). Copyright © 2020, reprinted from Ref. [127].

(Fig. 11) [127]. The authors reported that NCs with mesoporous silica on the surface of the conduits provide ME conversion, protein adsorption, and thus cell stimulation. Electromagnetized carbon porous NCs under a high-frequency magnetic field treatment facilitate ME conversion for the release of growth factor and cell stimulation to induce neuron cell differentiation and proliferation *in vitro* and *in vivo* [127]. However, no details on the parameters of electromagnetic field were presented in the study. Fig. 11a reveals a bioink composed of mesoporous carbon layers on a graphene oxide sheet (sandwich NCs), and 4-hydroxybutyl acrylate/urethanepolyethylene glycol-polypropylene glycol monomer was placed in a 3D printer resin bath. Then, UV light possessing a channel pattern in a ring was applied to cure the bioink to form a flexible composite NC@C with internal channels through DLP 3D printing. Fig. 11b shows that 3D printed NC@C loaded with a large payload of neuron growth factor (NFG) was implanted to implement its spatial distribution for the promotion of axon outgrowth after a peripheral nerve was transected 10 mm from the bifurcation point of the sciatic nerve of Sprague-Dawley rats. Upon receiving high-frequency magnetic field irradiation, the NFG encapsulated in NC@C revealed an excellent permeability and on-demand release enabling induction of the differentiation and proliferation of nerve cells *in vivo* while simultaneously supplying electromagnetic stimulation to cells. After the addition of NCs, the printed conduit and composite still revealed sufficient for successful application elastic and stretchable properties (Fig. 11c and d). The controllable roughness of the surface on a conduit by exposing NCs to 3D printing was achieved, which is an advantageous physical stimulus for

cell adhesion (Fig. 11e). In addition, through exquisite fabrication, the microchannels of NC conduits promoted cell alignment (Fig. 11f).

For providing an understanding of the orientation and growth of regenerated axons, the whole regenerated nerve from the proximal to the distal section in the conduit was harvested and stained with DAPI and β -III-tubulin to reveal the cell nuclei and regenerated axons, respectively. Fig. 12 displays a large area of CLSM images of immunohistochemically stained sciatic nerve defects from different treatments one month after implantation. It is seen that the autograft group had a thick nerve, curled and random fiber-like morphologies of regenerated axons were observed because the direct surgical suture led to the mismatch of axons. In addition, NGF-NC@C + MF (MF – treated with magnetic field) revealed a thicker nerve bundle compared with NGF-NC@C and NC@C, indicating that the growth of a nerve was promoted by ME stimulation and NGF release (shown as an inset). In further, a small distribution of axon orientation was observed in the conduit groups, which confirmed the effective regeneration of the high-frequency magnetic field treatment (i.e., ME stimulation-induced nerve differentiation mediated by NCs in the conduit, and NGF release enhanced cell growth). In addition, judging from the limb muscle weights and functions, the nerve recovery effects in NGFNC@C + MF were found to be excellent. A normal nerve was found to exhibit a nerve conduction velocity (NCV) of 47.5 m/s and a compound muscle action potential (CMAP) of 46.2 mV. At 1 month after surgery, the NGF-NC@C + MF group exhibited an NCV of 44.7 m/s and a CMAP of 44.9 mV, which were both higher compared with those of the NGF-NC@C group.

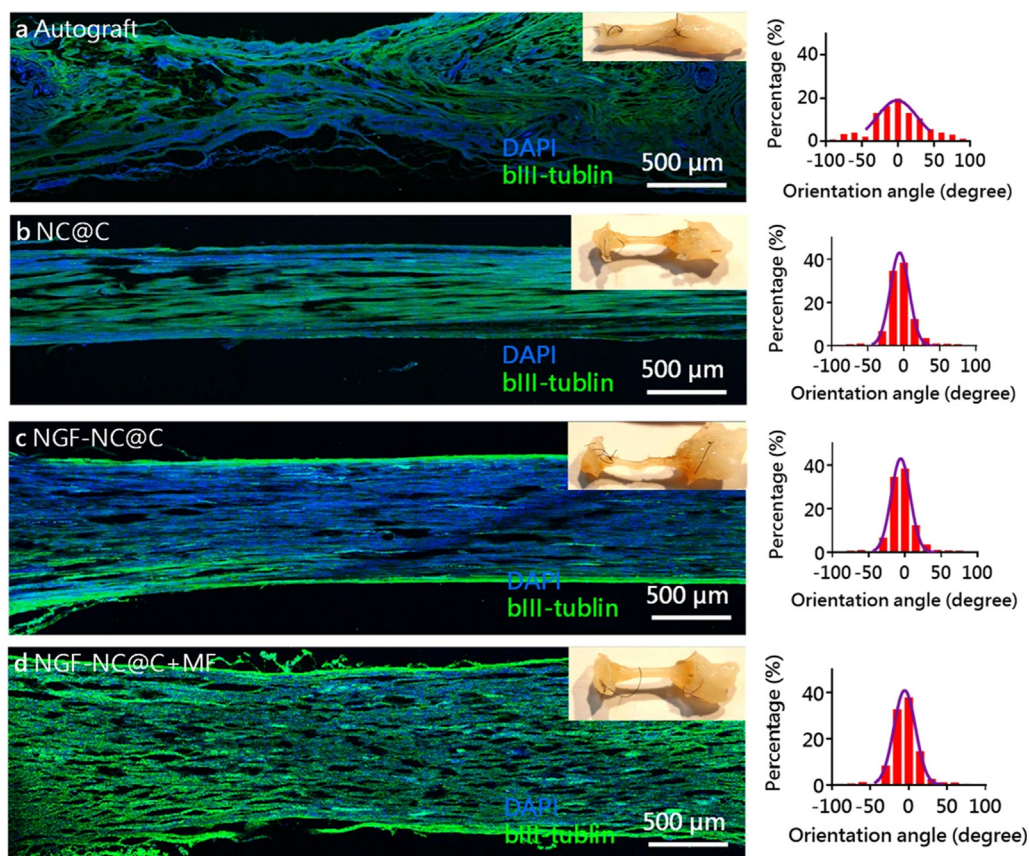


Fig. 12. Immunohistochemistry images of peripheral nerve regeneration. (a) Sciatic nerve defects harvested from an autograft, (b) NC@C, (c) NGF-NC@C, and (d) NGF-NC@C + MF ($n = 5$). The inserted images show the optical images, and the bar charts show the orientation analysis. Direct axonal outgrowth followed the microchannels of the conduit. Blue represents nuclei and green represents β -III-tubulin (axon). The orientation is from proximal to distal ($n = 5$). Copyright © 2020, reprinted from Ref. [127].

In summary, despite the active research and results described in the section, there is still a gap in the knowledge regarding the control of proliferation and differentiation of cells, as well as tissue apposition to ME scaffolds/implants via the ME effect. Most of the studies on electroactive materials were done using solely piezoelectric materials, which require deformation/loading to provide surface polarization [88,103,128–131]. In all of these cases, the movement of a person resulting in the mechanical deformation of a material/scaffold or mimicking this exposure ultrasound, etc. was used. These exposures have got their pros and cons, making it necessary for new research in the field of novel materials development. In the case of ME composites, the surface charge can be controlled in a more precise way by the variation of an externally applied magnetic field, which can also be applied for immobilized patients making them far more advantages in various tissue engineering applications.

4.3. Magnetoelectric effect for brain stimulation

The potential of ME nanomaterials to provide wireless stimulation of selective regions deep in the brain locally at the subneuronal level or vagus nerve stimulation cannot be underestimated [55,56,132]. This ability could open the door to definitive treatment for disabilities associated with motor and sensory impairments and cure patients with Parkinson's disease (PD) and some other neurodegenerative diseases. Both the central and peripheral nervous systems (CNS and PNS) are driven by electric signals and thus may be represented as electric circuits. A neurodegenerative disease occurs when one or several electric subcircuits have a defect or are completely broken. Local stimulation can help to repair such damaged subcircuits. It is noteworthy that electric-field triggered stimulation is the basis for many modern stimulation approaches like various forms of invasive direct-contact deep-brain stimulation (DBS) and low-efficacy transcranial magnetic stimulation (TMS) techniques [133,134]. However, these approaches are

severely limited in their capabilities. The DBS must make direct physical contacts with the neural network and is therefore limited to a finite number of implants. TMS interacts only indirectly with electrical circuits, and therefore, has very low efficiency and poor spatial resolution. In contrast, wireless ME-based stimulation can be performed locally, and therefore, can be completely non-invasive (or only mildly invasive) while achieving unprecedentedly high efficacy. The idea of using ME nanoparticles for brain stimulation to recover the communication between neurons in patients with PD was first discussed in a theoretical paper by Yue et al. in 2012 [135]. A few years later, Guduru et al. [136] reported the first *in vivo* ME-mediated modulation of brain EEG activity of mice by the external magnetic field via intravenous injection of core-shell CoFe_2O_4 - BaTiO_3 ME nanoparticles. These studies demonstrate that wireless stimulation with ME nanoparticles is really possible. In their *in vivo* experiments, the authors administrated a relatively small dose of the nanoparticles into the bloodstream intravenously through an injection of approximately 100 μg of ME materials in the tail of a mouse. The nanoparticles were pulled into the brain across the blood-brain barrier (BBB) via the application of a magnetic field gradient of approximately 3000 Oe/cm. The significantly increased concentration of the nanoparticles in the brain was confirmed through atomic and magnetic force microscopies (AFM and MFM), as well as through scanning electron microscopy (SEM) imaging of brain slices post euthanasia. To demonstrate wirelessly controlled stimulation, electroencephalographic (EEG) signals from EEG implants in correlation with an applied AC magnetic field of 100 Oe strength at a frequency in a range up to 100 Hz were measured. Thus, magnetic stimulation of the brain using ME nanoparticles requires a magnetic field intensity lower than that used for typical TMS [137]. The unique properties of ME nanoparticles, such as small size (~ 30 nm) and the ME effect not displayed by any other nanoparticles known to date, may provide significant improvements according to currently used techniques in terms of efficiency, accuracy, and tissue penetration for non-invasive brain stimulation.

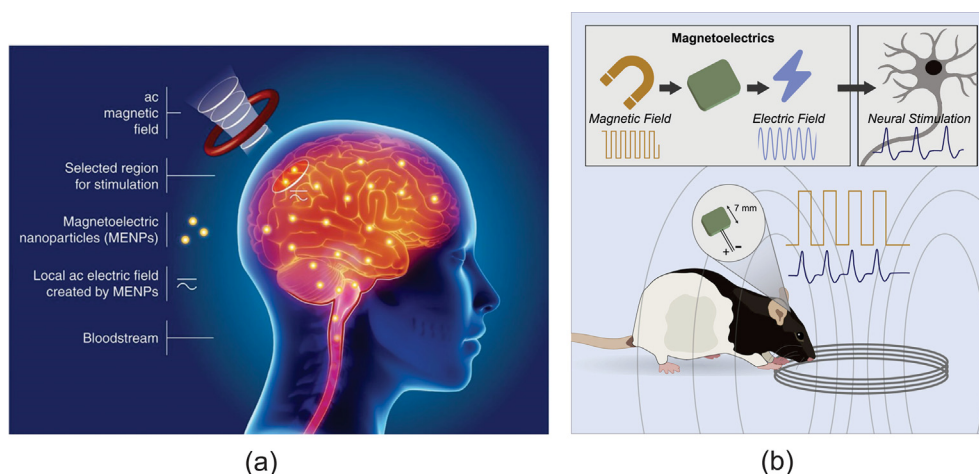


Fig. 13. (a) Illustration of a wireless electric stimulation with magnetolectric nanoparticles via application of AC magnetic fields. Reprinted with permission from Ref. [139]. (b) Schematic demonstrating of wireless deep brain stimulation in freely moving rodent model for Parkinson's disease. Reprinted with permission from Ref. [56] © 2020 Elsevier Inc.

Recently Nguyen et al. reported a non-invasive technique using core-shell CoFe_2O_4 - BaTiO_3 ME nanoparticles to wirelessly stimulate cortical neuronal activity [138]. The nanoparticles have been injected into a vein. The authors showed by *in vitro* and *in vivo* fluorescent and two-photon imaging techniques that ME nanoparticles can be drawn across the BBB and localized to a target cortical region without any apparent signs of neuroinflammation. Cortical activities in individual neurons and in a large neural network *in vivo* were induced by activating ME nanoparticles with a weak external magnetic field (100–500 Oe) at a specific frequency. Under the influence of a relatively weak magnetic field, the core of ME nanoparticles of cobalt ferrite (CoFe_2O_4) undergoes non-zero deformation due to the magnetostrictive effect. Due to the ME coupling, this deformation propagates through the lattice-matched interface to the neighboring shell of barium titanate (BaTiO_3), which, in turn, creates a local electric field (on the order of 1000 V/m) due to the piezoelectric effect. The concept of ME-based wirelessly controlled stimulation is shown schematically in Fig. 13a [139] and can be briefly described as follows: an external magnetic field of very low intensity is directed to the brain and causes fluctuations in the electrical charge in the nanoparticles, which can interact with neurons and stimulate neural pathways: a low-intensity field generates AC signals at the same frequency as the activity of a healthy nerve charge, and the vibration of a ME nanoparticle leads to the activation of neurons around it with the same frequency, that is, to their stimulation non-invasively.

The maximum effectiveness of wireless stimulation based on ME nanoparticles is achieved when nanoparticles are located on the surface of the neuronal membrane. As known [139], at rest, a typical value of the membrane potential is approximately -70 mV, and increasing by $+15$ mV triggers the firing of an action potential. The type of neuron and the specific location on the membrane surface determine the value of the electric field required to reach this threshold. MEs on the membrane must be able to locally generate an electric field strong enough to overcome the potential threshold for the ignition of action potentials. The results of a back-of-the-envelope-type estimation [140] demonstrated that the application of a magnetic field of 1000 Oe to a ME nanoparticle with an α of 100 mV/(Oe cm) would generate an electric field of 100 V/cm (10^4 V/m), and that would be enough to trigger firing of an action potential by a single nanoparticle. ME nanoparticles provide highly efficient stimulation when they act collectively and under the influence of periodic signals corresponding to periodic rhythms of brain waves. A relatively low-frequency periodic sequence of narrow pulses effectively stimulates the neural network at the local level [55,56], and may be useful for the treatment of depression, Parkinson's disease, and some

other neurodegenerative diseases. For example, Singer et al. [56] demonstrated that the wireless power method based on ME allows the use of magnetically powered miniature neural stimulators that operate at clinically significant frequencies ≥ 100 Hz. Millimeter-scale (about 7 mm) magnetolectric device has been used for DBS using a unit attached to the skull and wired to the deep brain (Fig. 13b). These ME stimulators can provide therapeutic deep brain stimulation in a free-roaming rodent model for Parkinson's disease.

Recently [55], a new study was published concerning wireless DBS in mice. For achieving wireless signal transmission to the insertion devices, ME nanoelectrodes that couple magnetic and electric signals (Fig. 14A,B) were used. ME nanoelectrodes were implanted into the subthalamic region by stereotaxic infusion and actuated using an external magnetic field at nonresonant carrier frequencies and in freely moving mice (Fig. 14C). Two-phase ME nanoparticles were prepared from magnetostrictive CoFe_2O_4 nanoparticles coated with a piezoelectric BaTiO_3 by sol-gel method (Fig. 14D-E). Magnetic stimulation of ME nanoparticles enables wireless modulation of neuronal activity *in vitro* and *in vivo*. Also reported was the therapeutic potential of this technology through its ability to modulate the activity of the motor cortex and non-motor thalamus, as well as to alter animal behavior.

It should be noted that, in order to perfectly recover any operation of the neural network with the help of ME nanoparticles, the individual action potentials should be triggered in any neural system at any time instance on demand. The ME coefficient is critical for this, and its increase depends on improving the properties of materials. It was reported [1] that the coefficient ME coefficient above 1 V/(Oe cm) can be achieved. The ME coefficient can be increased through a dc field biasing [141,142], and the ME effect strongly depends on the frequency [143–145]. In the case when both phases, magnetic and electric, resonate at the same frequency, the highest resonance will occur [146]. At the moment, most of these resonances in ME nanoparticles usually occur in the GHz range (e.g., from below 5 to over 10 GHz), while electromagnetic waves in this frequency range are strongly attenuated due to absorption by water [147,148]. The integration of extremely sensitive nanotechnology with advanced signal processing technologies should solve this problem. It is very important that after treatment, ME nanoparticles can be removed from the brain through the application of a magnetic field with a reverse gradient, as well as naturally. It has been shown on animal models that the nanoparticles are excreted within 2 months depending on their size [149] and also are non-toxic [150] to the brain and other major organs, such as kidneys, lungs, liver, etc. Perhaps in the near future, some other types of biodegradable ME nanoparticles will be developed, possibly made of biocompatible functionalized carbon materials.

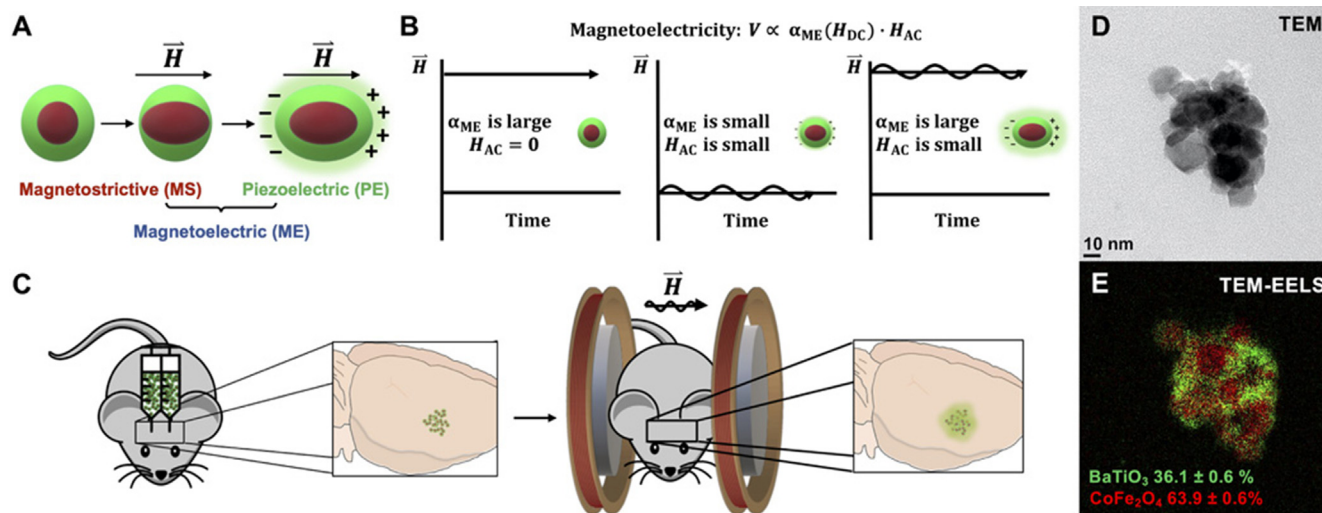


Fig. 14. Material and magnetolectric characterization of ME nanoparticles made from magnetostrictive and piezoelectric phases demonstrate wireless electric field generation. Schematic demonstrating two-phase magnetolectricity in materials made from magnetostrictive and piezoelectric materials that are strain-coupled (A). Schematic demonstrating the rationale for using a large DC magnetic field overlaid with an AC field to generate optimal magnetolectric output (B). Diagram of the method of *in vivo* ME nanoparticles administration. ME nanoparticles are injected bilaterally into the subthalamic region of mice and are wirelessly stimulated using an AC and DC magnetic field (C). Transmission electron microscope (TEM) (D) and TEM-electron energy loss spectroscopy (TEM-EELS) images (E) show ME nanoparticle morphology and BaTiO₃/CoFe₂O₄ phases (green and red, respectively), with quantitative elemental analysis measurement of the molar percentage of each material (E). ME nanoparticles were analyzed via x-ray powder diffraction (XRD) to confirm the perovskite crystal structure of BaTiO₃ (green) and the spinel crystal structure of CoFe₂O₄ (red). Reprinted with permission from Ref. [55] © 2021.

4.4. Magnetolectric effect for cancer treatment and drug delivery

Cancer is one of the deadliest diseases in the world for now. Despite significant progress in finding a cure, fundamental questions remain unresolved. Each successful therapy is not only limited to a few cancers but also has relatively low specificity for target cancer cells; while cancer cells can indeed be eradicated, many normal cells are sacrificed as collateral damage. ME nanoparticles that could be externally controlled are very promising for cancer treatment due to high-specificity targeted delivery and release of therapeutic drugs on demand.

As known [151], for the delivered drug to be bioactive, it is important to release it off the carrier nanoparticles when they reach the target site. The most important property of ME nanoparticles is the ability to release the load in any place at any time on demand. ME nanoparticles can be wirelessly controlled via the application of DC and AC magnetic fields. Using ME materials instead of single piezoelectric or magnetic nanoparticles adds more flexibility and functionality to the drug delivery and release process since both AC, DC magnetic, and ultrasonic activation can be used. Nair et al. showed [152] that, owing to the ME effect, the application of an AC magnetic field is equivalent to shaking the drug off the nanoparticles. Therefore, the conjugation strength between the drug and the nanoparticles can be made adequately strong to ensure no drug is released before the nanoparticles reach the target site. Only after the nanoparticles with the drug are pulled across the BBB and reach the target site in the brain, an AC magnetic field can be applied to trigger the desired high-efficacy release. The concept of the AC magnetic field-controlled drug release across the BBB can be schematically represented as follows: (1) Intravenous (IV) injection of drug-loaded nanoparticles, (2) the drug-loaded ME nanoparticles are pulled across the BBB via application of a DC magnetic field gradient (on the order of 3000 Oe/cm), (3) when, optionally through image guiding, ME nanoparticles can be localized at the intended site, a relatively weak AC magnetic field, with a strength of 100 Oe at a frequency of 100 Hz, is applied to release the drug.

In vitro BBB model was used to [152] that this ME nanoparticles concept could be used to deliver and release the well-known antiretroviral therapy 3'-azido-3'-deoxythymidine-5'-triphosphate (AZTTP) to

eliminate the HIV-1 virus hidden deep in the brain.

It is well known [18,19] that different cells, particularly their membranes, could be distinguished through their electric properties such as membrane potential, dielectric permittivity, conductivity, etc. For example, the membrane potentials of cancer cells can be quite different from those of their normal counterparts [153]. The membrane potential defines the energy required to break through the membrane for entering the cell. Electroporation is a well-established, highly specific process that is used to deliver biomolecules to cancer cells without affecting the surrounding normal cells of the same type [154]. Relatively strong electric fields (about 1000 V/cm) are used to electroporate cancer cells, but such strong fields can also damage the surrounding normal tissue. In the case of using ME materials for the induction of electroporation, strong fields are applied only in the local nanoscale region around the nanoparticles. That is why nanoparticle ME-induced electroporation, also known as nanoelectroporation, does not cause any field-sensitive side effects. The ME-triggered nanoelectroporation was used for the first time to deliver the well-known mitotic inhibitor paclitaxel into ovarian cancer cells while sparing the surrounding normal ovarian cells. Such experiments were conducted both *in vitro* and *in vivo*. It was reported [155,156] that drug-loaded ME nanoparticles showing relatively high specificity to cancer cells can penetrate the cancer cell membrane while sparing the surrounding healthy cells, and then release the drug intracellularly via application of d. c. and a. c. magnetic fields, respectively. *In vitro* and *in vivo* studies of ovarian cancer in mice carrying SKOV-3 human ovarian carcinoma xenografts have confirmed the hypothesis of a highly specific target delivery by drug-loaded ME nanoparticles [156].

The high specificity of nanoelectroporation was explained by the substantial difference in the membrane potential between the two cell types. The membrane potentials of ovarian cancer and normal cells are on the order of -5 and -50 mV, respectively. In other words, the field required to 'penetrate' normal cells must be ten times that of cancer cells. The physics behind nanoelectroporation was discussed in the paper by Stimphil et al. [157]. The mode of SEM known as the energy-dispersive spectroscopy (EDS) was used to directly measure the tissue specificity for this approach and to detect the presence of ME materials with nanoscale precision [156]. The EDS-SEM imaging combines the

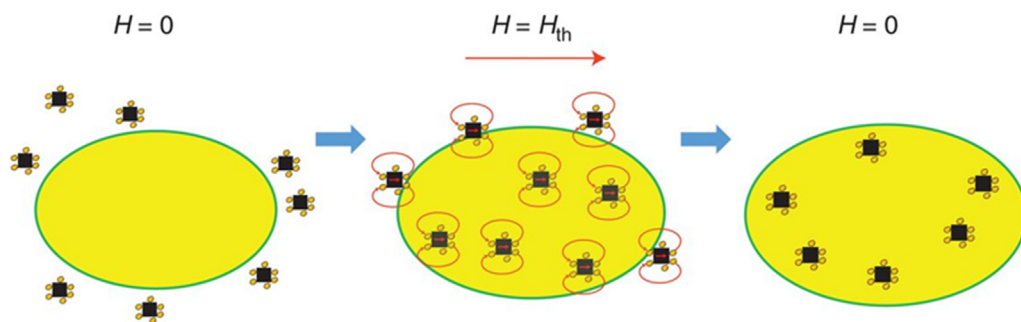


Fig. 15. Illustration of steps of the concept of the field-controlled ME-based nanoelectroporation to deliver drugs specifically into cancer cells. (1) Drug-loaded ME nanoparticles are administered into the cellular microenvironment of interest; (2) a DC magnetic field above the threshold value for the particular cancer cell line is applied to induce the process of nanoelectroporation; and (3) the magnetic field is turned off to trap the drug-loaded nanoparticles inside the cancer cells. Represented with permission from Ref. [139].

advantages of the elemental compositional analysis on par with that by mass spectroscopy and the high spatial resolution by SEM [149]. The concept of ME-triggered nanoelectroporation used to deliver drugs specifically into cancer cells via the application of a 100 Oe DC magnetic field is schematically shown in Fig. 15. It is very important to maintain the DC field between the thresholds of nanoelectroporation for cancer and normal cells, respectively, to provide the required specificity. After delivery of the loaded nanoparticles to cancer cells, a relatively weak AC magnetic field, with a strength of 30 Oe at a frequency of 100 Hz, was applied to release the drug on demand.

Recently it was reported [158] that 30-nm ME nanoparticles which consist of the core-shell composition of $\text{CoFe}_2\text{O}_4@ \text{BaTiO}_3$ demonstrate externally controlled high-efficacy binding with the hormone MIA690 and targeted specificity to glioblastoma cells and on-demand release of the peptide by application of DC and AC magnetic fields, respectively. Notably, due to the fundamental nature of the approach, ME materials can be used for intracellular delivery of any biomolecule, including nucleic acids, to enable genetic engineering or certain antitumor peptides for the treatment of glioblastomas, as described in Stewart et al. [158].

4.5. Wireless power transfer approaches and ME antennas

Medical implants have become commonplace in biomedicine, owing to their multiple benefits; however, they demand certain levels of power (e.g., $\sim 1\text{--}10$ and $\sim 10\text{--}100$ μW for pacemakers and neurostimulators, respectively). A fundamental challenge in developing miniature neural implants is delivering sufficient power to the devices inside the body. Accordingly, charging implants through wired power supplies presents severe drawbacks, as lead wires increase the risks of infections, restrict device deployment, and affect subject mobility [159]. The most common method to provide energy to an implanted electronic device is through a battery, as it is portable, reliable, and convenient. Nevertheless, batteries are often bulky and make up for a large portion of the volume of the implanted electronic device [160]. Additionally, they need to be replaced periodically, which is a significant economic and health burden, and the materials that compose them are toxic, making leakage a serious health concern [160,161].

External recharging based on radio frequencies is attenuated through

the tissue, thus limiting the level of power transmission. Furthermore, tissue damage in humans can occur upon exposure to a boosted transmitted power. Compared to wired or battery-powered implants, wirelessly powered battery-free neural stimulators have the potential to provide less invasive and longer-lasting interfaces for human nerves [63].

The list of the most prominent power transfer methods employed by implantable electronic devices found in the literature can be derived as follows: optical, electromagnetic, and ultrasound [160]. Electromagnetic methods, in their turn, are divided into near-field, mid-field, and far-field, inductive, and capacitive couplings, as well as ME ones, which is a relatively new ME wireless power transfer technology. Inductive coupling techniques seem to be the most advanced for powering implants; they utilize a pair of coils that must be physically close and well-aligned to allow for power transfer. Subsequently, the power transfer is dependent on the degree of the orientation, size, and distance between the coils [162]. Ultimately, these dependencies make this form of wireless power transfer most viable for implantable medical devices (e.g., pacemakers [163]) where the depth of the implant is relatively shallow, and the alignment of the coils can be well controlled. Table 2 presents a list of pros and cons of the different wireless power transfer methods, and Fig. 16 proposes a graphical representation of the comparison between them.

Mid-field and far-field electromagnetic wireless power transfer systems have also been widely used for power pacemakers [164,165], however, they can induce significant heating caused by radio frequency wave absorption in the human body, which absorption can both reduce system efficiency and pose a health risk to users [59]. The recoverable electromagnetic energy by radio frequency transmission or inductive coupling for micro-systems is usually low to enable a useful power supply at a communication distance greater than 50 mm [58,166]. In its turn, ultrasound is proposed as an efficient approach to power and communicate with millimeter-scale implants deep inside tissues [167]. Application of ultrasound leads to a volume reduction of the size of transducers/implants due to a shorter wavelength [168–170], which maintains the ability to operate at moderate depths in tissue and perform functions with moderate power requirements [171]. However, the acoustic transmitter must be in direct contact with the skin, and the

Table 2

Summary of pros and cons of each wireless power transfer method according to the literature review [160]. IC – inductive coupling, CC – capacitive coupling, MF – mid-field, FF – far-field, US – ultrasound, OW – optical, ME – magnetoelectric.

	IC	CC	MF	FF	US	OW	ME
advantages	Efficiency Small RX Well established	Delivered power Efficiency	Efficiency Small RX	High depth TX practicality	High depth Small RX High efficiency	High efficiency	Low absorption Small RX
limitations	Low depth Misalignment	Low depth High RX area TX practicality	Misalignment TX practicality	Efficiency High absorption	Misalignment Losses in interfaces Losses in bone	Low depth Absorption in tissue TX practicality Misalignment	Misalignment Early development Efficiency

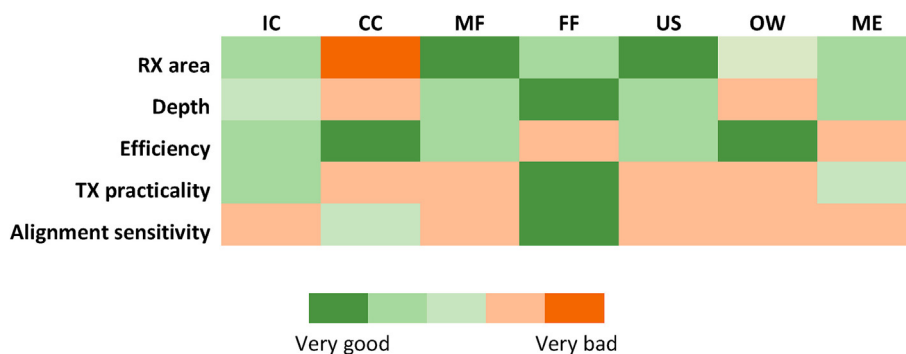


Fig. 16. Comparison of key parameters between wireless power transfer methods. © 2020 Elsevier B.V. Reprinted with permission from Ref. [160].

acoustic power transmission through the bone seems to be minimal due to a large acoustic impedance mismatch between soft tissues and bone, which results in the reflection of most of the acoustic energy.

Unlike acoustic and inductively coupled systems, alignment is not as critical for radio frequency wireless power transfer systems because receivers do not need to be tightly coupled to the transmitter. However, as the size of receivers decreases, the operating frequency must increase to a level where tissue tends to absorb and attenuate the transmitted signal, which is not only inefficient, but it is potentially hazardous because of associated tissue heating. A technology that could make efficient use of low-frequency electromagnetic power transfer at a distance could be a significant achievement for very small implantable systems [162]. The criteria, advantages, and limitations of the developed and most frequently used at the moment wireless power transfer technologies are reviewed in detail elsewhere [160].

When delivering power to neural implants using a radio frequency field, the carrier frequencies must be in the GHz range to match the resonant wavelengths of small antennas [172], causing high electromagnetic absorption in the body and violating safety limits, which will be discussed in detail in further. Near-field inductively powered devices primarily work at 13.56 MHz or higher, improving the quality factor of the miniaturized receiver (R_x) coil and its efficiency [173], also resulting in energy absorption by the body, and thus, requiring operation under certain restrictions. Inductive coupling technology is sensitive to alignment changes and inter-coil distance, resulting in excessive heat generation in tissues, damaging the metabolisms and immune system. In this regard, both technologies raise efficiency and safety concerns. In addition, *in vivo* movements, which are regarded as internal energy sources, yield low frequency and acceleration that are difficult to harvest [174].

Transducers based on acoustic energy via application of piezoelectric materials or electromagnetic energy via application of inductive coupling between coils or radio frequency transmission between antennas are among the most studied solutions of the energy transmission techniques for micro-systems in the biomedical field [171,175]. The development of a ME antenna indicated that for a given frequency, its wavelength could be five orders of magnitude shorter than the electromagnetic wavelength, thus enabling dramatic device miniaturization [176]. Furthermore, the typical operating frequency of ME systems is relatively low, in the range of tens of kHz, which enables a higher permissible applied magnetic field than that of resonant inductive coupling wireless power transfer systems [177].

Low-frequency magnetic fields possess several key merits, including (i) strong penetration and low tissue absorption in a specific range of parameters owing to low carrier frequencies; (ii) less sensitivity to changes in alignment (in comparison with inductive coupling); (iii) high output power and efficiency even with increasing miniaturization, due to the much smaller acoustic wavelength inside organic tissue (than that of electromagnetic waves) which results in the decrease of the receivers' size [59,63,160,162]. These characteristics make the ME generator a promising alternative to other wireless power transfer technologies,

especially for implantable medical devices [59]. Body-area wireless power transfer via high-frequency electric, magnetic, or electromagnetic fields represents safety issues, such as heating, owing to the power deposition in the human tissues. Therefore, the field strength and frequency must be adjusted to provide safe operation in all cases. The International Commission on Non-Ionizing Radiation Protection (ICNIRP) and the Institute of Electrical and Electronics Engineers (IEEE) standards are also applied. According to the ICNIRP regulation [178,179], the maximum SAR is set to be 2 W/kg per 10 g of tissue to stay within safety limit conditions. An example, according to the IEEE safety standards [180–182], at 70 470 Hz, the highest allowable amplitude of the magnetic field that can be applied to humans is 0.205 mT. With the same operating frequency and maximum magnetic field strength, the system under investigation is able to transfer up to 4.16 mW to a load resistance (which is equivalent to 3.85 mW with 197.2 μ T) [183]. This amount of power is sufficient to supply most of the biosensors. As an alternative example is that the IEEE standard for exposure to magnetic fields above 3000 Hz is limited to 163 A/m [182]. ME films operate under low-frequency magnetic fields (100 kHz–1 MHz), enabling them to penetrate the human body without substantial absorption, thus alleviating the safety limitations for power delivery [184]. For assessing the safety of ME power transfer for deep-body implants, the specific absorption rate (SAR) must be determined [63]. A deeper understanding of the safety concerns can be provided by taking into account Fig. 17 [185]. Fig. 17a depicts the simulation model of a two-port communication system. Since the Tx antenna is placed close to the GM-CSF (gray matter-cerebrospinal fluid) interface, the developed COMSOL model includes all layers except the edema because it is very far from the Tx port.

Fig. 17b displays the simulated path loss between Tx and Rx antennas as a function of frequency. From Maxwell's equation in a lossy media, one should know that tissue absorption is directly proportional to the conductivity of the tissue and inversely proportional to its relative permittivity. Thus, Fig. 17b reveals that the path loss increases with a higher operational frequency. Fig. 17c shows the simulated path loss along with brain layers at different frequencies. It is shown that most of the loss occurs in the scalp and CSF layers due to their high conductivity to permittivity ratio. In addition, the path loss is reduced with decreasing frequency. In addition, even in the GHz regime, the electromagnetic loss is very small in the skull. This is a significant advantage of electromagnetic waves compared to ultrasound ones, in which the loss rate in the skull is 22 dB/cm-MHz [186]. It implies that an acoustic-based implantable device [167] such as operating at the frequency of 10 MHz would have 110 dB loss in the skull alone. The results described above clearly show that wireless implantable devices operating in the low-frequency regime could be far more efficient than devices operating in the high-frequency range because the former ones will face much less tissue loss compared to the latter ones. Furthermore, a low tissue loss is especially important for passive implantable devices since there is little power available inside the body, and it is even more critical when implanting a device into the brain because the implanted component

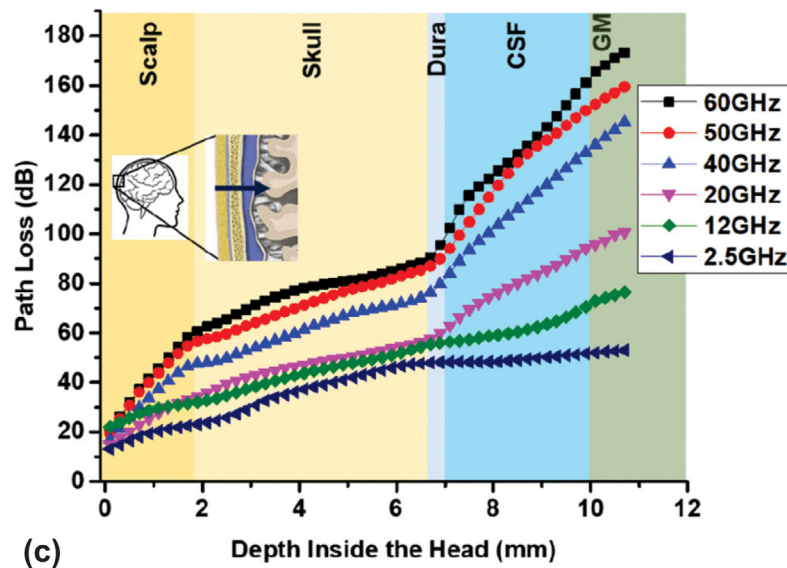
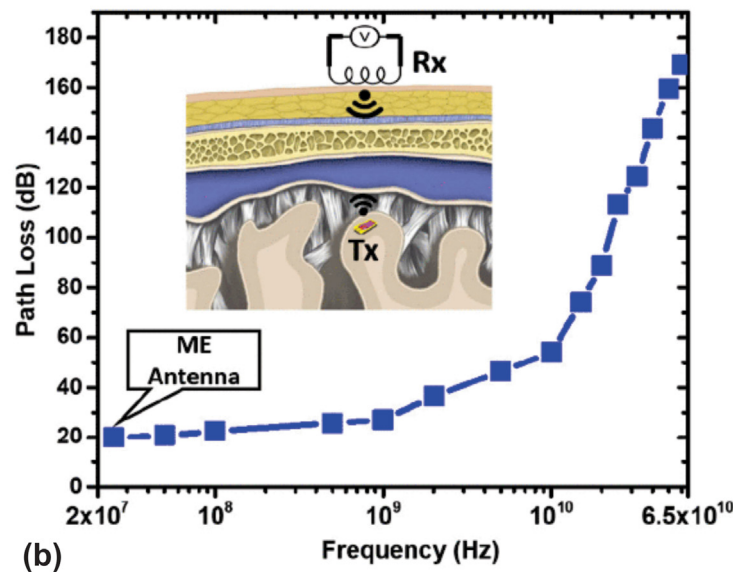
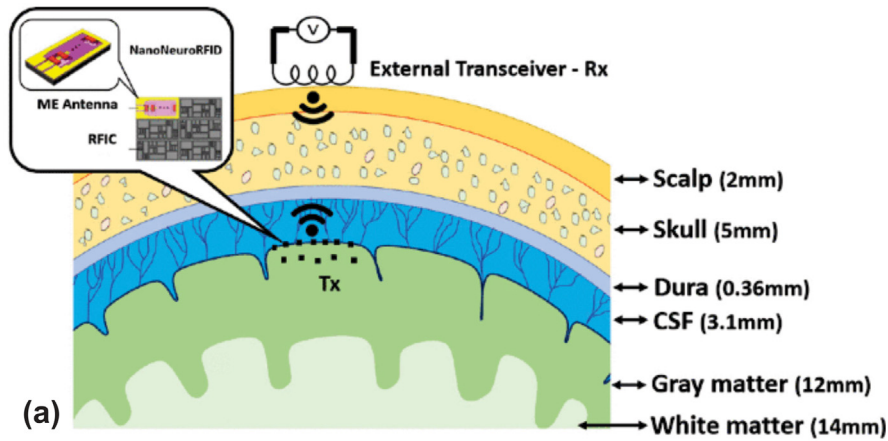


Fig. 17. (a) Finite element analysis simulation model of brain layers. The external receiver antenna is on the scalp, and the implanted device is close to the cerebrospinal fluid (CSF)-gray matter (GM) interface. (b) Path loss between receiver (Rx) and transmitter (Tx) antennas, where Rx is on the scalp outside the head and Tx is implanted on the CSF-GM interface. Path loss increases significantly with enhancing the operational frequency. An inset reveals the brain structure and the position of Tx and Rx antennas. (c) Path loss along with brain layers at different frequencies, where the layers are shown in the background. Most of the loss occurs in the scalp and CSF layers due to their low permittivity and high conductivity. Unlike acoustic waves, the loss of electromagnetic waves in the skull is very small, which is an upper hand for electromagnetic implantable devices. (Inset) Brain layers along the path. © [2019] IEEE. Adapted with permission from Ref. [185].

must be extremely small and batteries are not acceptable. Therefore, implanted systems based on ME antennas could be a breakthrough in the field of body implantable devices because these antennas are smaller than 200 μm in size and can work in 10 s or 100 s of MHz frequency range, while conventional inductive coils or antennas operating in a similar frequency range are more than a few centimeters in size [185]. An ultra-compact dual-band smart nanoelectromechanical systems ME

antenna with a size of 250 × 174 μm² that can efficiently perform wireless energy harvesting and sensing ultra-small magnetic fields, such as those arising from neural activities, is reported [187]. The ME antenna reveals a wireless power transfer efficiency 1–2 orders of magnitude higher than any other reported so far miniaturized micro-coil, allowing the wireless implantable medical devices to be compliant with the SAR limit and thus operating under safe radio frequency exposure. In

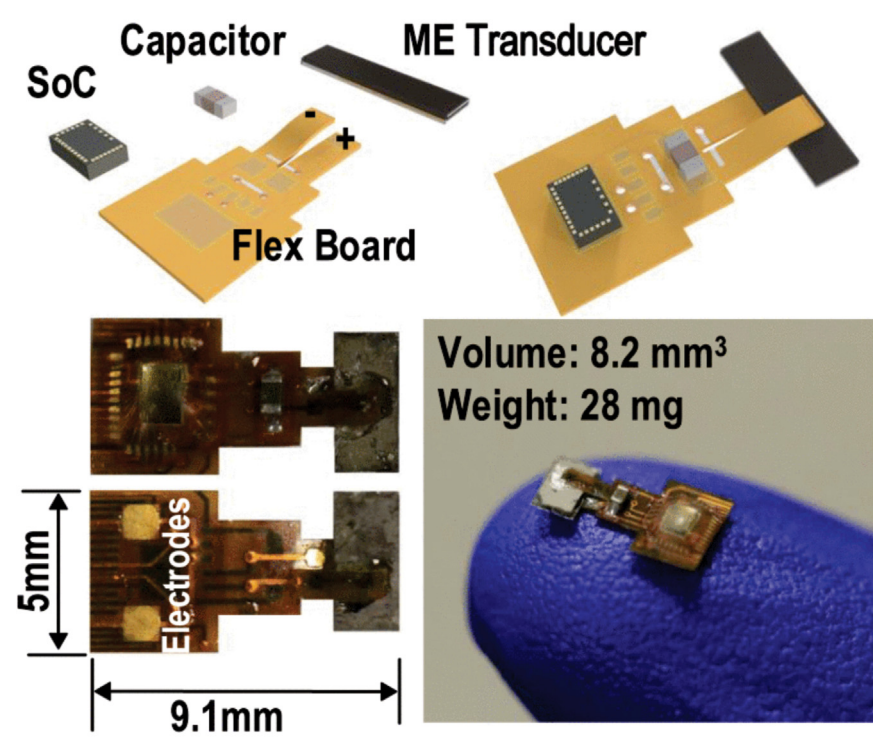
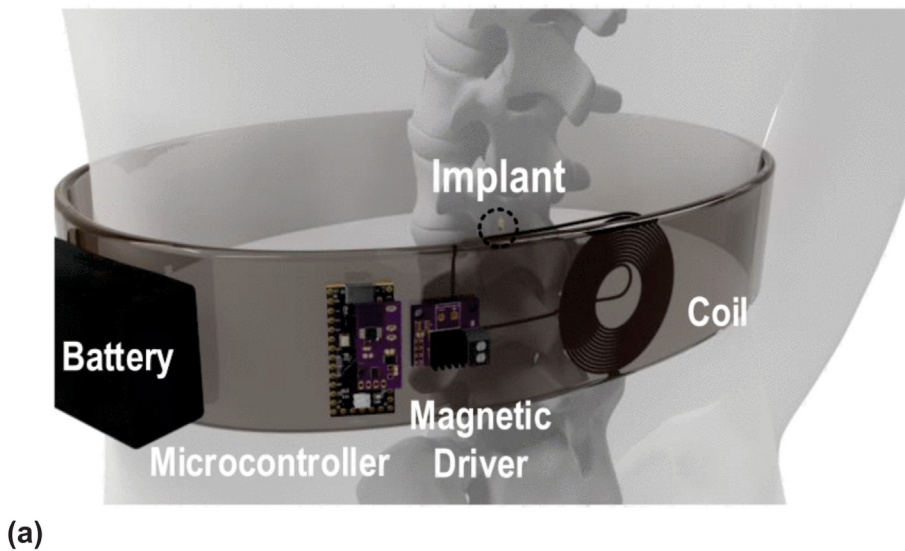


Fig. 18. (a) Conceptual diagram showing a wearable spinal cord neurostimulation system for pain relief, the implant is remotely powered via a magnetic field; (b) Illustrations of the proposed neurostimulation implant. ME element contains a nickel-coated lead zirconate titanate (PZT), and a Metglas, a magnetostrictive layer. © [2020] IEEE. Adapted, with permission from Ref. [63].

addition, the magnetic sensing capability of the proposed smart ME antenna, with a limit of detection of 300–500 pT at > 200 Hz, should allow the implantable medical devices to record neural magnetic fields from the brain without requiring differential recording.

The ICNIRP and the IEEE standards were applied to the lumped elements models, which were then used to optimize device dimensions within a volume of 2 mm³. An optimized ME device can produce 21.3 μW/mm³ and 31.3 μW/mm³ under the ICNIRP and IEEE standards, respectively, which are very attractive for a broad range of biomedical implants and wearable devices.

Encapsulated ME composites for the wirelessly powered brain implantable devices were reported [188]. Simulation results indicate that a polymer encapsulant, rather than creating a substrate clamping effect, increases the voltage output of the ME composite, which can be further improved via a careful polymer selection. These attributes are modeled using the finite element method with COMSOL Multiphysics software. A piezoelectric voltage of 3.77 V AC output at a magnetic field strength of 0.2 kOe was obtained. To the best of our knowledge, the highest ME power densities reported in the literature is 175 mW/cm³ [58,189]. This new technology can increase the power density and overpass the issues of directionality present in the inductive transmission technique, and open new prospects for wireless powering medical implants [99].

When electromagnetic energy at 2 GHz and ultrasound energy at 2 MHz are compared, the former reveals lower attenuation through tissue (1–2 dB/cm vs. 10–12 dB/cm [190]), a higher US Food and Drug Administration (FDA) limit for power flux (7.2 mW/mm² vs. 0.1 mW/mm² [191]) and a smaller wavelength (0.75 mm vs. 25 mm) for more efficient coupling to small implants [169]. A key challenge in developing wireless millimeter-scale stimulators is wireless power and communication that provide well-controlled, therapeutically relevant effects. A wireless, leadless, and battery-free implantable neural stimulator (that is 1.7 mm³ in size) incorporating a piezoceramic transducer, an energy-storage capacitor, and an integrated circuit was reported [169].

Stemming from the low tissue absorption, low misalignment sensitivity, and high power transfer efficiency, the ME effect enables the safe delivery of high power levels (a few mWs) at relatively low resonant frequencies (~ 0.25 MHz) to millimeter-sized implants deep inside the body (3 cm in depth) (Fig. 18a) [56,63]. Although various wireless radio frequency-based neural implants exploiting electromagnetic, inductive coupling, ultrasonic, and optical power transfer have been reported, achieving safe and reliable wireless power transfer within the size and power constraints of neural and other types of implants is still challenging [63]. The proposed device (Fig. 18b) features: (1) a miniature physical dimension of 8.2 mm³ and 28 mg, (2) adaptive system control and data transfer mechanisms robust under source amplitude variations, (3) a 90% chip efficiency due to its low static power down to 23.7 μW, and (4) the capability to perform fully programmable bi-phasic current

Table 3

A Comparison of the NanoNeuroRFID system design approach with some recently published wireless implantable devices. Re-designed based on [185].

Recording/ stimulation	Size, mm × mm	Approach	Reference
Micro electrodes (contact with tissue)	5 × 7.5	Electromagnetic	[193]
Micro electrodes (contact with tissue)	5 × 5	Electromagnetic	[194]
Micro electrodes (contact with tissue)	3 × 6.5	Ultrasound	[168]
Micro electrodes (contact, E-field recording)	3 × 1	Ultrasound (and electromagnetic for intermediate transceiver)	[170]
NanoNeuroRFID	1 × 1	Electromagnetic	[185]

stimulation covering 0.05–1.5 mA amplitude, 64–512 μs pulse width, and 0–0.2 kHz frequency ranges, making it appropriate for spinal cord stimulation for chronic pain treatment.

In general, the efficiency of the transferred power is dependent on the position of the transmitter relative to the receiver and the distance between them. In this context, a lot of research was done to provide direction-independent power transfer without significant losses due to possible misorientations between a receiver and a transmitter. The performance of the delivered to a resistive load power under uncertainties in ME receiver position and orientation was studied [183]. In further, a non-uniform applied magnetic field effect has also been considered. In the case of the studied experimental system, a maximum transferred power of 4.91 mW was reached at a distance of 3 cm between the centers of the ME transducer and the coil, in which the subsequent magnetic flux density was 225.8 μT. When the distance was increased to 6 cm, the generated power decreased to 1.97 mW. It was also revealed that the output power is proportional to the squared cosine of the misorientation angle, compared to the power reached at the zero-angle (nominal) position. It was found that the delivered power is less sensitive to misalignment since the width of the receiver is relatively small in comparison with the diameter of the transmit coil. In principle, the power generated at a specific load is a quadratic function of the effective magnetic field that is projected onto the operating direction of the ME laminated composite (i.e., the longitudinal axis in this case) [183].

Despite the fact that α_{ME} has been widely used as a standard criterion to determine the performance of a ME transducer, however, there is strong evidence that a higher α_{ME} does not always ensure higher optimum power delivered to the load. In general, many factors influence achievable power levels, including parameters and configurations of magnetostrictive and piezoelectric phases. It was shown that the

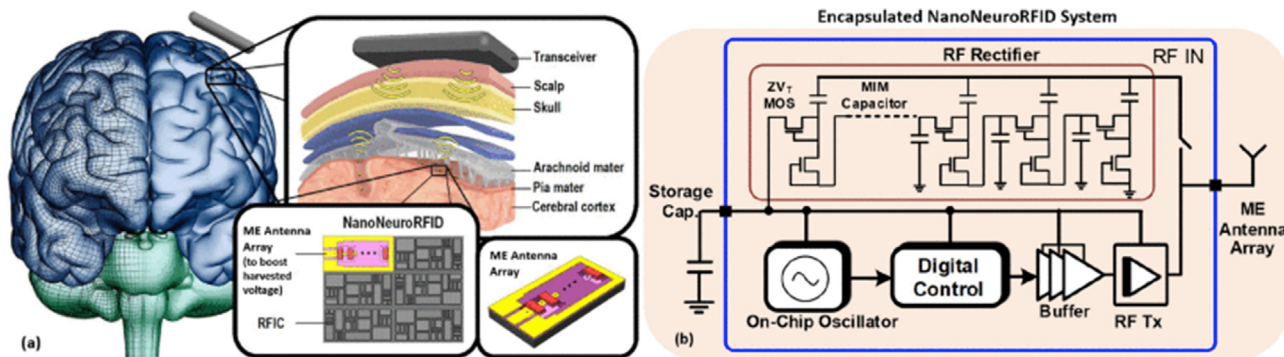


Fig. 19. (a) Overview of the wireless implantable NanoNeuroRFID environment. (b) Architecture of the implantable NanoNeuroRFID with energy harvesting, clock source, and radio frequency transmission capability. © [2019] IEEE. Adapted with permission from Ref. [185].

transduction factor between the mechanical and magnetic domains is also important for power optimization along with the mechanical-electrical transduction because it defines and limits the maximum power available for transfer to a resistive load [59].

Two configurations of composite multiferroic structures were investigated as the transmitter and receiver to introduce the concept of bidirectional strain-mediated multiferroic wireless energy transfer. Specifically, a stacked laminate tri-layer PZT/Terfenol-D/PZT was placed at the center of a concentric PZT/Terfenol-D hollow cylinder [192]. The first strain-mediated composite multiferroic wireless energy transfer configuration was tested by using ring composite as a transmitter and e laminated plates as a receiver. In the second configuration, the laminate plates were used as a transmitter, while the composite ring was a receiver. The composite cylinders, in conjunction with laminated plates, were successfully demonstrated as a novel technology of bi-directional ME-based wireless energy transfer. A peak extracted power of ~ 0.1 mW was reported, which is sufficient to wirelessly power a multitude of small electronic devices [192].

A novel wireless implantable device termed NanoNeuroRFID was also developed [185] (Fig. 19) with a novel multifunctional implantable design based on ME antennas. The device offers the following important advantages: (1) it operates in the low-frequency range of the electromagnetic spectrum in which tissue loss is low, and at the same time its antenna size is in the μ -scale range; (2) its loss in the skull is small, unlike ultrasound approach which has a significant loss in bone structures; (3) it does not utilize contact electrodes for recording action potential and is entirely encapsulated with a biocompatible material such as parylene, making it superior for long-time recording; (4) it is sub-mm in size and is suitable for large-scale (1000–10 000 devices) neural magnetic field transmissions with high temporal and spatial resolutions. The comparison of NanoNeuroRFID system with the results on different wireless implantable devices is presented in Table 3.

In spite of the described above advantages of ME composites and transducers for wireless power transfer, we believe the potential benefits of the ME effect have still not been studied in detail, which hinders the possibility for further implanted devices miniaturization; thus, additional research in the field is required. We believe that magnetic field penetrating through biological tissue without any harmful effect under the range of the specific parameters enables further improvement of ME transducers and allows the increase of the transferred power, which is less sensitive to the angular alignment between a receiver and a transmitter.

4.6. Prospective use of ME composites in optogenetics

The human brain is one of the most sophisticated and complex organs, which exist in nature [180]. Billions of neurons are burned per unit of time to implement a broad range of objectives and tasks. A better understanding of the brain activities and operation mechanisms will enable for a human being a lot of functionalities in medicine such as providing communication and interaction between the brain and computer, advanced prosthesis systems, etc. The fundamental part of this system understanding is the possibility to record the signals from the brain with very high temporal and spatial resolutions [187].

At present, a lot of studies have been done in the field of brain-related research over the past several decades, and a variety of tethered and untethered devices have been proposed to modulate the activity of neurons. It has been a great challenge to obtain a high density distributed network of tethered (electrical, optical, etc.) devices due to interconnection and wiring constraints related to them. Besides, tethered devices suffer from safety problems connected with biocompatibility and the presence of conductive wires [172,187,195]. On the contrary, a wireless approach enables overcoming these challenges. Sufficient progress has been recently achieved in the area of wireless neural interface devices. So far, electromagnetic and ultrasound are two major approaches available for implantable wireless communication and energy scavenging [185,

187].

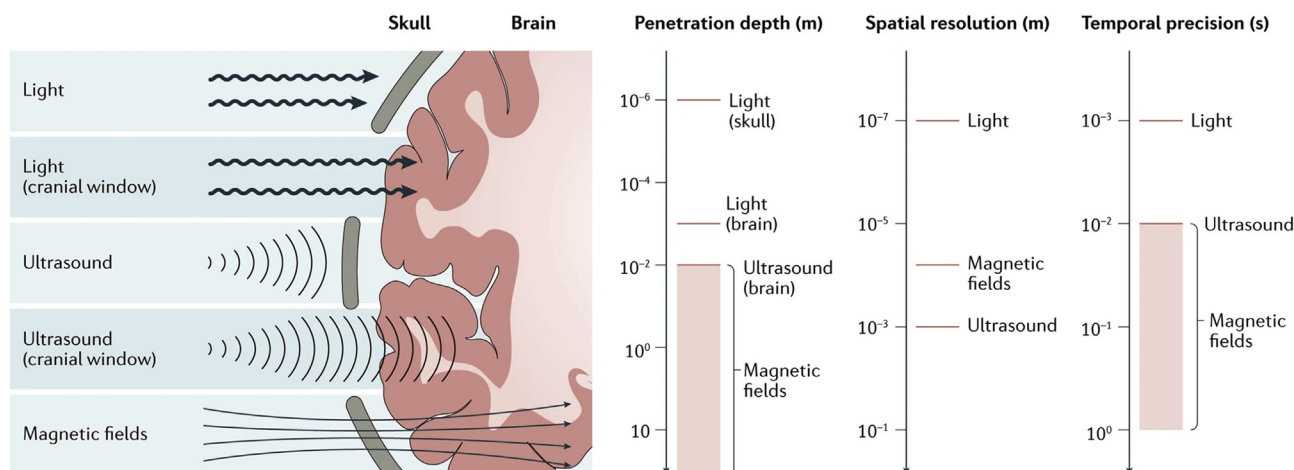
There are several non-invasive sensing methods that are clinically used which help to understand brain behavior, for example, magnetic resonance imaging (MRI), functional MRI, and computer tomography [196]. However, controlled millisecond stimulation deep inside the brain at a cellular level to match the natural speed of neural spike patterns in the brain is very hard to achieve. Hence, to decipher the mechanisms in the neurobiological systems and dissect various neural diseases, scientists have tried exploring the cells using a variety of biologically engineered techniques such as magnetic, electrical, genetic, chemical, optical, infrared, and ultrasound stimulations [196]. Although many original non-invasive approaches have been explored, the three most popular invasive techniques to access deep brain tissues at the cellular level are electrical, optogenetic, and chemical stimulation, which are initiated through electric fields, photostimulation, and pharmacological deliveries, respectively [196].

Optogenetics is a cutting-edge tool in neuroscience, which utilizes light-sensitive proteins and controlled illumination for neuromodulation [197]. Optogenetics genetically inserts photosensitive ion channels into a neuron's membrane and modulates the activity of neurons via blue light [198,199], which reveals impressive spatial and temporal resolutions and cell-type specificity. However, the tissue-penetrating capability is limited to a blue light, which usually makes the method invasive and requires the implantation of a light. The main advantage of optogenetics is the ability to demonstrate causal relationships by manipulating the activity of specific neurons and observing behavioral phenotypes. An optically powered and controlled wireless optogenetic system using near-infrared light for a high transmittance through live tissues was shown [197]. *In vivo* optogenetic stimulations using this system-induced whisker movement in channelrhodopsin-expressing freely moving mice, which confirmed that the photovoltaics-generated electrical power was sufficient, and the remote controlling system was successful. To provide a sophisticated optogenetic manipulation of neural circuits throughout the nervous system with limited disruption of the behavior of an animal, light-delivery systems beyond fiber optic tethering and bulky head-mounted wireless receivers are necessary.

The near-field inductive coupling has been used to power optogenetic stimulators in freely moving mice, which is highly effective when the coils are at or near the surface of the skin [56,200]. However, a relatively large cross-sectional area (70 mm^2) of the receiving coil and sensitivity to coil curvature could limit its application in implants that are deep inside the body.

An easy-to-fabricate, implantable wireless optogenetic device was reported in Ref. [172]. Its version (0.02 g , 10 mm^3) is two orders of magnitude lower than the alternative wireless optogenetic systems, which allows the implantation of the entire device subcutaneously. When a radio frequency power source and a controller are used, this implant generates sufficient light power for optogenetic stimulation with tissue heating below 1°C . It is shown that untethered optogenetic control throughout the nervous system (spinal cord, brain, and peripheral nerve endings) of behaving mice is thus possible, which allows for optogenetic experiments in animals behaving naturally with optogenetic manipulation of both peripheral and central targets [172]. The micro-LED, with emitted light power/input power $\sim 19\%$, was efficient over the range of light power densities suitable for optogenetic stimulation within the power density range $1\text{--}20 \text{ mW/mm}^2$.

Remote regulation of optogenetic proteins by a magnetoluminescence microdevice has been recently reported [201]. However, most of the frequently used microdevices utilize optical, acoustic, and magnetic stimuli offer application-specific advantages for neural stimulation and recording, as depicted in Fig. 20 [202]. Although optical stimulation and imaging approaches, such as infrared light [203], genetically encoded opsins [204], and calcium and voltage indicators [205] offer a superior spatial and temporal resolution, they are limited to penetration depths of $<1 \text{ mm}$ owing to tissue absorbance and scattering. Even three-photon excitation with a 1675 nm laser can only access brain structures not



Nature Reviews | Materials

Fig. 20. A schematic representation of tissue penetration by ultrasonic, optical, and magnetic stimuli. Electromagnetic waves in the visible and near-infrared optical spectrum allow superior spatial and temporal resolution but limited penetration depth ($\sim 1\text{--}1.5$ mm) [203,205]. Ultrasound allows accessing deeper brain regions (>5 cm) with a spatial resolution that is inversely proportional to the wavelength, which, in turn, scales inversely with the penetration depth (in general for ultrasound, spatial resolution is > 1 mm³, and temporal precision is > 10 ms) [207]. Alternating magnetic fields with low frequencies (<1000 Hz) and high amplitudes (0.1–2 T) inductively couple to the upper 0.1–1 cm of tissue [208]. Alternating magnetic fields with amplitudes of $\sim 1\text{--}100$ mT and frequencies in the low radio frequency range 100–1000 kHz penetrate through tissue unaffected [177]. The temporal precision of neural activity is dependent on the used magnetic scheme [202].

deeper than 1.5 mm [202,206].

The genetically encoded cells rapidly and selectively respond to light, enabling them to remedy various neurological diseases such as epileptic seizure, somniphobia, and Parkinsonism [209–211]. For optogenetic applications, flexible microscale light-emitting diode (f- μ LED) with high power efficiency, low heating, and thermal/humid/chemical stability can be an excellent light stimulation tool for freely moving animals by achieving conformal attachment on the brain cortex surface with minimal invasion [212,213]. The optogenetic stimulation was demonstrated as a form of the implantable electronic system that contains an

independent power source of conventional batteries [214,215]. However, the restricted lifetime (~ 60 months) of a battery may result in repeated replacements of the discharged battery every several years, which is a medically critical issue, especially for *in vivo* conditions [211, 216,217].

An organic electrolytic photocapacitor (OEPC) to perform chronic peripheral nerve stimulation via transduction of tissue-penetrating deep-red light into electrical signals has been developed to wirelessly modulate neural tissue [218]. The principle of the OEPC operation is based on efficient charge generation by nanoscale organic semiconductors

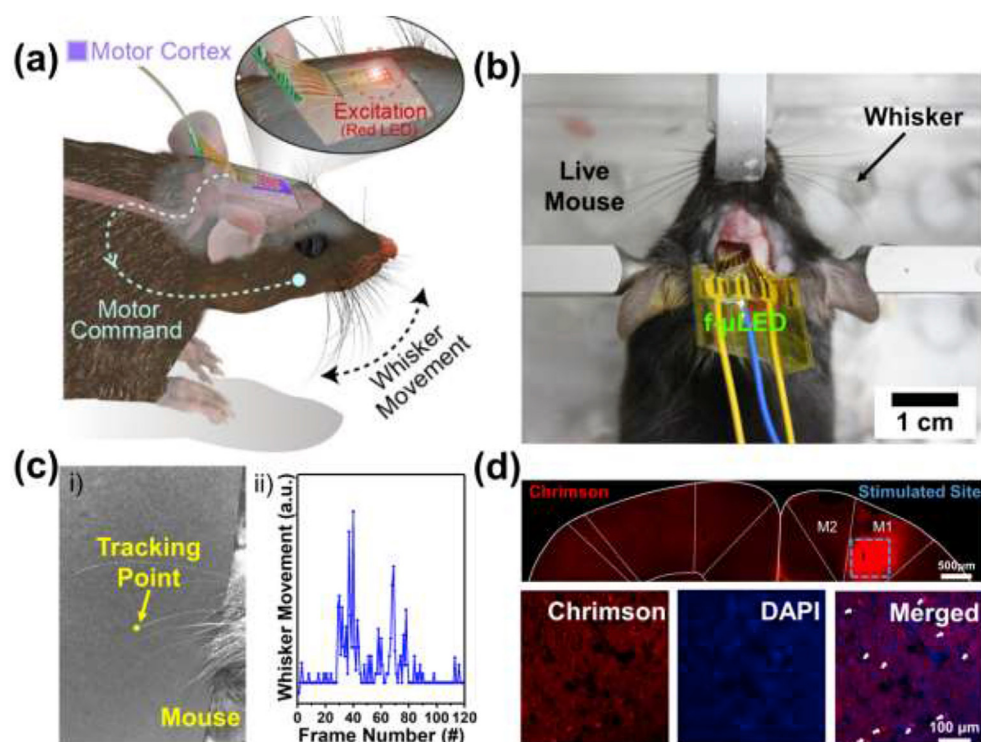


Fig. 21. (a) Schematic view of experimental procedures for energy-harvesting optogenetic brain stimulation. (b) Implantation of f- μ LED array underneath the mouse skull for stimulation of M1 (As a red light-activated channelrhodopsin variant, Chromson was expressed in the primary motor cortex). (c) i) Video snapshot tracking the whisker movements. The tracking point is shown as a yellow circle. ii) Relative whisker movements via f- μ LED stimulation with the operation of MMTENG. (d) Confocal fluorescent images of the mouse brain. The top is the expression of Chromson and the stimulation site in the motor cortex, whereas the bottom is a magnified image for the stimulated M1 site. Red color signals indicate the expression of tdTomato (a maker of Chromson), and the blue signals represent the DAPI (a maker of neural cells). © 2020 Elsevier Ltd. Reprinted with permission from Ref. [212].

containing nontoxic commercial pigments. The stimulation parameters typically involve irradiation with pulses of 50–1000 μs with the length 638 or 660 nm, which allows the actuation of the implant of ~ 1 cm below the skin. A rat sciatic nerve model was implemented to benchmark performance parameters of OEPCs first *ex vivo* and *in vivo*. The sustained ability to non-invasively mediate neurostimulation over 100 days was revealed. Thus, OEPC device with an ultralow volume of 0.1 mm^3 provides a high-efficiency biocompatible approach to wireless neuromodulation.

Magnetic fields are able to penetrate the body tissues without any harmful effects which makes their use a perspective in the wireless delivery of different stimuli to deep targets [219]. Magnetic stimuli should be imperceptible for many organisms, which is advantageous for small animal behavioral experiments, where the subject's ability to sense the application of a particular stimulus may compromise the obtained results. In optogenetics, where visible light leaking from the waveguides or scattered by the tissue may be seen peripherally by the subjects. One of the goals of magnetic neuromodulation strategies is to offer various deep-brain stimulation means with a system that does not rely on a physical connection to stimulation sites, which enables reduction of the deep-brain stimulation therapy invasiveness and tissue damage associated with the implanted hardware [219].

A wireless magnetic resonance device for optogenetic applications in an animal model was reported Ref. [220]. In the case of this remote-controlled wireless device, the electromagnetic field range (i.e., +5 cm and -5 cm of the outside coil) is larger than the range for the magnetic induction and radio frequency power sources, which allows controlling animals' behavior by the electromagnetic field effective range via photostimulation. The developed wireless remote-controlled device with a magnetic resonance technique can be used in many behavioral tasks in rats and mice. This novel technique serves as a helpful tool to modulate the neuronal activity of target neurons in specific brain areas for optogenetic experiments without adverse effects of high radio frequency.

A sophisticated optogenetic stimulating system by scavenging the wasted magnetic field of the home appliance was reported in Ref. 212. A flash-enhanced magneto-mechano-triboelectric nanogenerator (MMTENG) allowed optogenetic neuromodulation by operating a flexible micro-light-emitting diode (f- μLED). An optogenetic stimulator composed of MMTENG and f- μLED was implanted under a living mouse skull without mechanical damage [211]. The flash-stamped MMTENG effectively generated an open-circuit peak-to-peak voltage of 0.87 kV and a short-circuit current of 0.145 mA under a gentle alternating current magnetic field of 7 Oe. Maximum peak power of 8.1 mW was observed from the flash-induced harvester, which was 2.6 times higher than the non-treated device. The MMTENG generated a rectified output voltage of 134 V by a 60 Hz stray magnetic field of the home appliance, enabling it to operate the f- μLED continuously. The authors verified that the whisker movements of a living mouse were caused by the precise Chrimson activation in the light-emitted motor cortex. A schematic representation of experimental procedures to scavenge energy for optogenetic brain stimulation is presented in Fig. 21.

Fig. 21a reveals an experimental illustration of the energy-harvesting optogenetic modulation using a living mouse, f- μLED array operated by the MMTENG, and a simplified neural pathway corresponding to the whisker movement. Fig. 21b presents an image of an anesthetized mouse located on a stereotaxic fixture with the *in-vivo* f- μLED to stimulate the M1. For triggering the whisker movement of the mouse, the f- μLED was powered by the MMTENG with induction of a tiny AC magnetic field of 2.1 Oe at 60 Hz, resulting in the energy-harvesting optogenetic system could produce red LED light with ~ 10 ms duration by the rectified MMTENG output signal. During the optogenetic stimulation, the vibration of the whisker was tracked utilizing video capture and image analysis (Fig. 21c–I, additional video is provided in the original paper). Fig. 21c–ii presents the whisker movement triggered *via* the optogenetic procedure for 2 s (120 frames), and the tip position of the whisker was changed with an alternation during the recoding frames of a 1/60 s interval, which is compared to the control test.

Thus, the results revealed that the MMTENG device under a gentle magnetic field is an efficient energy-harvesting device for the optogenetic f- μLED to define the functions of mammalian cortical areas. After the optogenetic neuromodulation on the mouse brain, a postmortem histological analysis was done to verify the expression of Chrimson in the M1 region. With the settlement of Chrimson into the M1 neurons, the movement of the mouse whisker utilizing the *in vivo* f- μLED could be practical evidence of successful optogenetic manipulation [221,222]. The top of Fig. 20d reveals a confocal fluorescent image of the cortex to investigate the Chrimson injection site, and an intensive fluorescent red color signal (normally generated by tdTomato; a maker of Chrimson) is seen at the stimulation site of M1. Since the autofluorescence backgrounds (fixative-generated fluorescence and fluorescence of inherent tissue elements) of tdTomato overlapped on both the neural cells and brain tissue, the nuclei of the M1 neurons were dyed using 40 6-diamidino-2-phenylindole (DAPI) to confirm whether the Chrimson was expressed from neuronal cells [223,224]. If the DAPI (blue signal) and Chrimson (red signal) appeared at the same points, it means that these locations are Chrimson-modified neurons. The bottom images of Fig. 21d show magnified views of the stimulated M1 region. Even though the DAPI and Chrimson signals are widely distributed in the observed area, several red/blue superimposed signals (marked by white arrows) were discovered on the 'merged' image, where successful optogenetic stimulation with the f- μLED array is demonstrated. In addition, identical brain morphology confirmed the minimal damage to the frontal motor cortex after f- μLED implantation through DAPI staining. These results indicate that the energy-scavenging brain photostimulator is a powerful tool for investigating the neuro-muscular interactions and the ethological modulations of mammals. The continuous optogenetic manipulation by using the wasted magnetic field, including home, hospital, factory, and infrastructure, could be used as a novel therapeutic protocol to derive behavior change or even treat life-threatening neurodiseases [211]. Thus, to the best of our knowledge, there has been no ME transducer for wireless power transfer to a micro-LED for optogenetic stimulation of various brain activities; however, the ME effect was successfully utilized in combination with other energy scavenging approaches reported above and elsewhere [211].

5. Future challenges and conclusions

The development of effective methods to enhance bone healing, regeneration, and formation of strong bonding with artificial implants has always been among the most important research areas [114,225,226]. Although interesting bone repair strategies have already been developed, elaboration of novel smart materials as artificial implants is still challenging because successful implantable materials for bone tissue engineering must meet a specific set of requirements such as bioactivity, biocompatibility, mechanical strength and endurance, microstructure and porosity, as well as other important functional properties such as a quick reaction with its environment once being implanted.

There exist various ME composites for tissue engineering applications, which have been developed and studied so far. As an example, hybrid scaffolds of PHBV and cobalt ferrite nanoparticles after the degradation of the polymer due to the exposition of the CoFe_2O_4 revealed suitability for magneto- and electroactive tissue engineering applications [96]. However, cytotoxic effects may occur when the magnetic cobalt ferrite nanoparticles needed for magnetoactive applications are released. Thus, the substitution of cobalt ferrite by biocompatible ferrites, such as Fe_3O_4 or toxic element-free ferrites, e.g. MnFe_2O_4 , should be investigated. In this case, non-toxic fillers being released will provide no potential cytotoxic effect on cells or tissues. In addition, Fe_3O_4 nanoparticles are the only metal oxide nanoparticles approved by FDA for clinical use [52]. Thus, a widespread application of ME nanoparticles should face the challenge of FDA approval. Moreover, mechanical properties of the ME composites can deteriorate, such as compressive strength and Young's modulus, which are determined by the rigid enhancement effect of ME nanoparticles [52]. As a result, an optimization of the ME filler content in the composite should always be

accomplished.

Electroactive magnetically responsive materials which provide controlled reactions with the host and degrade within the physiological environment are still in development [43]. In addition, there are remaining challenges in the development of biocompatible composite ME scaffolds for tissue regeneration. Because composite ME materials exhibit both ME and magnetomechanical responses, it is a key to develop experiments that appropriately control and isolate these effects. Also, it is very important to develop methods to characterize ME materials and scaffolds to determine the most appropriate surface potential that the cells experience to better understand the physiological response [48]. Despite a lot of research on the efficiency of ME composites to control over cell differentiation, the underlying mechanisms of cellular osteogenic differentiation caused by magnetization variation for different ME composites are still not clear and have to be studied in sufficient detail [64].

The properties of electroactive materials vary as a function of frequency, and many biological processes also occur at specific frequencies. Thus, it is important to identify and validate testing conditions that most appropriately mimic physiological environment [48].

ME composites provide a microenvironment for the precise control of bone regeneration *in situ*, which holds much promise for achieving efficient bone repair in the clinic [126]. ME composites can also serve for antibacterial protection [227]. PVDF nanocomposites doped with nickel nanowires (1.5 wt.%) resulted in more than 55% of bacterial growth inhibition obtained by employing controlled dynamic magnetic conditions for representative gram-positive and gram-negative bacteria, compared to 25% inhibition obtained without magnetic stimuli application, with the antibiofilm activity being also improved upon dynamic conditions. However, the ME materials optimization and generated surface electric potential (i.e., its magnitude and polarity) may still increase the outcome of the antibacterial response.

In the near future, we are expecting a variety of applications of ME materials serving the wireless power transfer purpose for different miniaturized bioelectronic implantable devices. It has already been demonstrated that ME materials allow powering LEDs for optogenetic stimulators, small integrated circuits for physiological monitoring, or transmit data out for closed-loop bioelectronic devices [56, 160]. However, ME composites have not yet been implemented for implantable optogenetic devices, where, for example, micro-LED could have been placed directly on the surface of the ME transducer. In the case of wearable technologies, it is also necessary to further miniaturize magnetic field generators so that they can be battery-powered to allow their comfortable use. Besides the benefits of ME materials described in this review, some disadvantages should be noted, such as the limitation of magnetic activation in some devices. Compared to ultrasound and radio frequency wireless power relying on propagating waves, ME devices are powered by near-field magnetic fields. Thus, the depth allowing an effective powering of ME devices depends strongly on the size of the transmitter. On the contrary, the magnetic fields in a specific range reveal negligible absorption by the tissues allowing to increase the power in the transmitter still well below the safety limits. These considerations provide design tradeoffs to develop a system for miniature bioelectronic implants, where the constraints on the size of the transmitter, necessity to transmit through the air, and total power needed for the device functioning may be the major factors to choose one wireless power solution over another. ME materials have the potential to serve as a key needed for wireless power delivery to miniature neural stimulators and other bioelectronic devices for which the major challenge is transferring energy over distances of several centimeters without heating the tissue or suffering loss at interfaces between tissue, fat, bone, and air [56,63].

Authors' contributions

All authors have contributed equally to writing the manuscript. A.K.

contributed to conceptualization, supervision, and funding acquisition.

Declaration of competing interest

The authors declare that they have no known competing financial interests or personal relationships that could have appeared to influence the work reported in this paper.

Acknowledgments

This work was developed within the scope of the project CICECO-Aveiro Institute of Materials, refs. UIDB/50011/2020 and UIDP/50011/2020, financed by national funds through the FCT/MCTES. Part of this work was funded by national funds (OE), through FCT – Fundação para a Ciência e a Tecnologia, I.P., in the scope of the framework contract foreseen in the numbers 4, 5, and 6 of the article 23, of the Decree-Law 57/2016, of August 29, changed by Law 57/2017, of July 19. The financial support from the Ministry of Science and Higher Education of the Russian Federation is acknowledged (grant agreements #075-15-2021-588 from 1.06.2021).

References

- [1] H. Palneedi, V. Annareddy, S. Priya, J. Ryu, Status and perspectives of multiferroic magnetolectric composite materials and applications, *Actuators* 5 (2016) 9, <https://doi.org/10.3390/act5010009>.
- [2] T. Prabhakaran, J. Hemalatha, Poly(vinylidene fluoride)-based magnetolectric polymer nanocomposite films, in: S. Lanceros-Mendez, P. Martins (Eds.), *Magnetolectric Polymer-Based Composites: Fundamentals and Applications*, Wiley, 2017, <https://doi.org/10.1002/9783527801336.ch3c>.
- [3] J. Mundy, C. Brooks, M. Holtz, D.G. Schlom, Atomically engineered ferroic layers yield a room-temperature magnetolectric multiferroic, *Nature* 537 (2016) 523–527, <https://doi.org/10.1038/nature19343>.
- [4] S.W. Cheong, M. Mostovoy, Multiferroics: a magnetic twist for ferroelectricity, *Nat. Mater.* 6 (2007) 13–20, <https://doi.org/10.1038/nmat1804>.
- [5] Y. Wang, J. Li, D. Viehland, Magnetolectrics for magnetic sensor applications: status, challenges and perspectives, *Mater. Today* 17 (2014) 269–275, <https://doi.org/10.1016/j.mattod.2014.05.004>.
- [6] Y. Cheng, B. Peng, Z. Hu, Z. Zhou, M. Liu, Recent development and status of magnetolectric materials and devices, *Phys. Lett.* 382 (2018) 3018–3025, <https://doi.org/10.1016/j.physleta.2018.07.014>.
- [7] X. Liang, H. Chen, N.X. Sun, Magnetolectric materials and devices, *Apl. Mater.* 9 (2021) 41114, <https://doi.org/10.1063/5.0044532>.
- [8] N.A. Spaldin, R. Ramesh, Advances in magnetolectric multiferroics, *Nat. Mater.* 18 (2019) 203–212, <https://doi.org/10.1038/s41563-018-0275-2>.
- [9] J. Gao, Z. Jiang, S. Zhang, Z. Mao, Y. Shen, Z. Chu, Review of magnetolectric sensors, *Actuators* 10 (2021) 109, <https://doi.org/10.3390/act10060109>.
- [10] M.I. Bichurin, *Magnetolectric Composites*, Jenny Stanford Publishing, 2019, p. 296.
- [11] H. Chen, X. Liang, C. Dong, Y. He, N. Sun, M. Zaimbashi, Y. He, Y. Gao, P.V. Parimi, H. Lin, N.-X. Sun, Ultra-compact mechanical antennas, *Appl. Phys. Lett.* 117 (2020) 170501, <https://doi.org/10.1063/5.0025362>.
- [12] M.A. Kemp, M. Franzl, A. Haase, E. Jongewaard, M.T. Whittaker, M. Kirkpatrick, R. Sparr, A high Q piezoelectric resonator as a portable VLF transmitter, *Nat. Commun.* 10 (2019) 1715, <https://doi.org/10.1038/s41467-019-09680-2>.
- [13] N. Pereira, A.C. Lima, V. Correia, N. Perinka, S. Lanceros-Mendez, P. Martins, Magnetic proximity sensor based on magnetolectric composites and printed coils, *Materials* 13 (2020) 1729, <https://doi.org/10.3390/ma13071729>.
- [14] J.V. Vidal, A.V. Turutin, I.V. Kubasov, A.M. Kislyuk, D.A. Kiselev, M.D. Malinkovich, Y.N. Parkhomenko, S.P. Kobeleva, N.A. Sobolev, A.L. Kholkin, Dual vibration and magnetic energy harvesting with bidomain LiNbO₃-based composite, *IEEE Trans. Ultrason. Ferroelectr. Freq. Control* 67 (2020) 1219–1229, <https://doi.org/10.1109/TUFFC.2020.2967842>.
- [15] Z. Tiana, L. Xu, Y. Gao, S. Yuan, Z. Xia, Magnetic memory effect at room temperature in exchange coupled NiFe₂O₄/NiO nanogranular system, *Appl. Phys. Lett.* 111 (2017) 182406, <https://doi.org/10.1063/1.4997518>.
- [16] J. Scott, Room-temperature multiferroic magnetolectrics, *NPG Asia Mater.* 5 (2013) e72, https://doi.org/10.1007/978-3-319-02812-5_23.
- [17] D. Hitchens, Natural systems engineering, in: M. Aiguier, F. Boulanger, D. Krob, C. Marchal (Eds.), *Complex Systems Design & Management*, Springer, Cham, 2014, pp. 315–334, https://doi.org/10.1007/978-3-319-02812-5_23.
- [18] D. Shamoon, S. Lasquellec, C. Brosseau, Perspective: towards understanding the multiscale description of cells and tissues by electromechanobiology featured, *J. Appl. Phys.* 123 (2018) 240902, <https://doi.org/10.1063/1.5018723>.
- [19] P. Marracino, D. Havelka, J. Prusa, M. Liberti, J. Tuszynski, A.T. Ayoub, F. Apollonio, M. Cifra, Tubulin response to intense nanosecond-scale electric field in molecular dynamics simulation, *Sci. Rep.* 9 (2019) 10477, <https://doi.org/10.1038/s41598-019-46636-4>.

- [20] R. Jahns, R. Knochel, H. Greve, E. Woltermann, E. Lage, E. Quandt, Magnetolectric sensors for biomagnetic measurements, in: 2011 IEEE International Symposium on Medical Measurements and Applications, 2011, pp. 107–110, <https://doi.org/10.1109/MeMeA.2011.5966676>.
- [21] D. Viehland, M. Wittig, J. McCord, E. Quandt, Magnetolectric magnetic field sensors, *MRS Bull.* 43 (2018) 834–840, <https://doi.org/10.1557/mrs.2018.261>.
- [22] M.O. Özden, A. Teplyuk, O. Gümiş, D. Meyners, M. Höft, M. Gerken, Magnetolectric cantilever sensors under inhomogeneous magnetic field excitation, *AIP Adv.* 10 (2020) 25132, <https://doi.org/10.1063/1.5136239>.
- [23] D. Murzin, D.J. Mapps, K. Levada, V. Belyaev, A. Omelyanchik, L. Panina, V. Rodionova, Ultrasensitive magnetic field sensors for biomedical applications, *Sensors* 20 (2020) 1569, <https://doi.org/10.3390/s20061569>.
- [24] S.A. Tikhonova, P.V. Evdokimov, Y.Y. Filippov, T.V. Safronova, A.V. Garshev, I.M. Shcherbakov, V.E. Dubrov, V.I. Putlyayev, Electro- and magnetoactive materials in medicine: a review of existing and potential areas of application, *Inorg. Mater.* 56 (2020) 1319–1337, <https://doi.org/10.1134/S0020168520130038>.
- [25] P. Curie, Sur la symétrie dans les phénomènes physiques, symétrie d'un champ électrique et d'un champ magnétique, *J. Phys.* 3 (Ser. III) (1894) 393–415.
- [26] H. Schmid, Some symmetry aspects of ferroics and single phase multiferroics, *J. Phys. Condens. Matter* 20 (2008) 434201, <https://doi.org/10.1088/0953-8984/20/43/43420>.
- [27] D.N. Astrov, The magnetolectric effect in antiferromagnetics, *Sov. Phys. JETP* 11 (1960) 708–709.
- [28] V.J. Folen, G.T. Rado, E.W. Stalder, Anisotropy of the magnetolectric effect in Cr₂O₃, *Phys. Rev. Lett.* 6 (1961) 607–608, <https://doi.org/10.1103/PhysRevLett.6.607>.
- [29] W. Eerenstein, N.D. Mathur, J.F. Scott, Multiferroic and magnetolectric materials, *Nature* 442 (2006) 759, <https://doi.org/10.1038/nature05023>.
- [30] Y.F. Popov, A.M. Kadomtseva, G.P. Vorob'ev, A.K. Zvezdin, Discovery of the linear magnetolectric effect in magnetic ferroelectric BiFeO₃ in a strong magnetic field, *Ferroelectrics* 162 (1994) 135–140, <https://doi.org/10.1080/00150199408245098>.
- [31] J. Van Den Boomgaard, D.R. Terrell, R.A.J. Born, H.F.J.I. Giller, An in situ grown eutectic magnetolectric composite material, *J. Mater. Sci.* 9 (1974) 1705–1709, <https://doi.org/10.1007/BF00540770>.
- [32] J. Van Suchtelen, Product properties: a new application of composite materials, *Philips Res. Rep.* 127 (1972) 28–37.
- [33] R.E. Newnham, D.P. Skinner, L.E. Cross, Connectivity and piezoelectric-pyroelectric composites, *Mater. Res. Bull.* 13 (1978) 525–536, [https://doi.org/10.1016/0025-5408\(78\)90161-7](https://doi.org/10.1016/0025-5408(78)90161-7).
- [34] V. Corral-Flores, D. Bueno-Baques, D. Carrillo-Flores, J.A. Matutes-Aquino, Enhanced magnetolectric effect in core-shell particulate composites, *J. Appl. Phys.* 99 (2006) 81503, <https://doi.org/10.1063/1.2165147>.
- [35] G. Sreenivasulu, M. Popov, F.A. Chavez, S.L. Hamilton, P.R. Lehto, G. Srinivasan, Controlled self-assembly of multiferroic core-shell nanoparticles exhibiting strong magneto-electric effects, *Appl. Phys. Lett.* 104 (2014) 52901, <https://doi.org/10.1063/1.4863690>.
- [36] M.L. Bichurin, D.A. Fillipov, V.M. Petrov, V.M. Laletsin, G. Srinivasan, Resonance magnetolectric effects in layered magnetostrictive-piezoelectric composites, *Phys. Rev.* 68 (2003) 132408, <https://doi.org/10.1103/PhysRevB.68.132408>.
- [37] N. Pereira, A.C. Lima, S. Lanceros-Mendez, P. Martins, Magnetolectrics: three centuries of research heading towards the 4.0 industrial revolution, *Materials* 13 (2020) 4033, <https://doi.org/10.3390/ma13184033>.
- [38] D. Saveliev, D. Chashin, L. Fetisov, M. Shamonin, Y. Fetisov, Ceramic-heterostructure-based magnetolectric voltage transformer with an adjustable transformation ratio, *Materials* 13 (2020) 3981, <https://doi.org/10.3390/ma13183981>.
- [39] F. Narita, M. Fox, A review of piezoelectric, magnetostrictive, and magnetolectric materials and device technologies for energy harvesting applications, *Adv. Eng. Mater.* 20 (2017) 1700743, <https://doi.org/10.1002/adem.201700743>.
- [40] G. Srinivasan, Y.K. Fetisov, Microwave magnetolectric effects and signal processing devices, *Integr. Ferroelectr.* 83 (2005) 89–98, <https://doi.org/10.1080/10584580600949105>.
- [41] W. Kleemann, Multiferroic and magnetolectric nanocomposites for data processing, *J. Phys. D Appl. Phys.* 50 (2017) 223001, <https://doi.org/10.1088/1361-6463/aa6c04>.
- [42] J. Reenmann, P. Durdaut, S. Salzer, T. Demming, A. Piorra, E. Quandt, N. Frey, M. Hof, G. Schmidt, Evaluation of magnetolectric sensor systems for cardiological applications, *Measurement* 116 (2018) 230–238, <https://doi.org/10.1016/j.measurement.2017.09.047>.
- [43] C. Khatua, D. Bhattacharya, V. Krishna Balla, In situ electrical stimulation for enhanced bone growth: a minireview, *Med Devices Sens* 3 (2020) e10090, <https://doi.org/10.1002/mds3.10090>.
- [44] T. Zheng, Z. Yue, G.G. Wallace, Y. Du, P. Martins, S. Lanceros-Mendez, M. J. Higgins, Local probing of magnetolectric properties of PVDF/Fe₃O₄ electrospun nanofibers by piezoresponse force microscopy, *Nanotechnology* 28 (2017) 65707, <https://doi.org/10.1088/1361-6528/aa5217>.
- [45] K. Kapat, Quazi T.H. Shubhra, M. Zhou, S. Leeuwenburgh, Piezoelectric nano-biomaterials for biomedicine and tissue regeneration, *Adv. Funct. Mater.* 30 (2020) 1909045, <https://doi.org/10.1002/adfm.201909045>.
- [46] X. Zhang, L. Li, J. Ouyang, L. Zhang, J. Xue, H. Zhang, W. Tao, Electroactive electrospun nanofibers for tissue engineering, *Nano Today* 39 (2021) 101196, <https://doi.org/10.1016/j.nantod.2021.101196>.
- [47] C. Ribeiro, V. Correia, P. Martins, F.M. Gama, S. Lanceros-Mendez, Proving the suitability of magnetolectric stimuli for tissue engineering applications, *Colloids Surf., B* 140 (2016) 430–436, <https://doi.org/10.1016/j.colsurfb.2015.12.055>.
- [48] N.D. Ferson, A.M. Uhl, J.S. Andrew, Piezoelectric and magnetolectric scaffolds for tissue regeneration and biomedicine: a review, *IEEE Trans. Ultrason. Ferroelectrics Freq. Control* 68 (2021) 229–241, <https://doi.org/10.1109/TUFFC.2020.3020283>.
- [49] J. Zhai, S. Dong, Z. Xing, J. Li, D. Viehland, Giant magnetolectric effect in metglas/polyvinylidene-fluoride laminates, *Appl. Phys. Lett.* 89 (2006) 83507, <https://doi.org/10.1063/1.2337996>.
- [50] E. Díaz, B. Valle, S. Ribeiro, S. Lanceros-Mendez, J. Manuel Barandiarán, Development of magnetically active scaffolds for bone regeneration, *Nanomaterials* 8 (2018) 678, <https://doi.org/10.3390/nano8090678>.
- [51] S. Ribeiro, C. Ribeiro, E.O. Carvalho, C.R. Tubio, N. Castro, N. Pereira, V. Correia, A.C. Gomes, S. Lanceros-Méndez, Magnetically activated electroactive microenvironments for skeletal muscle tissue regeneration, *ACS Appl. Bio Mater.* 3 (2020) 4239–4252, <https://doi.org/10.1021/acsabm.0c00315>.
- [52] C. Shuai, W. Yang, C. He, S. Peng, C. Gao, Y. Yang, F. Qi, P. Feng, A magnetic micro-environment in scaffolds for stimulating bone regeneration, *Mater. Des.* 185 (2020) 108275, <https://doi.org/10.1016/j.matdes.2019.108275>.
- [53] A. Reizabal, R. Brito-Pereira, M.M. Fernandes, N. Castro, V. Correia, C. Ribeiro, C.M. Costa, L. Perez, J.L. Vilas, S. Lanceros-Méndez, Silk fibroin magnetoactive nanocomposite films and membranes for dynamic bone tissue engineering strategies, *Materialia* 12 (2020) 100709, <https://doi.org/10.1016/j.mtla.2020.100709>.
- [54] N. Abzan, M. Kharaziha, S. Labbaf, Development of three-dimensional piezoelectric polyvinylidene fluoride-graphene oxide scaffold by non-solvent induced phase separation method for nerve tissue engineering, *Mater. Des.* 167 (2019) 107636, <https://doi.org/10.1016/j.matdes.2019.107636>.
- [55] K.L. Kozielski, A. Jahanshahi, H.B. Gilbert, Y. Yu, Ö. Erin, D. Francisco, F. Alosaimi, Y. Temel, M. Sitti, Nonresonant powering of injectable nanoelectrodes enables wireless deep brain stimulation in freely moving mice, *Sci. Adv.* 7 (2021) eabc4189, <https://doi.org/10.1126/sciadv.abc4189>.
- [56] A. Singer, S. Dutta, E. Lewis, Z. Chen, J.C. Chen, N. Verma, B. Avants, A.K. Feldman, J. O'Malley, M. Beierlein, C. Kemere, J.T. Robinson, Magnetolectric materials for miniature, wireless neural stimulation at therapeutic frequencies, *Neuron* 107 (2020) 631–643, <https://doi.org/10.1016/j.neuron.2020.05.019>.
- [57] P. Martins, S. Lanceros-Mendez, Polymer-based magnetolectric materials, *Adv. Funct. Mater.* 23 (2013) 3371–3385, <https://doi.org/10.1002/adfm.201202780>.
- [58] K. Malleron, A. Gensbittel, H. Talleb, Z. Ren, Experimental study of magnetolectric transducers for power supply of small biomedical devices, *Microelectron. Eng.* 88 (2019) 184–189, <https://doi.org/10.1016/j.mejo.2018.01.013>.
- [59] K. Agarwal, R. Jegadeesan, Y.X. Guo, N.V. Thakor, Wireless power transfer strategies for implantable bioelectronics, *IEEE Rev. Biomed. Eng.* 10 (2017) 136–161, <https://doi.org/10.1109/RBME.2017.2683520>.
- [60] B. Hermenegildo, C. Ribeiro, L. Pérez-Álvarez, J.L. Vilas, D.A. Learmonth, R.A. Sousa, P. Martins, S. Lanceros-Méndez, Hydrogel-based magnetolectric microenvironments for tissue stimulation, *Colloids Surf., B* 181 (2019) 1041–1047, <https://doi.org/10.1016/j.colsurfb.2019.06.023>.
- [61] E.O. Carvalho, C. Ribeiro, D.M. Correia, G. Botelho, S. Lanceros-Mendez, Biodegradable hydrogels loaded with magnetically responsive microspheres as 2D and 3D scaffolds, *Nanomaterials* 10 (2020) 2421, <https://doi.org/10.3390/nano10122421>.
- [62] C. Khatua, D. Bhattacharya, B. Kundu, V. Krishna Balla, S. Bodhak, S. Goswami, Multiferroic reinforced bioactive glass composites for bone tissue engineering applications, *Adv. Eng. Mater.* 20 (2018) 1800329, <https://doi.org/10.1002/adem.201800329>.
- [63] Z. Yu, J.C. Chen, F.T. Alrashdan, B.W. Avants, Y. He, A. Singer, J.T. Robinson, K. Yang, MagnNi: a magnetolectrically powered and controlled wireless neurostimulating implant, *IEEE Trans. Biomed. Circuits. Syst.* 14 (2020) 1241–1252, <https://doi.org/10.1109/TBCAS.2020.3037862>.
- [64] B. Tang, X. Shen, Y. Yang, Z. Xu, J. Yi, Y. Yao, M. Cao, Y. Zhang, H. Xia, Enhanced cellular osteogenic differentiation on CoFe₂O₄/P(VDF-TrFE) nanocomposite coatings under static magnetic field, *Colloids Surf., B* 198 (2021) 111473, <https://doi.org/10.1016/j.colsurfb.2020.111473>.
- [65] A. Omelyanchik, V. Antipova, C. Gritsenko, V. Kolesnikova, D. Murzin, Y. Han, A.V. Turutin, I.V. Kubasov, A.M. Kisluky, T.S. Ilna, D.A. Kiselev, M. Voronova, M.D. Malinkovich, Y.N. Parkhomenko, M. Silibin, E.N. Kozlova, D. Peddis, K. Levada, L. Makarova, A. Amirov, V. Rodionova, Boosting magnetolectric effect in polymer-based nanocomposites, *Nanomaterials* 11 (5) (2021) 1154, <https://doi.org/10.3390/nano11051154>.
- [66] C. Shuai, W. Yang, S. Peng, C. Gao, W. Guo, Y. Lai, P. Feng, Physical stimulations and their osteogenesis-inducing mechanisms, *Int. J. Bioprint.* 4 (2018) 138–158, <https://doi.org/10.18063/IJB.v4i2.138>.
- [67] M. Navede-Ul-Haq, V.V. Shvartsman, G. Constantinescu, H. Trivedi, S. Salamon, J. Landers, H. Wende, D.C. Lupascu, Effect of Al₃₊ modification on cobalt ferrite and its impact on the magnetolectric effect in BCZT-CFO multiferroic composites, *J. Mater. Sci.* 52 (2017) 13402–13413, <https://doi.org/10.1007/s10853-017-1444-4>.
- [68] Y. Zong, Z. Yue, P. Martins, J. Zhuang, Y. Du, S. Lanceros-Mendez, M.J. Higgins, Magnetolectric coupling in nanoscale 0-1 connectivity, *Nanoscale* 10 (2018) 17370–17377, <https://doi.org/10.1039/C8NR05182H>.
- [69] G. Backman, B. Lawton, N.A. Morley, Magnetostrictive energy harvesting: materials and design study, *IEEE Trans. Magn.* 55 (2019) 4700206, <https://doi.org/10.1109/TMAG.2019.2891118>.
- [70] P.J. Praveen, V.R. Monaji, S.D. Kumar, V. Subramanian, D. Das, Enhanced magnetolectric response from lead-free (Ba_{0.85}Ca_{0.15})(Zr_{0.1}Ti_{0.9})O₃ –

- CoFe₂O₄ laminate and particulate composites, *Ceram. Int.* 44 (2018) 4298–4306, <https://doi.org/10.1016/j.ceramint.2017.12.018>.
- [71] J. Rani, V.K. Kushwaha, P.K. Patel, C.V. Tomy, Exploring magnetolectric coupling in trilayer [Ba(Zr_{0.2}Ti_{0.8})O_{3-0.5}(Ba_{0.7}Ca_{0.3})TiO₃]/CoFe₂O₄/[Ba(Zr_{0.2}Ti_{0.8})O_{3-0.5}(Ba_{0.7}Ca_{0.3})TiO₃] thin film, *J. Alloys Compd.* 863 (2021) 157702, <https://doi.org/10.1016/j.jallcom.2020.157702>.
- [72] J. Wang, Y. Zhang, M.P.K. Sahoo, T. Shimada, T. Kitamura, P. Ghosez, T.-Y. Zhang, Giant magnetolectric effect at the graphone/ferroelectric interface, *Sci. Rep.* 8 (2018) 12448, <https://doi.org/10.1038/s41598-018-30010-x>.
- [73] I.R. Reddy, P.M. Oppeneer, K. Tarafder, Route to achieving giant magnetolectric coupling in BaTiO₃/Sr₂CoO₃F perovskite heterostructures, *Phys. Rev. B* 98 (2018) 140401, <https://doi.org/10.1103/PhysRevB.98.140401>.
- [74] P.D. McGary, B.J.H. Stadler, Electrochemical deposition of Fe_{1-x}Ga_x nanowire arrays, *J. Appl. Phys.* 97 (2005) 10R503, <https://doi.org/10.1063/1.1851435>.
- [75] Y. He, C. Jiang, W. Wu, B. Wang, H. Duan, H. Wang, T. Zhang, J. Wang, J. Liu, Z. Zhang, P. Stamenov, J.M.D. Coey, H. Xu, Giant heterogeneous magnetostriction in FeGa alloys: effect of trace element doping, *Acta Mater.* 109 (2016) 177–186, <https://doi.org/10.1016/j.actamat.2016.02.056>.
- [76] Y. He, X. Ke, C. Jiang, N. Miao, H. Wang, J.M.D. Coey, Y. Wang, H. Xu, Interaction of trace rare-Earth dopants and nanoheterogeneities induces giant magnetostriction in Fe-Ga alloys, *Adv. Funct. Mater.* 28 (2018) 1800858–1800859, <https://doi.org/10.1002/adfm.201800858>.
- [77] A.E. Clark, J.B. Restorff, M. Wun-Fogle, T.A. Lograsso, D.L. Schlagel, Magnetostrictive properties of body-centered cubic Fe-Ga and Fe-Ga-Al alloys, *IEEE Trans. Magn.* 36 (2000) 3238–3240, <https://doi.org/10.1109/20.908752>.
- [78] M.P. Ruffoni, S. Pascarelli, R. Grössinger, R. Sato Turtelli, C. Bormio-Nunes, R.F. Pettifer, Direct measurement of intrinsic atomic scale magnetostriction, *Phys. Rev. Lett.* 101 (2008) 147202–147204, <https://doi.org/10.1103/PhysRevLett.101.147202>.
- [79] A.B. Flatau, B.J.H. Stadler, J. Park, K. Sai Madhukar Reddy, P.R. Downey, C. Mudivarthi, M. Van Order, Magnetostrictive Fe-Ga Nanowires for actuation and sensing applications, in: M. Vázquez (Ed.), *Magnetic Nano- and Microwires. Design, Synthesis, Properties and Applications*, second ed., Elsevier, 2020, pp. 737–776.
- [80] A. Pateras, R. Harder, S. Manna, B. Kiefer, R.L. Sandberg, S. Trugman, J.W. Kim, J. de la Venta, E.E. Fullerton, O.G. Shpyrko, E. Fohtung, Room temperature giant magnetostriction in single-crystal nickel nanowires, *NPG Asia Mater.* 11 (2019) 59, <https://doi.org/10.1038/s41427-019-0160-8>.
- [81] C. Ribeiro, V. Sencadas, D.M. Correia, S. Lanceros-Méndez, Piezoelectric polymers as biomaterials for tissue engineering applications, *Colloids Surf., B* 136 (2015) 46–55, <https://doi.org/10.1016/j.colsurfb.2015.08.043>.
- [82] M. Minary-Jolandan, M.-F. Yu, Uncovering nanoscale electromechanical heterogeneity in the subfibrillar structure of collagen fibrils responsible for the piezoelectricity of bone, *ACS Nano* 3 (2009) 1859–1863, <https://doi.org/10.1021/nn900472n>.
- [83] E. Fukada, I. Yasuda, On the piezoelectric effect of bone, *J. Phys. Soc. Jpn.* 12 (1957) 1158–1162, <https://doi.org/10.1143/JPSJ.12.1158>.
- [84] E. Fukada, I. Yasuda, Piezoelectric effects in collagen, *Jpn. J. Appl. Phys.* 3 (1964) 117–121, <https://doi.org/10.1143/JJAP.3.117>.
- [85] A.N. Koppes, A.M. Seggio, D.M. Thompson, Neurite outgrowth is significantly increased by the simultaneous presentation of schwann cells and moderate exogenous electric fields, *J. Neural. Eng.* 8 (2011) 46023, <https://doi.org/10.1088/1741-2560/8/4/046023>.
- [86] R. Green, M.R. Abidian, Conducting polymers for neural prosthetic and neural interface applications, *Adv. Mater.* 27 (2015) 7620–7637, <https://doi.org/10.1002/adma.201501810>.
- [87] M.M. Fernandes, D.M. Correia, C. Ribeiro, N. Castro, V. Correia, S. Lanceros-Méndez, Bioinspired three-dimensional magnetoactive scaffolds for bone tissue engineering, *ACS Appl. Mater. Interfaces* 11 (2019) 45265–45275, <https://doi.org/10.1021/acsami.9b14001>.
- [88] R.A. Surmenev, T. Orlova, R.V. Chernozem, A.A. Ivanova, A. Bartasyte, S. Mathur, M.A. Surmeneva, Hybrid lead-free polymer-based nanocomposites with improved piezoelectric response for biomedical energy-harvesting applications: a review, *Nano Energy* 62 (2019) 475–506, <https://doi.org/10.1016/j.nanoen.2019.04.090>.
- [89] B. Mavčić, V. Antolić, Optimal mechanical environment of the healing bone fracture/osteotomy, *Int. Orthop.* 36 (2012) 689–695, <https://doi.org/10.1007/s00264-012-1487-8>.
- [90] D. Sarkar, M.-C. Chu, S.-J. Cho, Ceramic - polymer nanocomposite: alternate choice of bone, *J. Korean Ceram. Soc.* 45 (2008) 309–319, <https://doi.org/10.4191/kcers.2008.45.6.309>.
- [91] M. Zhao, Electrical fields in wound healing—An overriding signal that directs cell migration, *Semin. Cell Dev. Biol.* 20 (2009) 674–682, <https://doi.org/10.1016/j.semcdb.2008.12.009>.
- [92] D.G. Woo, M.S. Shim, J.S. Park, H.N. Yang, D.R. Lee, K.H. Park, The effect of electrical stimulation on the differentiation of hESCs adhered onto fibronectin-coated gold nanoparticles, *Biomaterials* 30 (2009) 5631–5638, <https://doi.org/10.1016/j.biomaterials.2009.07.026>.
- [93] Z. Schwartz, B.J. Simon, M.A. Duran, G. Barabino, R. Chaudhri, B.D. Boyan, Pulsed electromagnetic fields enhance BMP-2 dependent osteoblastic differentiation of human mesenchymal stem cells, *J. Orthop. Res.* 26 (2008) 1250–1255, <https://doi.org/10.1002/jor.20591>.
- [94] S. Meng, M. Rouabhia, Z. Zhang, Electrical stimulation modulates osteoblast proliferation and bone protein production through heparin-bioactivated conductive scaffolds, *Bioelectromagnetics* 34 (2013) 189–199, <https://doi.org/10.1002/bem.21766>.
- [95] S.A.M. Tofail, J. Bauer, Electrically polarized biomaterials, *Adv. Mater.* 28 (2016) 5470–5484, <https://doi.org/10.1002/adma.201505403>.
- [96] L. Amaro, D.M. Correia, P.M. Martins, G. Botelho, S.A.C. Carabineiro, C. Ribeiro, S. Lanceros-Méndez, Morphology dependence degradation of electro- and magnetoactive poly(3-hydroxybutyrate-co-hydroxyvalerate) for tissue engineering applications, *Polymers* 12 (2020) 953, <https://doi.org/10.3390/polym12040953>.
- [97] C. Ribeiro, D.M. Correia, S. Ribeiro, M.M. Fernandes, S. Lanceros-Méndez, Piezo- and magnetolectric polymers as biomaterials for novel tissue engineering strategies, *MRS Adv.* 3 (2018) 1671–1676, <https://doi.org/10.1557/adv.2018.223>.
- [98] E. Esmaeili, M. Soleimani, M. Adel Ghiassi, S. Hatamie, S. Vakilian, M. Soufi Zomorrod, N. Sadeghzadeh, M. Vossoughi, S. Hosseinzadeh, Magnetolectric nanocomposite scaffold for high yield differentiation of mesenchymal stem cells to neural-like cells, *J. Cell. Physiol.* 234 (2019) 13617–13628, <https://doi.org/10.1002/jcp.28040>.
- [99] G. Rizzo, V. Loyau, R. Nocua, J. Christophe Lourme, E. Lefeuvre, Potentiality of magnetolectric composites for Wireless Power Transmission in medical implants, in: 13th International Symposium on Medical Information and Communication Technology (ISMICT), 2019, p. 18813511, <https://doi.org/10.1109/ISMICT.2019.8743873>.
- [100] Y. Liu, X. Zhang, C. Cao, Y. Zhang, J. Wei, Y. J. Li, W. Liang, Z. Hu, J. Zhang, Y. Wei, X. Deng, Built-in electric fields dramatically induce enhancement of osseointegration, *Adv. Funct. Mater.* 27 (2017) 1703771, <https://doi.org/10.1002/adfm.201703771>.
- [101] C. Ribeiro, J. Pärssinen, V. Sencadas, V. Correia, S. Miettinen, V. P. Hytönen, S. Lanceros-Méndez, Dynamic piezoelectric stimulation enhances osteogenic differentiation of human adipose stem cells, *J. Biomed. Mater. Res.* 103 (2015) 2172–2175, <https://doi.org/10.1002/jbm.a.35368>.
- [102] B. Liu, L. Chen, C. Shao, F. Zhang, K. Zhou, J. Cao, D. Zhang, Improved osteoblasts growth on osteomimetic hydroxyapatite/BaTiO₃ composites with aligned lamellar porous structure, *Mater. Sci. Eng. C* 61 (2016) 8–14, <https://doi.org/10.1016/j.msec.2015.12.009>.
- [103] R.A. Surmenev, R.V. Chernozem, I.O. Pariy, M.A. Surmeneva, A review on piezo- and pyroelectric responses of flexible nano- and micropatterned polymer surfaces for biomedical sensing and energy harvesting applications, *Nano Energy* 79 (2021) 105442, <https://doi.org/10.1016/j.nanoen.2020.105442>.
- [104] S.M. Damaraju, Y. Shen, E. Elele, B. Khusid, A. Eshghinejad, J. Li, M. Jaffe, T. Livingston Arinze, Three-dimensional piezoelectric fibrous scaffolds selectively promote mesenchymal stem cell differentiation, *Biomaterials* 149 (2017) 51–62, <https://doi.org/10.1016/j.biomaterials.2017.09.024>.
- [105] G.G. Genchi, E. Sinibaldi, L. Ceseracciu, M. Labardi, A. Marino, S. Marras, G. De Simoni, V. Mattoli, G. Ciofani, Ultrasound-activated piezoelectric P(VDF-TrFE)/boron nitride nanotube composite films promote differentiation of human SaOs-2 osteoblast-like cells, *Nanomed. Nanotechnol. Biol. Med.* 14 (2018) 2421–2432, <https://doi.org/10.1016/j.nano.2017.05.006>.
- [106] H.M. Huang, S.Y. Lee, W.C. Yao, C.T. Lin, C.Y. Yeh, Static magnetic fields upregulate osteoblast maturity by affecting local differentiation factors, *Clin. Orthop. Relat. Res.* 447 (2006) 201–208, <https://doi.org/10.1097/01.blo.0000203464.35561.be>.
- [107] Z. Yue, Y. Qi, M. Yang, X. Zhan, L. Fang, H. Jing, Z. Gu, Y. Wu, Protein corona of magnetic hydroxyapatite scaffold improves cell proliferation via activation of mitogen-activated protein kinase signaling pathway, *ACS Nano* 11 (2017) 3690–3704, <https://doi.org/10.1021/acsnano.6b08193>.
- [108] M. Arjmand, A. Ardeshirylajimi, H. Maghsoudi, E. Azadian, Osteogenic differentiation potential of mesenchymal stem cells cultured on nanofibrous scaffold improved in the presence of pulsed electromagnetic field, *J. Cell. Physiol.* 233 (2017) 1061–1070, <https://doi.org/10.1002/jcp.25962>.
- [109] J. Wang, Y. An, F. Li, D. Li, D. Jing, T. Guo, E. Luo, C. Ma, The effects of pulsed electromagnetic field on the functions of osteoblasts on implant surfaces with different topographies, *Acta Biomater.* 10 (2014) 975–985, <https://doi.org/10.1016/j.actbio.2013.10.008>.
- [110] N. Castro, M.M. Fernandes, C. Ribeiro, V. Correia, R. Minguez, S. Lanceros-Méndez, Magnetic bioreactor for magneto-, mechano- and electroactive tissue engineering strategies, *Sensors* 20 (2020) 3340, <https://doi.org/10.3390/s20123340>.
- [111] D.M. Correia, V. Sencadas, C. Ribeiro, P.M. Martins, P. Martins, F.M. Gama, G. Botelho, S. Lanceros-Méndez, Processing and size range separation of pristine and magnetic poly(L-lactic acid) based microspheres for biomedical applications, *J. Colloid Interface Sci.* 476 (2016) 79–86, <https://doi.org/10.1016/j.jcis.2016.05.012>.
- [112] P.M. Martins, S. Ribeiro, C. Ribeiro, V. Sencadas, A.C. Gomes, F.M. Gama, S. Lanceros-Méndez, Effect of poling state and morphology of piezoelectric poly(vinylidene fluoride) membranes for skeletal muscle tissue engineering, *RSC Adv.* 3 (2013) 17938–17944, <https://doi.org/10.1039/C3RA43499K>.
- [113] F. Mushtaq, H. Torlakcik, Q. Vallmajo-Martin, E. Can Siringil, J. Zhang, C. Röhrig, Y. Shen, Y. Yu, X.-Z. Chen, R. Müller, B.J. Nelson, S. Pané, Magnetolectric 3D scaffolds for enhanced bone cell proliferation, *Appl. Mater. Today* 16 (2019) 290–300, <https://doi.org/10.1016/j.apmt.2019.06.004>.
- [114] R.A. Surmenev, M.A. Surmeneva, A.A. Ivanova, Significance of calcium phosphate coatings for the enhancement of new bone osteogenesis – a review, *Acta Biomater.* 10 (2014) 557–579, <https://doi.org/10.1016/j.actbio.2013.10.036>.
- [115] B. Tang, J. Zhuang, L. Wang, B. Zhang, S. Lin, F. Jia, L. Dong, Q. Wang, K. Cheng, W. Weng, Harnessing cell dynamic responses on magnetolectric nanocomposite films to promote osteogenic differentiation, *ACS Appl. Mater. Interfaces* 10 (2018) 7841–7851, <https://doi.org/10.1021/acsami.7b19385>.

- [116] Y. Zhang, L. Chen, J. Zeng, K. Zhou, D. Zhang, Aligned porous barium titanate/hydroxyapatite composites with high piezoelectric coefficients for bone tissue engineering, *Mater. Sci. Eng. C* 39 (2014) 143–149, <https://doi.org/10.1016/j.msec.2014.02.022>.
- [117] H. Shokrollahi, F. Salimi, A. Doostmohammadi, The fabrication and characterization of barium titanate/akermanite nano-bio-ceramic with a suitable piezoelectric coefficient for bone defect recovery, *J Mech Behav Biomed Mater* 74 (2017) 365–370, <https://doi.org/10.1016/j.jmbmm.2017.06.024>.
- [118] Q. Wang, J. Yang, W. Zhang, R. Khoie, Y. Li, J. Zhu, Z. Chen, Manufacture and cytotoxicity of a lead-free piezoelectric ceramic as a bone substitute-consolidation of porous lithium sodium potassium niobate by cold isostatic pressing, *Int. J. Oral Sci.* 1 (2009) 99–104, <https://doi.org/10.4248/ijos.09005>.
- [119] M. Kitsara, A. Blanquer, F.A. Murillo, V. Humblot, S. De Bragança Vieira, C. Nogués, E. Ibáñez, J. Esteve, L. Barrios, Permanently hydrophilic, piezoelectric PVDF nanofibrous scaffolds promoting unaided electromechanical stimulation on osteoblasts, *Nanoscale* 11 (2019) 8906–8917, <https://doi.org/10.1039/C8NR10384D>.
- [120] Y. Li, X. Dai, Y. Bai, Y. Liu, Y. Wang, Q. Liu, F. Yan, Z. Tang, X. Zhang, X. Deng, Electroactive BaTiO₃ nanoparticle-functionalized fibrous scaffolds enhance osteogenic differentiation of mesenchymal stem cells, *Int. J. Nanomed.* 12 (2017) 4007–4018, <https://doi.org/10.2147/IJN.S135605>.
- [121] T. Amna, M.S. Hassan, F.A. Sheikh, H.K. Lee, K.-S. Seo, D. Yoon, I.H. Hwang, Zinc oxide-doped poly(urethane) spider web nanofibrous scaffold via one-step electrospinning: a novel matrix for tissue engineering, *Appl. Microbiol. Biotechnol.* 97 (2013) 1725–1734, <https://doi.org/10.1007/s00253-012-4353-0>.
- [122] X. Zhang, C. Zhang, Y. Lin, P. Hu, Y. Shen, K. Wang, S. Meng, Y. Chai, X. Dai, X. Liu, Y. Liu, X. Mo, C. Cao, S. Li, X. Deng, L. Chen, Nanocomposite membranes enhance bone regeneration through restoring physiological electric microenvironment, *ACS Nano* 10 (2016) 7279–7286, <https://doi.org/10.1021/acsnano.6b02247>.
- [123] Y. Bai, X. Dai, Y. Yin, J. Wang, X. Sun, W. Liang, Y. Li, X. Deng, X. Zhang, Biomimetic piezoelectric nanocomposite membranes synergistically enhance osteogenesis of deproteinized bovine bone grafts, *Int. J. Nanomed.* 14 (2019) 3015–3026, <https://doi.org/10.2147/IJN.S197824>.
- [124] M. Schult, E. Buckow, H. Seitz, Experimental studies on 3D printing of barium titanate ceramics for medical applications, *Curr. Dir. Biomed. Eng.* 2 (2016) 95–96, <https://doi.org/10.1515/cdbme-2016-0024>.
- [125] A. Marino, J. Barsotti, G. de Vito, C. Filippeschi, B. Mazzolai, V. Piazza, M. Labardi, V. Mattoli, G. Ciofani, Two-photon lithography of 3D nanocomposite piezoelectric scaffolds for cell stimulation, *ACS Appl. Mater. Interfaces* 7 (2015) 25574–25579, <https://doi.org/10.1021/acsaami.5b08764>.
- [126] W. Liu, F. Zhang, Y. Yan, C. Zhang, H. Zhao, B. Chin Heng, Y. Huang, Y. Shen, J. Zhang, L. Chen, X. Wen, X. Deng, Remote tuning of built-in magnetoelectric microenvironment to promote bone regeneration by modulating cellular exposure to arginylglycylaspartic acid peptide, *Adv. Funct. Mater.* 31 (2021) 2006226, <https://doi.org/10.1002/adfm.202006226>.
- [127] J.-H. Fang, H.-H. Hsu, R.-S. Hsu, C.-K. Peng, Y.-J. Lu, Y.-Y. Chen, S.-Y. Chen, S.-H. Hu, 4D printing of stretchable nanocookie@conduit material hosting biocues and magnetoelectric stimulation for neurite sprouting, *NPG Asia Mater.* 12 (2020) 61, <https://doi.org/10.1038/s41427-020-00244-1>.
- [128] I.O. Paryi, A.A. Ivanova, V.V. Shvartsman, D.C. Lupascu, G.B. Sukhorukov, M.A. Surmeneva, R.A. Surmenev, Poling and annealing of piezoelectric poly(vinylidene fluoride) micropillar arrays, *Mater. Chem. Phys.* 239 (2020) 122035, <https://doi.org/10.1016/j.matchemphys.2019.122035>.
- [129] I.O. Paryi, A.A. Ivanova, V.V. Shvartsman, D.C. Lupascu, G.B. Sukhorukov, T. Ludwig, A. Bartaszyte, S. Mathur, M.A. Surmeneva, R.A. Surmenev, Piezoelectric response in hybrid micropillar arrays of poly(vinylidene fluoride) and reduced graphene oxide, *Polymers* 11 (2019) 1065, <https://doi.org/10.3390/polym11061065>.
- [130] C. Ribeiro, C.M. Costa, Daniela M. Correia, J. Nunes-Pereira, J. Oliveira, P. Martins, R. Gonçalves, V. F. Cardoso, S. Lanceros-Méndez, Electroactive poly(vinylidene fluoride)-based structures for advanced applications, *Nat. Protoc.* 13 (2018) 681–704, <https://doi.org/10.1038/nprot.2017.157>.
- [131] Z. Liu, X. Wan, Z.L. Wang, L. Li, Electroactive biomaterials and systems for cell fate determination and tissue regeneration: design and applications, *Adv. Mater.* (2021) 2007429, <https://doi.org/10.1002/adma.202007429>.
- [132] F.R. Carreno, A. Frazer, Vagus nerve stimulation for treatment-resistant depression, *Neurotherapeutics* 14 (2017) 716–727, <https://doi.org/10.1007/s13311-017-0537-8>.
- [133] F. Fregni, A. Pascual-Leone, Technology insight: noninvasive brain stimulation in neurology—perspectives on the therapeutic potential of rTMS and tDCS, *Nat. Clin. Pract. Neurol.* 3 (2007) 383–393, <https://doi.org/10.1038/ncpneu0530>.
- [134] M.L. Kringsbach, N. Jenkinson, S.L. Owen, T.Z. Aziz, Translational principles of deep brain stimulation, *Nat. Rev. Neurosci.* 8 (2007) 623–635, <https://doi.org/10.1038/nrn2196>.
- [135] K. Yue, R. Guduru, J. Hong, P. Liang, M. Nair, S. Khizroev, Magneto-electric nanoparticles for non-invasive brain stimulation, *PLoS One* 7 (2012) e44040, <https://doi.org/10.1371/journal.pone.0044040>.
- [136] R. Guduru, P. Liang, J. Hong, A. Rodzinski, A. Hadjikhani, J. Horstmyer, E. Levstev, S. Khizroev, Magnetoelectric 'spin' on stimulating the brain, *Nanomedicine (Lond)* 10 (2015) 2051–2061, <https://doi.org/10.2217/nmm.15.52>.
- [137] J. Rothwell, Transcranial brain stimulation: Past and future, *Brain. Neurosci. Adv.* 2 (2018), 32166172 <https://doi.org/10.1177/2398212818818070>.
- [138] T. Nguyen, J. Gao, P. Wang, A. Nagesetti, P. Andrews, S. Masood, Z. Vriesman, P. Liang, S. Khizroev, X. Jin, In vivo wireless brain stimulation via non-invasive and targeted delivery of magnetoelectric nanoparticles, *Neurotherapeutics* (2021), <https://doi.org/10.1007/s13311-021-01071-0>.
- [139] S. Khizroev, Technobiology's enabler: the magnetoelectric nanoparticle, *Cold Spring Harb Perspect Med* 9 (2019) a034207, <https://doi.org/10.1101/cshperspect.a034207>.
- [140] H. Ye, A. Steiger, Neuron matters: electric activation of neuronal tissue is dependent on the interaction between the neuron and the electric field, *J. NeuroEng. Rehabil.* 12 (2015) 65, <https://doi.org/10.1186/s12984-015-0061-1>.
- [141] R.A. Islam, V. Bedekar, N. Poudyal, J.P. Liu, S. Priya, Magnetoelectric properties of core-shell particulate nanocomposites, *J. Appl. Phys.* 104 (2008) 104111, <https://doi.org/10.1063/1.3013437>.
- [142] Y. Shi, N. Li, Y. Wang, J. Ye, An analytical model for nonlinear magnetoelectric effect in laminated composites, *Compos. Struct.* 263 (2021) 113652, <https://doi.org/10.1016/j.compstruct.2021.113652>.
- [143] C. Popov, H. Chang, P.M. Record, E. Abraham, R.W. Whatmore, Z. Huang, Direct and converse magnetoelectric effect at resonant frequency in laminar piezoelectric-magnetostrictive composite, *J. Electroceram.* 20 (2008) 53–58, <https://doi.org/10.1007/s10832-007-9184-5>.
- [144] K.H. Cho, S. Priya, Direct and converse effect in magnetoelectric laminate composites, *Appl. Phys. Lett.* 98 (2011) 232904, <https://doi.org/10.1063/1.3584863>.
- [145] W. Liu, A.E. Miroshnichenko, D.N. Neshev, Y.S. Kivshar, Broadband unidirectional scattering by magneto-electric core-shell nanoparticles, *ACS Nano* 6 (2012) 5489–5497, <https://doi.org/10.1021/nn301398a>.
- [146] M. Popov, G. Sreenivasulu, V.M. Petrov, F.A. Chavez, G. Srinivasan, High frequency magneto-dielectric effects in self-assembled ferrite-ferroelectric core-shell nanoparticles, *AIP Adv.* 4 (2014) 97117, <https://doi.org/10.1063/1.4895591>.
- [147] C.R. Chandra, P.S.N. Bharani, Y.R. Kumar, Frequently dependent attenuation of EM radiation on biological tissues, *Int J Adv Res EEI* 3 (2014) 12094–12099, <https://doi.org/10.15662/ijareeie.2014.0309031>.
- [148] M.C. Ziskin, S.I. Alekseev, K.R. Foster, Q. Balzano, Tissue models for RF exposure evaluation at frequencies above 6 GHz, *Bioelectromagnetics* 39 (2018) 173–189, <https://doi.org/10.1002/bem.22110>.
- [149] A. Hadjikhani, A. Rodzinski, P. Wang, A. Nagesetti, R. Guduru, P. Liang, C. Runowicz, S. Shahbazmohamadi, S. Khizroev, Biodistribution and clearance of magnetoelectric nanoparticles for nanomedical applications using energy dispersive spectroscopy, *Nanomedicine (Lond)* 12 (2017) 1801–1822, <https://doi.org/10.2217/nmm-2017-0080>.
- [150] A. Kaushik, R. Jayant, R. Nikkhal-Moshaie, V. Bhardwaj, U. Roy, Z. Huang, A. Ruiz, A. Yndart, V. Atluri, N. El-Hage, K. Khalili, M. Nair, Magnetically guided central nervous system delivery and toxicity evaluation of magneto-electric nanocarriers, *Sci. Rep.* 6 (2016) 25309, <https://doi.org/10.1038/srep25309>.
- [151] F.M. Veronese, G. Pasut, PEGylation, successful approach to drug delivery, *Drug Discov. Today* 10 (2005) 1451–1458, [https://doi.org/10.1016/S1359-6446\(05\)03575-0](https://doi.org/10.1016/S1359-6446(05)03575-0).
- [152] M. Nair, R. Guduru, P. Liang, J. Hong, V. Sagar, S. Khizroev, Externally controlled on-demand release of anti-HIV drug using magneto-electric nanoparticles as carriers, *Nat. Commun.* 4 (2013) 1707, <https://doi.org/10.1038/ncomms2717>.
- [153] M. Yang, W.J. Brackenbury, Membrane potential and cancer progression, *Front. Physiol.* 4 (2013) 1–10, <https://doi.org/10.3389/fphys.2013.00185>.
- [154] M.R. Prausnitz, V.G. Bose, R. Langer, J.C. Weaver, Electroporation of mammalian skin: a mechanism to enhance transdermal drug delivery, *Proc. Natl. Acad. Sci. Unit. States Am.* 90 (1993) 10504–10508, <https://doi.org/10.1073/pnas.90.22.10504>.
- [155] R. Guduru, P. Liang, C. Runowicz, M. Nair, V. Atluri, S. Khizroev, Magnetoelectric nanoparticles to enable field-controlled high-specificity drug delivery to eradicate ovarian cancer cells, *Sci. Rep.* 3 (2013), <https://doi.org/10.1038/srep02953>, 2953–2953.
- [156] A. Rodzinski, R. Guduru, P. Liang, A. Hadjikhani, T. Stewart, E. Stimpfil, C. Runowicz, R. Cote, N. Altman, R. Datar, S. Khizroev, Targeted and controlled anticancer drug delivery and release with magnetoelectric nanoparticles, *Sci. Rep.* 6 (2016), <https://doi.org/10.1038/srep20867>, 20867–20867.
- [157] E. Stimpfil, A. Nagesetti, R. Guduru, T. Stewart, A. Rodzinski, P. Liang, S. Khizroev, Physics considerations in targeted anticancer drug delivery by magnetoelectric nanoparticles, *Appl. Phys. Rev.* 4 (2017) 21101, <https://doi.org/10.1063/1.4978642>.
- [158] T.S. Stewart, A. Nagesetti, R. Guduru, P. Liang, E. Stimpfil, A. Hadjikhani, L. Salgueiro, J. Horstmyer, R. Cai, A. Schally, S. Khizroev, Magnetoelectric nanoparticles for delivery of antitumor peptides into glioblastoma cells by magnetic fields, *Nanomedicine (Lond)* 13 (2018) 423–438, <https://doi.org/10.2217/nmm-2017-0300>.
- [159] R. Biran, D.C. Martin, P.A. Tresco, The brain tissue response to implanted silicon microelectrode arrays is increased when the device is tethered to the skull, *J. Biomed. Mater. Res.* 82 (2007) 169–178, <https://doi.org/10.1016/j.jbios.2020.112781>.
- [160] H. Dinis, P.M. Mendes, A comprehensive review of powering methods used in state-of-the-art miniaturized implantable electronic devices, *Biosens. Bioelectron.* 172 (2021) 112781, <https://doi.org/10.1016/j.bios.2020.112781>.
- [161] B.D. Truong, S. Roundy, Experimentally validated model and power optimization of a magnetoelectric wireless power transfer system in free-free configuration, *Smart Mater. Struct.* 29 (2020) 85053, <https://doi.org/10.1088/1361-665X/ab90a2>.
- [162] T. Rupp, B.D. Truong, S. Williams, S. Roundy, Magnetoelectric transducer designs for use as wireless power receivers in wearable and implantable Applications, *Materials* 12 (2019) 512, <https://doi.org/10.3390/ma12030512>.

- [163] P. Abiri, A. Abiri, R.R.S. Packard, Y. Ding, A. Yousefi, J. Ma, M. Bersohn, K.-L. Nguyen, D. Markovic, S. Moloudi, T.K. Hsiai, Inductively powered wireless pacing via a miniature pacemaker and remote stimulation control system, *Sci. Rep.* 7 (2017) 6180, <https://doi.org/10.1038/s41598-017-06493-5>.
- [164] G. Monti, P. Arcuti, L. Tarricone, Resonant inductive link for remote powering of pacemakers, *IEEE Trans. Microw. Theor. Tech.* 63 (2015) 3814–3822, <https://doi.org/10.1109/TMTT.2015.2481387>.
- [165] T. Campi, S. Cruciani, F. Palandrani, V. De Santis, A. Hirata, M. Feliziani, Wireless power transfer charging system for airds and pacemakers, *IEEE Trans. Microw. Theor. Tech.* 64 (2016) 633–642, <https://doi.org/10.1109/TMTT.2015.2511011>.
- [166] H. Talleb, Z. Ren, Finite element modeling of a magnetoelectric energy transducer including the load effect, *IEEE Trans. Magn.* 51 (2015) 1–5, <https://doi.org/10.1109/TMAG.2014.2357492>, 7401305.
- [167] D. Seo, J.M. Carmena, J.M. Rabaey, M.M. Maharbiz, E. Alon, Model validation of untethered, ultrasonic neural dust motes for cortical recording, *J. Neurosci. Methods* 244 (2015) 114–122, <https://doi.org/10.1016/j.jneumeth.2014.07.025>.
- [168] J. Charthad, T.C. Chang, Z. Liu, A. Sawaby, M.J. Weber, S. Baker, F. Gore, S.A. Felt, A. Arabbian, A mm-sized wireless implantable device for electrical stimulation of peripheral nerves, *IEEE Trans. Biomed. Circuits Syst.* 12 (2018) 257–270, <https://doi.org/10.1109/TBCAS.2018.2799623>.
- [169] D.K. Piech, B.C. Johnson, K. Shen, M.M. Ghanbari, K.Y. Li, R.M. Neely, J.E. Kay, J.M. Carmena, M.M. Maharbiz, R. Muller, A wireless millimetre-scale implantable neural stimulator with ultrasonically powered bidirectional communication, *Nat. Biomed. Eng.* 4 (2020) 207–222, <https://doi.org/10.1038/s41551-020-0518-9>.
- [170] D. Seo, R.M. Neely, K. Shen, U. Singhal, E. Alon, J.M. Rabaey, J.M. Carmena, M.M. Maharbiz, Wireless recording in the peripheral nervous system with ultrasonic neural dust, *Neuron* 91 (2016) 529–539, <https://doi.org/10.1016/j.neuron.2016.06.034>.
- [171] H. Basaeri, D. Christensen, S. Roundy, A review of acoustic power transfer for biomedical implants, *Smart Mater. Struct.* 25 (2016) 123001, <https://doi.org/10.1088/0964-1726/25/12/123001>.
- [172] K.L. Montgomery, A.J. Yeh, J.S. Ho, V. Tsao, S.M. Iyer, L. Grosenick, E.A. Ferenczi, Y. Tanabe, K. Deisseroth, S. L. Delp, A.S.Y. Poon, Wirelessly powered, fully internal optogenetics for brain, spinal and peripheral circuits in mice, *Nat. Methods* 12 (2015) 969–974, <https://doi.org/10.1038/nmeth.3536>.
- [173] A. Burton, S.N. Obaid, A. Vázquez-Guardado, M.B. Schmit, T. Stuart, Le Cai, Z. Chen, I. Kandela, C.R. Haney, E.A. Waters, H. Cai, J.A. Rogers, L. Lu, P. Gutruf, Wireless, battery-free subdermally implantable photometry systems for chronic recording of neural dynamics, *Proc. Natl. Acad. Sci.* 117 (2020) 2835–2845, <https://doi.org/10.1073/pnas.1920073117>.
- [174] R. Hinchet, H.-J. Yoon, H. Ryu, M.-K. Kim, E.-K. Choi, D.-S. Kim, S.-W. Kim, Transcutaneous harvesting energy using energy conversion capacitive triboelectric technology, *Science* 365 (2019) 491–494, <https://doi.org/10.1126/science.aan3997>.
- [175] S.H. Song, A. Kim, B. Ziaie, Omnidirectional ultrasonic powering for millimeterscale implantable devices, *IEEE Trans. Biomed. Eng.* 62 (2015) 2717–2723, <https://doi.org/10.1109/TBME.2015.2444854>.
- [176] T. Nan, H. Lin, Y. Gao, A. Matyushov, G. Yu, H. Chen, N. Sun, S. Wei, Z. Wang, M. Li, X. Wang, A. Belkessam, R. Guo, B. Chen, J. Zhou, Z. Qian, Y. Hui, M. Rinaldi, M.E. McConney, B.M. Howe, Z. Hu, J.G. Jones, G.J. Brown, N.X. Sun, Acoustically actuated ultra-compact nems magnetoelectric antennas, *Nat. Commun.* 8 (2017) 296, <https://doi.org/10.1038/s41467-017-00343-8>.
- [177] B.A. Kramer, C.-C. Chen, M. Lee, J.L. Volakis, Fundamental limits and design guidelines for miniaturizing ultra-wideband antennas, *IEEE Antenn. Propag. Mag.* 51 (2009) 57–69, <https://doi.org/10.1109/MAP.2009.5338684>.
- [178] Int. Commission on Non-Ionizing Radiation Protection 1998 Guidelines for limiting exposure to time-varying electric, magnetic and electromagnetic fields (up to 300 ghz), *Health Phys.* 75 (1998) 494–522.
- [179] D. McRobbie, Concerning guidelines for limiting exposure to time-varying electric, magnetic and electromagnetic fields (1 hz-100 khz), *Health Phys.* 100 (2011) 442, <https://doi.org/10.1097/HP.0b013e318f06c86>.
- [180] IEEE, IEEE Standard for Safety Levels with Respect to Human Exposure to Radio Frequency Electromagnetic Fields, 3 kHz to 300 GHz, *IEEE Std C95.1-2005 (Revision of IEEE Std C95.1-1991)*, 2006, pp. 1–238.
- [181] IEEE Standard for Safety Levels with Respect to Human Exposure to Electromagnetic Fields, 0–3 kHz, *IEEE Std C95.6-2002, 2002, 1-0*.
- [182] IEEE Standard for Safety Levels with Respect to Human Exposure to Electric, Magnetic, and Electromagnetic Fields, 0 Hz to 300 GHz, "IEEE, Tech. Rep., ISBN: 9781504455480.
- [183] B.D. Truong, E. Andersen, C. Casados, S. Roundy, Magnetoelectric wireless power transfer for biomedical implants: effects of non-uniform magnetic field, alignment and orientation, *Sens. Actuators, A* 316 (2020) 112269, <https://doi.org/10.1016/j.sna.2020.112269>.
- [184] J. Young, M.-T. Wang, I. Brezovich, Frequency/depth-penetration considerations in hyperthermia by magnetically induced currents, *Electron. Lett.* 16 (1980) 358–359, https://doi.org/10.1049/el_19800255.
- [185] M. Zaeimbashi, H. Lin, C. Dong, X. Liang, M. Nasrollahpour, H. Chen, N. Sun, A. Matyushov, Y. He, X. Wang, C. Tu, Y. Wei, Y. Zhang, S.S. Cash, M. Onabajo, A. Shrivastava, N. Sun, NanoNeuroRFID: a wireless implantable device based on magnetoelectric antennas, *IEEE J. Electromagn. RF Microw. Med. Biol.* 3 (2019) 206–215, <https://doi.org/10.1109/JERM.2019.2903930>.
- [186] *Diagnostic Ultrasound: Physics and Equipment*, Cambridge Univ. Press, Cambridge, U.K., 2010.
- [187] M. Zaeimbashi, *Methods and Techniques for Magnetic Neural Stimulation and Recording*, PhD thesis, 2020. ProQuest Number: 28090985.
- [188] E. McGlynn, R. Das, H. Heidari, Encapsulated magnetoelectric composites for wirelessly powered brain implantable devices, in: 2020 27th IEEE International Conference on Electronics, Circuits and Systems (ICECS), 2020, pp. 1–4, <https://doi.org/10.1109/ICECS49266.2020.9294847>.
- [189] R.C. O'Handley, J.K. Huang, D. Currier Bono, J. Simon, Improved wireless, transcutaneous power transmission for in vivo applications, *IEEE Sensor. J.* 8 (2008) 57–62, <https://doi.org/10.1109/JSEN.2007.912899>.
- [190] J. Timot, K.L. Shepard, Bioelectronic devices: wirelessly powered implants, *Nat. Biomed. Eng.* 1 (2017) 51, <https://doi.org/10.1038/s41551-017-0051>.
- [191] Information for Manufacturers Seeking Marketing Clearance of Diagnostic Ultrasound Systems and Transducers, FDA, 2008, pp. 1–64. <https://www.fda.gov/downloads/UCM070911.pdf>.
- [192] S. Newacheck, G. Youssef, Wireless energy transfer based on strain-mediated composite multiferroics, *Smart Mater. Struct.* 29 (2020) 15014, <https://doi.org/10.1088/1361-665X/ab545b>.
- [193] H. Lyu, J. Wang, J.H. La, J.M. Chung, A. Babakhani, An energy-efficient wirelessly powered millimeter-scale neurostimulator implant based on systematic codesign of an inductive loop antenna and a custom rectifier, *IEEE Trans. Biomed. Circuits Syst.* 12 (2018) 1131–1143, <https://doi.org/10.1109/TBCAS.2018.2852680>.
- [194] C.-L. Yang, C.-K. Chang, S.-Y. Lee, S.-J. Chang, L.-Y. Chiou, Efficient four-coil wireless power transfer for deep brain stimulation, *IEEE Trans. Microw. Theor. Tech.* 65 (2017) 2496–2507, <https://doi.org/10.1109/TMTT.2017.2658560>.
- [195] F. Wu, L.W. Tien, F. Chen, J.D. Berke, D. I. Kaplan, E. Yoon, Silkbacked structural optimization of high-density flexible intracortical neural probes, *J-MEMS* 24 (2015) 62–69, <https://doi.org/10.1109/JMEMS.2014.2375326>.
- [196] R. Qazi, *Novel Class of Chronic and Implantable Wireless Optofluidic (wOF) Neural Devices for in Vivo Drug Delivery and Optogenetics in Freely Moving Animals*, PhD thesis, 2019.
- [197] J. Jeong, J. Jung, D. Jung, J. Kim, H. Ju, T. Kim, J. Lee, An implantable optogenetic stimulator wirelessly powered by flexible photovoltaics with near-infrared (NIR) light, *Biosens. Bioelectron.* 180 (2021) 113–139, <https://doi.org/10.1016/j.bios.2021.113139>.
- [198] E.S. Boyden, F. Zhang, E. Bamberg, G. Nagel, K. Deisseroth, Millisecond-timescale, genetically targeted optical control of neural activity, *Nat. Neurosci.* 8 (2005) 1263–1268, <https://doi.org/10.1038/nn1525>.
- [199] Y. Wang, L. Guo, Nanomaterial-enabled neural stimulation, *Front. Neurosci.* 10 (2016) 69, <https://doi.org/10.1016/j.front.2016.06.004>.
- [200] G. Shin, A.M. Gomez, R. Al-Hasani, Y. Ra Jeong, J. Kim, Z. Xie, A. Banks, S. Min Lee, S. Youn Han, C. Jong Yoo, J.-L. Lee, S. Hee Lee, J. Kurniawan, J. Tureb, Z. Guo, J. Yoon, S. Il Park, S. Yun Bang, J.A. Rogers, Flexible near-field wireless optoelectronics as subdermal implants for broad applications in optogenetics, *Neuron* 93 (2017) 509–521, <https://doi.org/10.1016/j.neuron.2016.12.031>, e3.
- [201] Y. Zhang, X. Zhang, H. Wang, Y. Tian, H. Pan, L. Zhang, F. Wang, J. Chang, Remote regulation of optogenetic proteins by a magneto-luminescence microdevice, *Adv. Funct. Mater.* 31 (2021) 2006357, <https://doi.org/10.1002/adfm.202006357>.
- [202] R. Chen, A. Canales, P. Anikeeva, Neural recording and modulation technologies, *Nat. Rev. Mater.* 2 (2017) 16093, <https://doi.org/10.1038/natrevmats.2016.93>.
- [203] J.D. Wells, C. Kao, E.D. Jansen, P.E. Konrad, A. Mahadevan-Jansen, Application of infrared light for in vivo neural stimulation, *J. Biomed. Opt.* 10 (2005) 64003, <https://doi.org/10.1117/1.2121772>.
- [204] O. Yizhar, L.E. Fenno, T.J. Davidson, M. Mogri, K. Deisseroth, Optogenetics in neural systems, *Neuron* 71 (2011) 9–34, <https://doi.org/10.1016/j.neuron.2011.06.004>.
- [205] T. Knopfel, Genetically encoded optical indicators for the analysis of neuronal circuits, *Nat. Rev. Neurosci.* 13 (2012) 687–700, <https://doi.org/10.1038/nrn3293>.
- [206] N.G. Horton, K. Wang, D. Kobat, C.G. Clark, F.W. Wise, C.B. Schaffer, C. Xu, In vivo three-photon microscopy of subcortical structures within an intact mouse brain, *Nat. Photonics* 7 (2013) 205–209, <https://doi.org/10.1038/nphoton.2012.336>.
- [207] W. Legon, T. F Sato, A. Opitz, J. Mueller, A. Barbour, A. Williams, W.J. Tyler, Transcranial focused ultrasound modulates the activity of primary somatosensory cortex in humans, *Nat. Neurosci.* 17 (2014) 322–329, <https://doi.org/10.1038/nn.3620>.
- [208] M. Hallett, Transcranial magnetic stimulation: a primer, *Neuron* 55 (2007) 187–199, <https://doi.org/10.1016/j.neuron.2007.06.026>.
- [209] A.V. Gourine, V. Kasymov, N. Marina, F.G. Tang, M.F. Figueiredo, S. Lane, A.G. Teschemacher, K.M. Spyer, K. Deisseroth, S. Kasparov, Astrocytes control breathing through pH-dependent release of ATP, *Science* 329 (2010) 571–575, <https://doi.org/10.1126/science.1190721>.
- [210] J. Tonnesen, A.T. Sorensen, K. Deisseroth, C. Lundberg, M. Kokaia, Optogenetic control of epileptiform activity, *Proc. Natl. Acad. Sci. U.S.A.* 106 (2009) 12162–12167, <https://doi.org/10.1073/pnas.0901915106>.
- [211] H.E. Lee, J.H. Park, D. Jang, J.H. Shin, T.H. Im, J.H. Lee, S.K. Hong, H.S. Wang, M.S. Kwak, M. Peddigari, C.K. Jeong, Y. Min, C.H. Park, J.-J. Choi, J. Ryu, W.-H. Yoon, D. Kim, K.J. Lee, G.-T. Hwang, Optogenetic brain neuromodulation by stray magnetic field via flash-enhanced magneto-mechano-triboelectric nanogenerator, *Nano Energy* 75 (2020) 104951, <https://doi.org/10.1016/j.nanoen.2020.104951>.
- [212] H.E. Lee, J.H. Shin, J.H. Park, S.K. Hong, S.H. Park, S.H. Lee, J.H. Lee, I.S. Kang, K.J. Lee, Micro light-emitting diodes for display and flexible biomedical applications, *Adv. Funct. Mater.* 29 (2019) 1808075, <https://doi.org/10.1002/adfm.201808075>.
- [213] S.H. Lee, J. Kim, J.H. Shin, H.E. Lee, I.S. Kang, K. Gwak, D.S. Kim, D. Kim, K.J. Lee, Optogenetic control of body movements via flexible vertical light-emitting diodes on brain surface, *Nano Energy* 44 (2018) 447–455, <https://doi.org/10.1016/j.nanoen.2017.12.011>.

- [214] A.R. Adamantidis, F. Zhang, A.M. Aravanis, K. Deisseroth, L. De Lecea, Neural substrates of awakening probed with optogenetic control of hypocretin neurons, *Nature* 450 (2007) 420–424, <https://doi.org/10.1038/nature06310>.
- [215] S.H. Yun, S.J.J. Kwok, Light in diagnosis, therapy and surgery, *Nat. Biomed. Eng.* 1 (2017), <https://doi.org/10.1038/s41551-016-0008>, 0008.
- [216] Y. Zhao, C.B. Liu, Z.X. Liu, W.H. Luo, L.Z. Li, X. Cai, D. Liang, Y.Z. Su, H. Ding, Q. Wang, L. Yin, J.S. Guan, M.M. Luo, X. Sheng, Wirelessly operated, implantable optoelectronic probes for optogenetics in freely moving animals, *IEEE Trans. Electron. Dev.* 66 (2019) 785–792, <https://doi.org/10.1109/TED.2018.2882397>.
- [217] G.T. Hwang, Y. Kim, J.H. Lee, S. Oh, C.K. Jeong, D.Y. Park, J. Ryu, H. Kwon, S.G. Lee, B. Joung, D. Kim, K.J. Lee, Self-powered deep brain stimulation via a flexible PIMNT energy harvester, *Energy Environ. Sci.* 8 (2015) 2677–2684, <https://doi.org/10.1039/C5EE01593F>.
- [218] M. Silverå-Ejneby, M. Jakešová, J.J. Ferrero, L. Migliaccio, Z. Zhao, M. Berggren, D. Khodagholy, V. Dėrek, J. Gėlinas, E.D. Głowacki, A chronic photocapacitor implant for noninvasive neurostimulation with deep red light, *bioRxiv* (2020), <https://doi.org/10.1101/2020.07.01.182113>, 2020.07.01.182113.
- [219] M.G. Christiansen, A.W. Senko, P. Anikeeva, Magnetic strategies for nervous system control, *Annu. Rev. Neurosci.* 42 (2019) 271–293, <https://doi.org/10.1146/annurev-neuro-070918-050241>.
- [220] A.C. Tsai, A. Chih Wei Huang, Y. Hao Yu, Chii-Shyang Kuo, C.-C. Hsu, Y. San Lim, B. Chuang Shyu, A wireless magnetic resonance device for optogenetic applications in an animal model, *Sensors* 20 (2020) 5869, <https://doi.org/10.3390/s20205869>.
- [221] K. Oda, J. Vierock, S. Oishi, S. Rodriguez-Rozada, R. Taniguchi, K. Yamashita, J.S. Wiegert, T. Nishizawa, P. Hegemann, O. Nureki, Crystal structure of the red light-activated channelrhodopsin Chrimson, *Nat. Commun.* 9 (2018) 3949, <https://doi.org/10.1038/s41467-018-06421-9>.
- [222] V. Sreenivasan, K. Karmakar, F.M. Rijli, C.C.H. Petersen, Parallel pathways from motor and somatosensory cortex for controlling whisker movements in mice, *Eur. J. Neurosci.* 41 (2015) 354–367, <https://doi.org/10.1111/ejn.12800>.
- [223] J. Kapuscinski, DAPI: a DNA-specific fluorescent probe, *Biotech. Histochem.* 70 (1995) 220–233, <https://doi.org/10.3109/10520299509108199>.
- [224] R.M. Rich, D.L. Stankowska, B.P. Maliwal, T.J. Sorensen, B.W. Laursen, R.R. Krishnamoorthy, Z. Gryczynski, J. Borejdo, I. Gryczynski, R. Fudala, Elimination of autofluorescence background from fluorescence tissue images by use of timegated detection and the AzaDiOxaTriAngulenium (ADOTA) fluorophore, *Anal. Bioanal. Chem.* 405 (2013) 2065–2075, <https://doi.org/10.1007/s00216-012-6623-1>.
- [225] S.N. Gorodzha, M.A. Surmeneva, R.A. Surmenev, Fabrication and characterization of polycaprolactone cross-linked and highly-aligned 3-D artificial scaffolds for bone tissue regeneration via electrospinning technology, *IOP Conf. Ser.: Mater. Sci. Eng.* 98 (2015) 12024, <https://doi.org/10.1088/1757-899X/98/1/012024>.
- [226] R.A. Surmenev, M.A. Surmeneva, A critical review of decades of research on calcium phosphate-based coatings: how far are we from their widespread clinical application? *Curr. Opin. Biomed. Eng.* 10 (2019) 35–44, <https://doi.org/10.1016/j.cobme.2019.02.003>.
- [227] M.M. Fernandes, P. Martins, D.M. Correia, E.O. Carvalho, F.M. Gama, M. Vazquez, C. Bran, S. Lanceros-Mendez, Magnetolectric polymer-based nanocomposites with magnetically controlled antimicrobial activity, *ACS Appl. Bio Mater.* 4 (2021) 559–570, <https://doi.org/10.1021/acsbm.0c01125>.